Dissertation
submitted to the
Combined Faculty of Natural Sciences and Mathematics
of the Ruperto Carola University Heidelberg, Germany
for the degree of
Doctor of Natural Sciences

Presented by
M.Sc. Daniela Schweinfurth
Born in: Gronau (Westf.)
Oral examination: 17 July 2020

Characterisation of Protein-Very Long Chain Fatty Acid-Containing Sphingolipid Interactions

Referees: Prof. Dr. Britta Brügger

Prof. Dr. Marius Lemberg

Table of Contents

List of Figures

List of Tables

List of Abbreviations

°C	Degree celsius
A2B5	Cell surface ganglioside epitope
aa	Amino acid
AcOH	Acetic acid
AGPS	Alkylglycerol phosphate synthase
Akt	Protein kinase B (also PKB)
ALCAM/CD166 antigen	Activated leukocyte cell adhesion molecule
Amp	Ampicillin
AP-1	Activator protein 1
aPC	Ester-linked PC
APS	Ammoniumperoxodisulfat
ASGR1	Asiaglycoprotein receptor 1
BbsI	Restriction endonuclease
BSA	Bovine serum albumin
BSG	Basigin
C	Carbon atom
C-terminal	Carboxy-terminal
C16	16 carbon atoms
C18	18 carbon atoms
C1P	Ceramide-1-phosphate
cAMP	Cyclic adenosine monophosphate
Cas9	CRISPR associated protein 9
Cav3	Caveolin-3
CCM	cholesterol-consensus motif
CCTop	CRISPR-Cas9 target online predictor
CD	Cluster of differentiation
CD46	Membrane cofactor protein
CD63	CD63 antigen
CD81	CD81 antigen
CD8a	T-cell surface glycoprotein CD8 alpha chain
CD9	CD9 antigen
CDS	Coding DNA sequence
CE	Cholesterol ester
Cer	Ceramide
CerS	Ceramide Synthase
CerS2	Ceramide Synthase 2
CGT	Galactosyltransferase
$CHCl_3$	Chloroform
Chol	Cholesterol
cm	Centimeter
CMT	Charcot-Marie-Tooth
CMV	Cytomegalovirus
CNS	Central nervous system
CNX	Calnexin
CO2	Carbon dioxide
CoA	Coenzyme A
COPI	Coat-protein I
CREB	Cyclic AMP response element-binding protein

CRISPR	Clustered Regularly Interspaced Short Palindromic Repeats
CST	3'phosphoadenosine-5'phosphosulfate:cerebroside sulfotransferase
CuAAC	copper (I)-catalysed azide alkyne cycloaddition
$CuBF_4$	Tetrakis(acetonitrile)copper(I) tetrafluoroborate
$CuSO_4$	Copper(II) sulfate pentahydrate
CXN	Calnexin
Cy2	Cyanine Dye 2
D_6	Deutero
DAG	Diacylglycerol
DAG1	Dystroglycan
DAPI	4',6-diamidino-2-phenylindole
dbcAMP	dibutyryl cAMP
ddH_2O	Double distilled water
de novo	from the beginning (lat.)
DGC	Dystrophin-containing complex
DH5α	*E.coli* cells
DMD	Duchenne muscular dystrophy
DMEM	Dulbecco's modified Eagle's medium
DMSO	Dimethyl sulfoxide
DNA	Deoxyribonucleic acid
DNase	Desoxyribonuclease
dNTP	Deoxynucleotide triphosphates
DRM	Detergent-resistant membrane
E. coli	*Escherichia coli*
e.g.	Exempli gratia (lat.), for example
ECM	Extracellular matrix
EDTA	Ethylenediaminetetraacetic acid
EGF	Epidermal growth factor
EGFR	Epidermal growth factor receptor
ELOVL	Elongation of very long chain fatty acids protein
EM	Electron microscopy
EMB	Embigin
EMBL	European Molecular Biology Laboratory
ePC	Ether PC
ER	Endoplasmic reticulum
esiRNA	Endo-ribonuclease prepared siRNA
et al.	and others (lat.)
EtOH	Ethanol
FA	Fatty acid
FA2H	Fatty acid 2-hydroxylase
FACS	Fluorescence activated cell sorting
FB1	Fumonisin B1
FBS	Fetal bovine serum
FGF	Fibroblast growth factor
FGFR	Fibroblast growth factor receptor
Fiji	Fiji is Just Image J software
FLAG	Popypeptide protein tag, DYKDDDDK
FWD	Forward
g	Gram
GalCer	Galactosylceramide
GAPDH	Glycerinaldehyd-3-phosphat-Dehydrogenase

GD1	Disialoganglioside 1
GD2	Disialoganglioside 2
GD3	Disialoganglioside 3
gDNA	Genomic DNA
GFP	Green fluorescent protein
GlcCer	Glucosylceramide
GM3	Monosialodihexosylganglioside
GM4	Monosialoganglioside
GNPAT	Glyceronephosphate O-acyltransferase
GO	Gene ontology
GPCR	G-protein-coupled receptors
GPL	Glycerophospholipid
Grb2	Growth factor receptor-bound protein 2
gRNA	Guide RNA
GSL	Glycosphingolipid
GT3	Trisialodihexosylganglioside
H	Heavy
HBSS	Hank's balanced salt solution
HCl	Hydrochloric acid
HEK	Human embryonic kidney
HeLa	Henrietta Lacks, Human epithelial carcinoma cells
HEPES	2-[4-(2-Hydroxyethyl)piperazin-1-yl]ethanesul- fonic acid
Hex2Cer	Dihexosylceramide
HexCer	Hexosylceramide (Glc- or GalCer)
HPTLC	High performance thin layer chromatography
HS	Horse serum
ICAM1	Intracellular adhesion molecule 1
IFITM3	Interferon-induced transmembrane protein 3
IGF-1	Insulin-like growth factor-1
In silico	Performed on computer or via computer simulation
in vitro	In glass (lat.)
in vivo	Within the living (lat.)
IPP2A	Inhibitor 2 of PP2A
IRS-1	Insulin receptor subtrate-1
ITGA5	Integrin alpha 5
ITGB1	Integrin beta 1
Kan	Kanamycin
kb	Kilobases
KBM7	Chronic myelogenous Leukemia cell line
kDa	Kilodalton
L	Light
L1CAM	Neural cell adhesion molecule 1
LacCer	Lactosylceramide
LAMP	Lysosome associated protein
LAMP1	Lysosome-associated membrane glycoprotein 1
LAMP2	Lysosome-associated membrane glycoprotein 2
LB	Lysogenic broth or Luria Bertani
LC	Liquid chromatrography
LCFA	Long chain fatty acid
L_D	Liquid disordered
LG	Laminin G
lgSF	Cell wall protein from *Lactobacillus gallinarum*

L_O	Liquid ordered
Log10	Decadic logarithm
Log2	Binary logarithm
LOH1	LAG one homologue 1
LPC	Lyso-PC
LSM	Laser Scanning Microscope
LYN	Tyrosine-protein kinase
M	Molar
m	Meter
MAG	Myelin-associated glycoprotein
MAM	Mitochondria-associated membranes
MBP	Myelin basic protein
MCAM	Cell surface glycoprotein MUC18
MDS	Molecular dynamics simulations
mdx	Mouse model for DMD, point mutation in DMD gene, leading premature STOP codon
MEME	Multiple EM for Motif Elicitation
MeOH	Methanol
mff	Mitochondrial fission factor
mg	Milligram
min	Minute
mRNA	Messenger RNA
MS	Multiple sclerosis
MS	Mass spectrometry
MUC18	Cell surface protein MUC18
MW	Molecular weight
MβCD	Methyl-β-cyclodextrin
N-linked	Asparagine-linked
NaCl	Sodium chloride
NaOH	Sodium hydroxide
NF-155	155-kDa neurofascin
nm	Nanometer
nM	Nanomolar
NP40	Nonidet P40
NPC1	Niemann-pick type C1
NPC2	Niemann-pick type C2
NPTN	Neuroplasin
nt	Nucleotides
O-linked	Serine or threonine-linked
OH	Hydroxyl
OLG	Oligodendrocyte
Oli-neu	OPC cell line stably expressing t-*neu* oncogene
OPC	Oligodendroglial progenitor cells
p	Phosphorylated
P/S	Penicillin/Streptomycin
p24 (TMED2)	Transmembrane emp24 domain-containing protein 2 (p24)
PA	Phosphatidic acid
pac	Photoactivatable- and clickable
pacFA	Photoactivatable- and clickable fatty acid
pacSL	Photoactivatable- and clickable sphingolipid
pacSph	Photoactivatable and clickable sphingosine
PAGE	Polyacrylamide gel electrophoresis

PANTHER	Classification system
pBJ5	Mammalian expression vector
PBS	Phosphate buffered saline
PBS-T	Phosphate buffered saline Tween20
PC	Phosphatidylcholine
PCR	Polymerase chain reaction
PE	Phosphatidylethanolamine
PFA	Paraformaldehyde
PG	Phosphatidylglycerol
pH	*Potentia hydrogenii (lat.)*
PI	Phosphatidylinositol
pl	Plasmalogen
pl-PE	Plasmalogen ethanolamine
PI3 kinase	Phosphoinositide 3-kinase
PIC	Protease Inhibitor Cocktail
PKA	Protein kinase A
PKCζ	protein kinase ζ
PL-PD	Protein-lipid pulldown
PLL	Poly-L-lysine
PLP	Proteolipid protein
PNS	Post-nuclear supernatant
PP2A	Protein phosphatase 2A
PREC	Precursor ion scanning
PS	Phosphatidylserine
PUFAs	Polyunsaturated FAs
QTRAP	Mass spectrometer
Rab	Ras-related in brain
REV	Reverse
Rho-family GTPases	Family of small signaling G proteins
RMPI	Roswell Park Memorial Institute
RNA	Ribonucleic acid
rpm	Rounds per minute
RT	Room temperature
s	Second
S1P	Sphingosine 1-phosphate
SATO	Cell culture media for Oli-*neu*
SD	Standard deviation
SDS	Sodium dodecyl sulfate
SEM	Standard error of mean
SGalCer	Sulfatide
SGCE	Epsilon-sarcoglycan
SGMS	Sphingomyelin synthase
SGPL1	Sphingosine 1-phosphate lyase
sgRNA	Single guide RNA
SH3	SRC homology domain 3
SILAC	Stable-isotope labelling in cell culture
siRNA	Silencing RNA
siSGMS1	siRNA targeting SGMS1
siUGCG	siRNA targeting UGCG
SL	Sphingolipid
SLC1A5	Neutral amino acid transporter B(0)
SLC38A2	Sodium-coupled neutral amino acid transporter 2

SM	Sphingomyelin
SNAP	Soluble N-ethylmaleimide-sensitive-factor attachment
SNARE	SNAP receptor
Sph	Sphingosine
SQS	Squalene synthase
ST3GAL1	ST3 beta-galactoside alpha-2,3-sialytransferase 1
STRING	Search tool for the retrieval of interacting genes/proteins
STXs	Syntaxins
SV40	Simian virus 40
TAE	Tris acetate EDTA
TAG	Triacylglycerol
TBTA	Tris[(1-benzyl-1*H*-1,2,3-triazol-4-yl)methyl]amine
TCEP	Tris(2carboxyethyl)phosphine hydrochloride
TE	Trypsin-EDTA
TEA	Triethylamine
TEMED	Tetramethylethylendiamine
TFR	Transferrin receptor (also TfR)
TGOLN2	Trans Golgi network protein 2
TIT	Tri-iodo-thyrodine
TMD	Transmembrane domain
TOPCONS	Consensus prediction of membrane topology and signal peptides
TOR	Target of rapamycin
Tris	Tris(hydroxymethyl)aminomethane
UDP	Uridindiphosphat
UGCG	Glucosylceramide synthase (also GCS)
ULCFAs	Ultra long chain fatty acids
UV	Ultraviolet
V	Volt
v/v	Volume per volume
VLC	Very long chain
VLCFA	Very long chain fatty acid
w/o	without
w/v	Weight per volume
WT	Wild type
WW	Molecular protein domain, named after presence of two conserved tryptophans (W)
xg	Acceleration of gravity
αDG	α-dystroglycan
βDG	β-dystroglycan
µg	Microgram
µM	Micromolar

1. Summary/ Zusammenfassung

Sphingolipids that differ in their acyl chains have different effects on physiological and pathophysiological processes. Some of the roles can be explained by the biophysical characteristics of sphingolipids with different acyl chain lengths, but direct intracellular targets of especially very long chain fatty acid-containing sphingolipids remain largely unknown. Therefore we previously established a proteomic approach to identify direct interaction partners of very long chain fatty acid-containing sphingolipids in a cellular system. In this PhD thesis, the data obtained from the proteomic approach were bioinformatically analysed and validated. Biochemical assays were performed to further characterise a subset of the identified proteins, including the membrane protein dystroglycan, with respect to structural and functional aspects of their interactions with sphingolipids. Functional studies in oligodendrocytes were performed to investigate a specific role of dystroglycan with very long chain fatty acid-containing sphingolipids in myelin.

The obtained bioinformatic analyses revealed a broad spectrum of functions of very long chain fatty acid-containing sphingolipids. The identified interaction appeared to play roles in e.g. membrane/vesicle fusion and diverse adhesion processes. Several of the identified proteins were functionally connected, indicating a preference for the same local lipids within multiprotein complexes. Selected protein-lipid interactions from the proteomic approach were successfully validated. To define the interacting lipid species of these interactions, different assays were performed. The sphingolipid metabolism was modified by two different approaches, siRNA-mediated knockdowns and knockouts of targeting enzymes of the sphingolipid biosynthesis pathway. The results were not unambiguous due to a lack of specificity within the highly connected sphingolipid network.

Among the multiple suggested functions of very long chain fatty acid-containing sphingolipids, they fulfil an important function in myelin stability, however the underlying molecular mechanisms are not yet understood. Like very long chain fatty acid-containing sphingolipids, dystroglycan was suggested to be important for myelin stability and the myelination process itself. Therefore dystroglycan-very long chain fatty acid-containing sphingolipids interactions and their putative functions were investigated in oligodendrocytes. An interaction of dystroglycan with sphingolipids was observed and additional data suggested a role of very long chain

fatty acid-containing sphingolipids in dystroglycan trafficking to the plasma membrane. The cellular system established in this work will help to elucidate specific interactions of sphingolipids with dystroglycan and to understand their functional implications during myelination in oligodendrocytes.
Concluding, these data provide novel insights into the role of very long chain fatty acid-containing sphingolipids in multiple biological processes and hinted at a role of these lipids in trafficking of dystroglycan to the plasma membrane in oligodendrocytes.

Sphingolipide mit verschiedener Fettsäurezusammensetzung haben unterschiedliche Einflüsse auf physiologische und pathophysiologische Prozesse. Nur einige dieser Effekte können durch die biophysikalischen Eigenschaften der Sphingolipide erklärt werden. Insbesondere die direkten intrazellulären Interaktionspartner von sehr langkettigen Sphingolipiden sind bisher nicht bekannt. In dieser Arbeit wurden, aufbauend auf den Daten einer bereits vorliegenden proteomweiten Analyse, die die direkten intrazellulären Interaktionspartner von sehr langkettigen Sphingolipiden untersucht hat, weitergehende Untersuchungen durchgeführt.
Die Daten wurden bioinformatisch ausgewertet, der Versuch wurde validiert und weitere biochemische Experimente wurden durchgeführt, um einige der identifizierten Interaktionen weiter zu charakterisieren. Des Weiteren wurde in Oligodendrozyten die Funktion der Interaktion zwischen Dystroglycan und sehr langkettigen Sphingolipiden während der Myelinisierung untersucht.
Die bioinformatische Datenauswertung ergab ein weitreichendes Wirkungsspektrum der identifizierten Interaktionen. Diese umfassen unter anderem Rollen in der Membran-/Vesikelfusion und verschiedener Adhäsionsprozessen. Viele der identifizierten Proteine waren funktionell miteinander verbunden, was auf eine Präferenz für dieselbe Lipidumgebung in Multiproteinkomplexen hindeutet. Ausgewählte Protein-Lipid-Interaktionen wurden erfolgreich validiert. Um die genaue Lipidspezies der Interaktionen zu definieren, wurden verschiedene Experimente durchgeführt. Diese umfassten die siRNA-basierende Reduktion oder vollständige Gen-Knockouts bestimmter Enzyme im Sphingolipidstoffwechsel.

Aufgrund des komplexen Sphingolipidstoffwechsels sind die Ergebnisse bisher nicht eindeutig.

Von den vielen vermuteten Funktionen sehr langkettiger Sphingolipide ist vor allem der Einfluss auf die Stabilität von Myelin beschrieben worden. Allerdings sind auch hier die molekularen Mechanismen nicht bekannt. So wie für die sehr langkettigen Sphingolipide wurde auch für Dystroglycan eine Funktion in der Myelinstabilität sowie in der Myelinisierung selbst beschrieben. Aus diesem Grund wurde die Interaktion von Dystroglycan mit sehr langkettigen Sphingolipiden in Oligodendrozyten untersucht. Sowohl die Interaktion selbst, als auch der Transport von Dystroglycan zur Plasmamembran durch sehr langkettige Sphingolipide, wurde in Oligodendrozyten identifiziert. Das entwickelte zelluläre System ist dafür geeignet, auch in nachfolgenden Versuchen die funktionellen Auswirkungen dieser Interaktion weitergehend zu untersuchen.

Zusammenfassend haben die Daten dieser Arbeit einen neuen Einblick in die Rolle der sehr langkettigen Sphingolipide in verschiedene biologischen Prozessen gegeben. Des Weiteren wurde erstmals ein Einfluss von Lipiden auf den Transport von Dystroglycan in Oligodendrozyten beschrieben.

2. Introduction

2.1. Lipids as Modulators of Protein Function

Thousands of different lipids make up biological membranes. This enormous degree of structural diversity of lipids contradicts their long-time recognised single roles in barrier functions and energy metabolism. Cells synthesize proteins to actively modulate their lipidome. Various genetic diseases with mutations within these enzymes demonstrate multiple functions of lipids in physiology[1]. Described roles of lipids include functions as structural membrane components, energy and heat sources, signalling molecules, protein recruitment platforms and substrates for post-translational protein-lipid modifications[2]. This section introduces the biochemical background of lipid diversity before focussing on sphingolipid metabolism and functions of lipids in myelin. Finally, roles of lipids by interacting with proteins and methods to study protein-lipid interactions will be introduced.

2.1.1. Lipid Diversity

The major membrane lipids are assigned to three categories: glycerol-phospholipids (GPLs), sphingolipids (SLs) and cholesterol (Figure 2.1)[3]. In GPLs, a glycerol is linked to two fatty acids chains and a phosphorylated alcohol. Is the phosphate not further modified, the resulting lipid is phosphatidic acid (PA). The addition of different head groups like serine, ethanolamine, choline, glycerol and inositol form different GPL species, namely phosphatidylserine (PS), phosphatidyl-ethanolamine (PE), phosphatidylcholine (PC), diphosphatidylglycerol (cardiolipin) and phosphatidylinositol (PI), respectively. The diversity of GPLs is further increased by variations of fatty acid chain length, double bond number, double bond positions and the degree of hydroxylation[2]. Also the combination of fatty acids at the *sn-1* and *sn-2* position increases structural diversity[2].

The backbone of SLs is a sphingosine, an amino alcohol containing a long, unsaturated hydrocarbon chain, which is N-linked to a fatty acid chain. Diversity arises from the variety in length and type of the sphingoid base (long chain base, LCB), N-acyl chain and head group[2]. The addition of a choline headgroup forms sphingomyelin (SM), whereas the addition of glucose or galactose forms the cerebrosides glucosylceramide (GlcCer) or galactosylceramide (GalCer),

respectively[4]. More complex glycolipids, such as gangliosides (e.g. GM3, GD3, GD1), show branched chains of multiple sugar residues[4].

Cholesterol is different to other lipid categories. It is a steroid, made up of four interconnected hydrocarbon rings and is not varying much in structure. However, when regarding compositional diversity, cholesterol is enriched at the plasma membrane compared to other organelle membranes[3]. Thus, the multiple described functions of lipids are not solely achieved by the diversity of chemical structures of cellular lipids. Especially during signalling, compositional diversities become important[5]. Lipid compositions are different between species, between tissues or cells within an organism, between different organelles as well as between membrane leaflets and even in membrane subdomains[2].

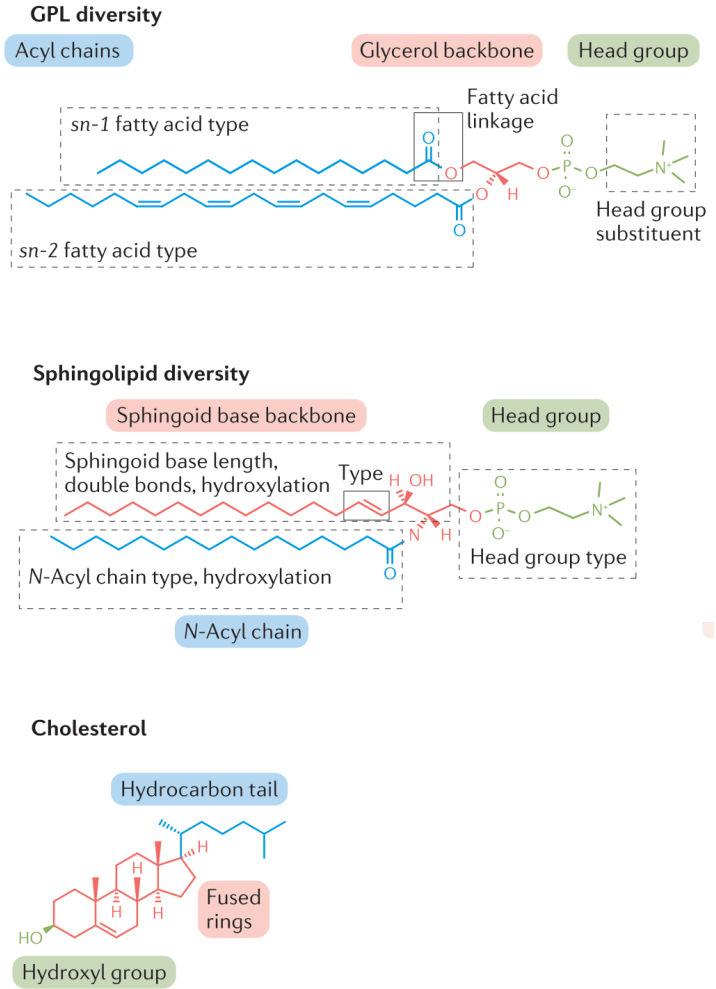

Figure 2.1 Classification of Membrane Lipids Based on Their Structure
Glycerophospholipids (GPLs) have a glycerol backbone with fatty acids at the sn-1 and sn-2 position. Head group is a esterified phosphoric acid with, for example, an attached choline head group, forming phosphatidylcholine. Sphingolipids have a sphingoid base, a N-linked acyl chain and a head group. Cholesterol is a sterol. Adapted and modified from[2]

At the level of subcellular diversity, membrane nanodomains (also called “lipid rafts”[6]) especially appear important for signalling and sorting[2,3]. These nanodomains are defined as dynamic sterol-SL-enriched nanoscale assemblies in the plane of the bilayer that associate and dissociate on a sub-second timescale[7]. As these nanodomains are enriched in cholesterol[6], the identity of components within these domains can be investigated by employing cyclodextrin which extracts cholesterol from the membrane[8]. This is further described in section 2.1.6.

2.1.2. Sphingolipid Metabolism

About 40 enzymes and metabolites are involved in the regulation and catalysis of different SL species[9]. The *de novo* synthesis of SLs starts with the condensation of the activated lipid palmitoyl-CoA and L-serine forming 3-keto-dihydrosphingosine by the serine palmitoyltransferase complex (Figure 2.2 Aa)[10]. After reduction to dihydrosphingosine, (Dihydro)ceramide synthases (CerSs) catalyse the formation of various dihydroceramides by linking a fatty acid to the C2-amino group[11], which initiates the diversification of SLs.

Mammals synthesize six different CerS isoforms, each showing a preference for the acyl-chain length of the fatty acid[12]. Furthermore, CerSs show a strong compartment- and tissue-specific expression[12], indicating particular roles of their lipid products in the respective organelles or tissues. For instance, CerS2 catalyses the formation of ceramide with very long chain fatty acids (VLCFA; C22-C24) and is strongly expressed in liver, kidney, bone marrow and in oligodendrocytes (OLGs) during active myelination (refer to section 2.1.3.2 and 2.1.5)[13–15]. Desaturation of dihydroceramide at the C4-C5 position forms ceramide[16]. Ceramide is also generated by the action of CerS employing sphingosine from the catabolism of complex SLs (salvage pathway)[12].The phosphorylation of ceramide (Figure 2.2 Ab) or sphingosine (Figure 2.2 Af) results in the synthesis of bioactive ceramide-1-phosphate (C1P) or sphingosine-1-phosphate (S1P), respectively. Many different functions of these bioactive metabolites are described including roles in cell migration, cell proliferation, apoptosis and inflammation[17]. Ceramide is catabolised to sphingosine by the action of a Ceramidase (Figure 2.2 Af). Further phosphorylation to S1P allows the escape from the SL pathway by the action of the Sphingosine-1-phosphate lyase (S1P lyase or SGPL1; Figure 2.2 Ag), which

degrades S1P to hexadecanal and ethanolamine 1-phosphate. This further results in the formation of fatty acyl-CoAs[17], which are also substrates for the synthesis of lipids of other categories.

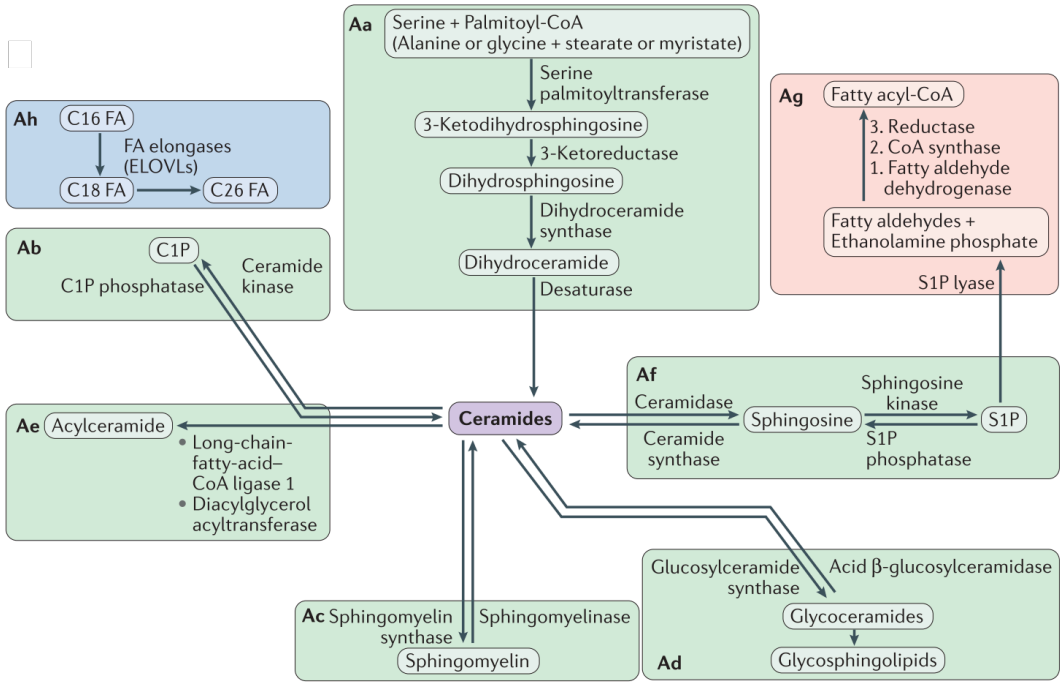

Figure 2.2 Pathways of Sphingolipid Metabolism
The *de novo* biosynthetic pathway of sphingolipid metabolism resulting in the formation of ceramide (Aa). Metabolism of ceramide to various sphingolipids (Ab-Ad). Synthesis of ceramide-1-phosphate (C1P, Ab). Synthesis of sphingomyelin (Ac). Synthesis of glycosphingolipids (Ad). Acylation of ceramides to form 1-O-acyl-ceramide (Ae). Sphingolipid catabolic pathways resulting in the formation of sphingosine-1-phosphate (S1P, Af). Exit from sphingolipid pathway by S1P lyase resulting in the formation of fatty-acyl-CoA (Ag). Fatty acid (FA) elongation by Elongation of very long chain fatty acid proteins (ELOVLs) forming very long chain fatty acids (for example C26 FA, Ah). Adapted and modified from[9].

Complex SLs are divided into three major groups, depending on the primary residue attached to their C1-hydroxy headgroup. Sphingomyelin synthases (SGMSs) attach a choline head group from PC to ceramide, forming the major cellular SL class sphingomyelin (Figure 2.2 Ac) which is essential for cellular viability[10,18]. Glycosphingolipids (GSLs) are not essential for cellular viability, but are owning multiple functions in mammalian development and tissue specific functions (Section 2.1.3.3)[4]. GlcCer is synthesised from ceramide and UDP-glucose by the enzyme glucosylceramide synthase (UGCG, Figure 2.2 Ad) and could be further glycosylated by the activity of glucosyltransferases resulting in

more than 300 species of GSLs[4]. Ceramide can be galactosylated to form GalCer by the enzyme galactosyltransferase (CGT). CGT is expressed only in a few tissues, among them the central nervous system, indicating particular functions of these lipid species[10]. Subsequent sulfation of GalCer by cerebroside sulfotransferase (CST) forms sulfogalactolipids whereas sialyation forms the GM4 ganglioside[4]. Ceramide may also be metabolised to acylceramide and stored in lipid droplets (Figure 2.2 Ae). Finally, the action of Elongation of very long chain fatty acid proteins (ELOVLs) provide substrates for the synthesis of VLCFA SL species (C24-C26; Figure 2.2 Ah) and other long chain fatty acid (LCFA) SL species[19].

2.1.3. Metabolism and Functions of Lipids in Myelin

During active myelination, the myelin-membrane surface area expands strongly[20]. An enormous amount of lipids is generated in a relatively short period of time[21]. Besides their synthesis, lipid and protein transport has to be regulated precisely and every step is pivotal for the assembly and maintenance of myelin[22]. This section describes the development of oligodendrocyte progenitor cells to myelinating oligodendrocytes, followed by the synthesis of lipids during active myelination. Finally roles of lipids in myelin will be outlined.

2.1.3.1. Development of Oligodendrocytes

In CNS, OLGs synthesize myelin, a specialised lipid-rich membrane. Myelin membrane arrangement along a neuron, including precisely localised gaps, allows action potentials to be propagated far more rapidly compared to an unmyelinated neuron[23]. Different developmental steps are occurring to become a myelinating OLG: First, oligodendroglial progenitor cells (OPCs) develop in the ventricular zones of the brain and migrate into the developing white matter in which they finally form an evenly spaced network of process-bearing cells[24]. Early OPCs are bipolar, migratory, proliferative cells which are distinguished by specific monoclonal antibodies[25]. The antibody A2B5 recognises specific surface gangliosides such as GD3, GT3 and O-acetylated GT3, which are downregulated as the OPCs develop into mature OLGs (Figure 2.3)[26]. These early progenitors develop into late progenitors, recognised by the antibody A2B5 as well as O4, a specific monoclonal

antibody against an sulphated glycolipid[25]. O4 recognises sulfatides in all developmental stages with varying fatty acid chain length compositions during differentiation[27]. Originally, it was thought that O4 recognises an unknown sulphated lipid other than sulfatide, termed POA[27]. Late progenitors mature into the transient "Pre-GalCer" stage in which the proliferation is strongly reduced and terminal differentiation begins. These cells are marked by immunoreactivity against the antibody R-mAb which recognises GalCer and sulfatide[28]. During terminal differentiation, OLGs finally develop complex branched processes and abundantly synthesise GalCer, which is recognised by the antibody O1, and sulfatide, recognised by the antibody O4[26].

Furthermore, in myelinating OLGs specific proteins are expressed in high quantities. These include myelin-specific proteins like myelin-associated glycoprotein (MAG), myelin basic protein (MBP) and proteolipid protein (PLP, section 2.1.3.3)[22]. Mature OLGs form "myelin-like" membranous sheets *in vitro* and axon-enwrapping myelin sheaths *in vivo*[26]. The process of myelin biosynthesis and wrapping is highly complex and described in the sections 2.1.3.2 and 2.1.3.3.

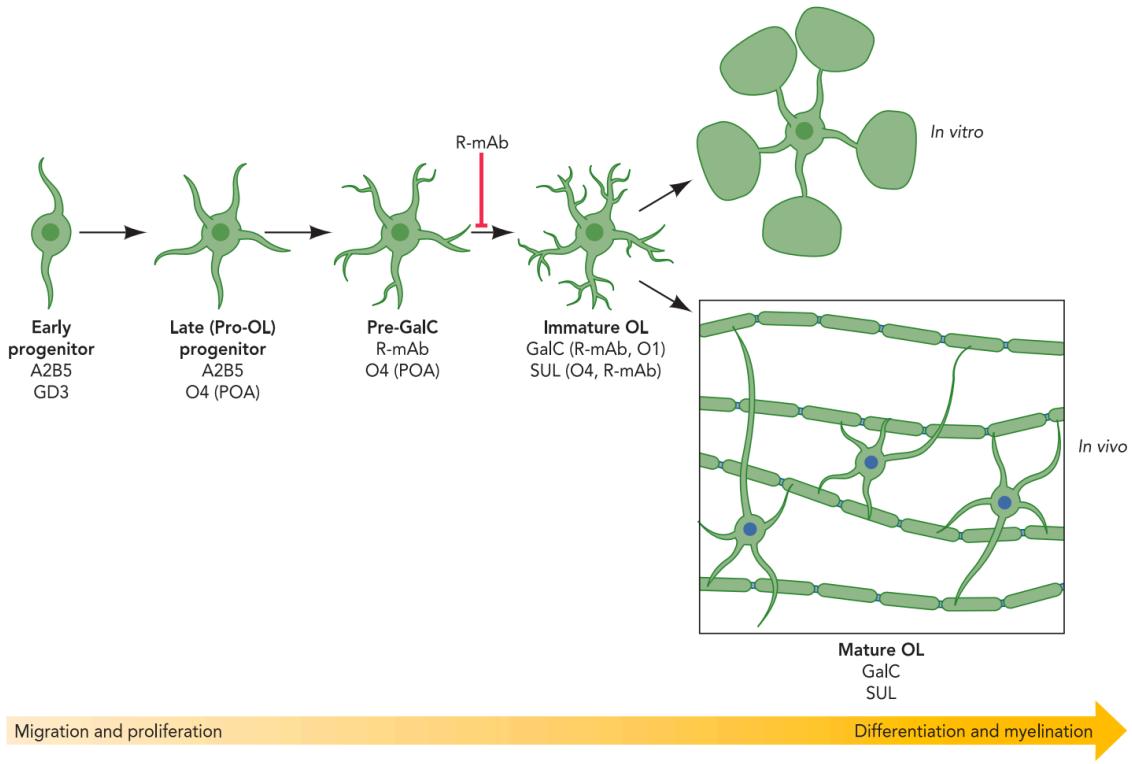

Figure 2.3 Schematic Illustration of Oligodendrocyte Differentiation
Each step of oligodendrocyte development is defined by the expression of different marker proteins and lipids. GalC, Galactoylceramide; OL, oligodendrocyte; POA, pro-oligodendroblast antigen; SUL, sulfatide; GD3 a ganglioside. A2B5, O4, O1, R-mAb, targeting different glycan structures. Adapted from[26].

2.1.3.2. Metabolism and Trafficking of Lipids in Myelinating Oligodendrocytes

During active myelination, OLGs generate an enormous amount of lipids in a relatively short time[21]. Remarkable 70-80% of myelin's dry weight consists of lipids, in particular cholesterol, GalCer, ethanolamine plasmalogen and sulfatide[21,29]. Myelin is extraordinary stable which is mostly based on the lipid composition with high levels of saturated, long chain fatty acids together with the enrichment of GSLs and cholesterol[24].

Oligodendroglial cholesterol synthesis appears to be coupled to the speed of myelination as the knockout of the first and rate-limiting step of cholesterol synthesis strongly delays myelination[30]. In the ER, the majority of cholesterol is synthesised *de novo* from ketone bodies instead of glucose which is used by most cell types[31]. Squalene synthase (SQS) catalyses the first step committed to the biosynthesis of sterols[30]. After a complex process of cholesterol synthesis, two different pathways are assumed by which cholesterol is transported from the ER to myelin. Either by vesicular transport along microtubules together with integral membrane proteins after passing the Golgi, or by a direct route from ER to the plasma membrane by lipid exchange and carrier molecules (lipid transfer proteins)[21,32]. Externally endocytosed cholesterol enters the late endosome/lysosome before reaching the ER via Niemann-pick type C1 (NPC1) and C2 (NPC2) protein-depended mechanisms.

GalCer and sulfatides with 24:0 and 24:1 FAs are among the most common myelin lipids[27,33] and even serve as measure of myelin biogenesis in brain (Section 2.1.3.1). Gangliosides and sulfatides are synthesised from GlcCer and GalCer, respectively (detailed GSL metabolism described in section 2.1.2). To obtain a majority of VLCFA GSLs, the CerS2 enzyme is strongly upregulated in myelinating OLGs[34]. Imaging mass-spectrometry identified shifting sulfatide species during the development of OLG (Figure 2.4)[27,35]. In early stages of OLG development C16:0 and hydroxylated C18-OH species predominate, whereas in later stages and in adult brain C24 species dominate[27]. Furthermore, the ratio of hydroxylated to non-hydroxylated sulfatide species increases with age[27,35]. About 50% of the GalCer and sulfatide species are hydroxylated in mature myelin, which also increases the packing density in myelin[36]. The synthesis of GSLs starts in the ER with the synthesis of ceramide (Section 2.1.2). CGT is also localised in the ER and

catalyses the formation of GalCer[37]. For the synthesis of sulfatide, GalCer is transported to the Golgi apparatus where CST is localised, catalysing the 3-O sulfation of the galactose residue[26]. Both lipids are likely transported by vesicular transport to the plasma membrane starting at the trans-Golgi network. GalCer may also employ a non-vesicular route by glycolipid transfer proteins directly from the ER to the plasma membrane[38,39].

However, even if similar trafficking pathways are taken, both GalCer and sulfatide do not colocalise within sheaths. They are found in distinct domains, most likely reflecting differences in sorting, trafficking and also function[22]. GalCer is localised to compact myelin, whereas sulfatide localises to the non-compact myelin regions (Section 2.1.3.3). Also in cultured OLGs, GalCer is found in sheets, whereas sulfatide localises to the cell body and primary and secondary processes[40]. Thus, myelinating OLGs are polarised cells with distinct membrane surfaces. It is unclear how cells segregate the lipid localisation, however it may be suggested that the majority of GalCer circumvents the Golgi and is indeed targeted directly to the myelin membrane[40].

Gangliosides are only present in small amounts in myelin membranes, however they represent a major fraction of the neuronal membrane[21].

Ethanolamine plasmalogens are also strongly enriched in myelin and levels correlate with the degree of myelination[41]. Differently to other GPLs, ethanolamine contains a vinyl ether linkage at the *sn-1* position and an ester linkage at the *sn-2* position with mostly saturated and monosaturated fatty acids. Generally, ethanolamine plasmalogens form compressed, thicker and rigid lipid bilayers[42], which enables a compact and stable structure in combination with the saturated fatty acids[41]. Plasmalogen synthesis starts in peroxisomes through the action of glyceronephosphate O-acyltransferase (GNPAT) and alkylglycerol phosphate synthase (AGPS) and is completed in the ER[43]. Also for plasmalogen lipids, the trafficking to the plasma membrane occurs via Golgi and endosomal compartments, or via non-vesicular pathways using lipid transporter proteins[41].

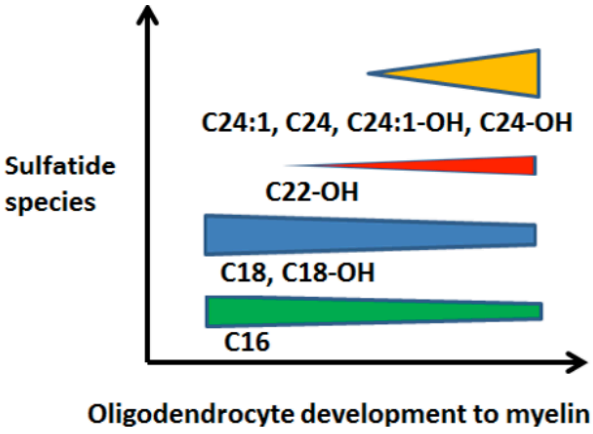

Figure 2.4 Sulfatide Species Changes During Oligodendrocyte Development
Lipid species were annotated according to their molecular composition as follows. Sum of carbon atoms in the FAs:sum of double bonds in the FAs-OH (hydroxylated). Adapted from[35]

As introduced in section 2.1.1, plasma membrane lipids are not diffusing freely in the lateral plane of the bilayer but are rather transiently confined to small 'nanodomains'[5]. Thus, domains of different composition and physical properties are coexisting in the lateral plane, being able to mediate platforms that regulate OLG behaviour and soring of different myelin proteins[26,29,44]. These domains are enriched in cholesterol, GPLs and phospholipids with saturated fatty acids, thereby creating a ordered ("liquid ordered", L_O) lipid environment compared to the more fluid ("liquid disordered", L_D) remainder[29].

Summarising, the myelin membrane lipid composition is special. Beside the functional roles in stability there are likely specific roles and functions beyond stability and insulation.

2.1.3.3. Functions of Myelin Lipids

The high lipid to protein ratio and the lipid composition of myelin are unique compared to other membranes[45]. The biosynthesis of these lipids is complex (Section 2.1.3.2) and deregulations are described for demyelinating diseases such as multiple sclerosis (MS), Charcot-Marie-Tooth (CMT) disease and Alzheimer[46–48], indicating important functional roles of lipids in myelin. The interaction between lipids and proteins is described to be important for the protein transport to, and the molecular organisation of proteins within the myelin sheath[22]. The mentioned structural properties of myelin lipids are important to impose stability for the long-term maintenance of myelin (Section 2.1.3.2)[21].

Myelin is a multi-layered structure which is built by wrapping the myelin sheath around the target axon. The outer leaflets of the myelin membrane thereby oppose each other which creates the intraperiod line, while the condensed cytoplasmic surface can be seen as major dense line by electron microscopy (EM, Figure 2.5)[45]. The 'nodes of Ranvier', are un-myelinated segments where sodium channels for saltatory conduction are localised[49]. The myelinated segment is divided into the internode area (compact myelin) in the middle of the sheath, and the paranode region (un-compact myelin) at the edges which are distinct in their molecular composition[20]. Especially GalCer together with PLP and MBP localise in compact myelin, whereas e.g. 155-kDa neurofascin (NF-155) and sulfatide localise in the paranodal region[22,50] (Figure 2.5, section 2.1.3.2).

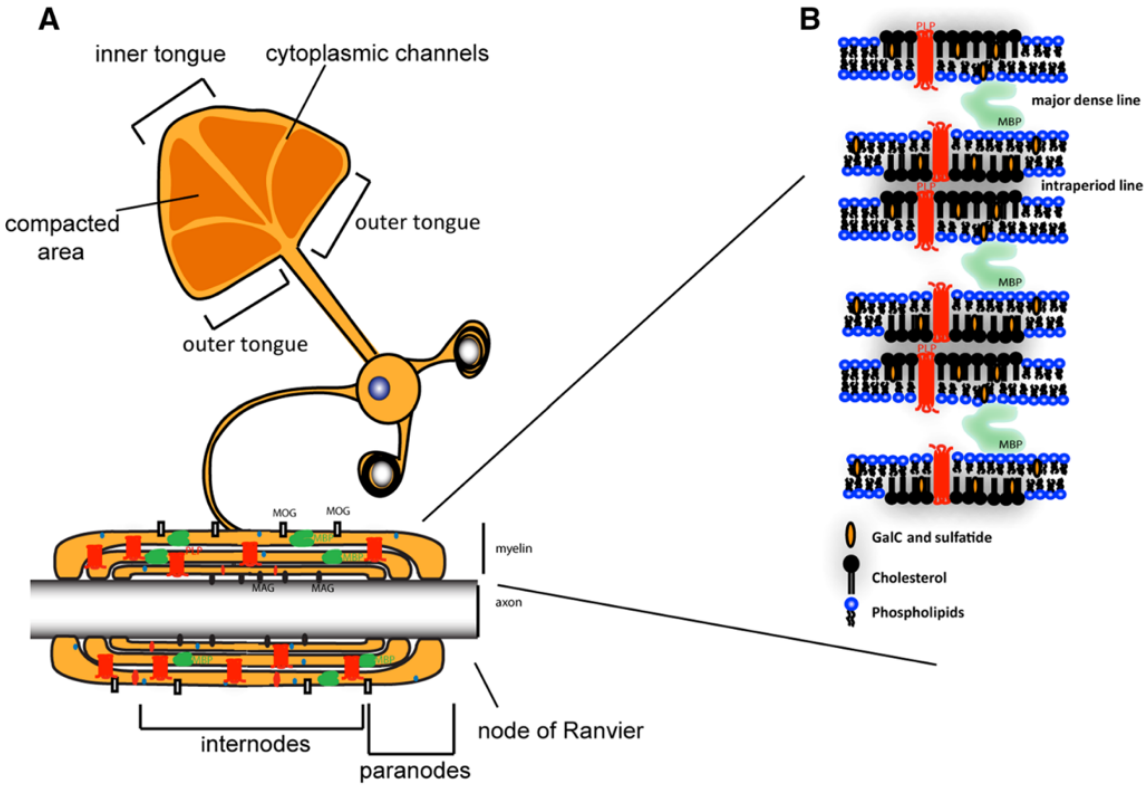

Figure 2.5 Schematic Illustration of the Myelin Structure
A. Schematic illustration of an unfolded myelin sheath and enwrapment of axons by myelin. PLP is shown in red, MBP is shown in green**. B. Myelin membrane organisation and localisation of major myelin lipids and proteins**. GalC and sulfatide of two opposing membranes are bringing myelin layers in close contact via hydrophobic interactions. MBP, myelin basic protein; MOG, myelin basic protein; MAG, myelin associated glycoprotein; PLP, proteolipid protein; GalC, Galactosyl-ceramide. Adapted and modified from[45].

Cholesterol is the only essential lipid for myelin membrane growth[30,51]. As mentioned in section 2.1.3.2, OLG specific knockout of the cholesterol synthesis by targeting the SQS enzyme strongly perturbs myelination and is only possible due to the uptake of cholesterol from exogenous sources[30]. Furthermore, SQS-knockout mice downregulated mRNA for major myelin proteins indicating that the precise stoichiometry of lipids and proteins is essential for myelin biogenesis[30]. After uptake from exogenous sources, NPC1 is required for cholesterol mobilisation. Mouse models of Niemann-Pick type C disease (owing a gene mutation in NPC1) show a drastic reduction in the number of myelinated axons[52]. A conditional OLG-specific knockout of NPC1 as well as a neuron-specific knockout show defects in myelin formation with an arrest in OLG maturation, indicating that cholesterol from different sources is required for proper myelination[53]. Cholesterol might coordinate myelin assembly by different mechanisms. Firstly, it might be coordinated by regulating the global metabolism of myelinating OLGs by targeting signalling pathways that control energy supply or protein translation. Secondly, it may be coordinated by direct regulation of transcription factors or by cholesterol mediated trafficking of major myelin proteins to the growing myelin membrane[21].

VLCFA GalCer and sulfatide are the most typical myelin lipids[26]. Mutations in CerS2 result in greatly reduced levels of VLCFA SLs and a massive decrease in GalCer and sulfatides in myelin[54]. Mutant mice show focal detachments of myelin lamellae which is progressing with age[54]. This probably indicates changes in the expression or localisation of adhesion molecules between or within lamellae[54]. The level of MBP is reduced by 20% in these mutant mice[54] which is described to be positioned by the lipid environment in myelin membranes[55]. Patients with mutations in ELOVL1 that reduce its enzymatic activity, show reduced levels of VLCFA SLs and hypomyelinations[56]. ELOVL1 knockout mice die shortly after birth[57], thus no conclusions on myelin phenotypes can be drawn.

A mutant mouse lacking CGT is still be able to produce myelin, however it is exhibiting myelin abnormalities. These mutant mice show reduced myelin thickness, redundant myelin outfoldings and vacuole formation, paranodal abnormalities and die early[58]. At paranodal junctions, axoglial contacts are severely detaching from the axons[21]. CST knockout mice also show this paranodal phenotype[59]. Thus, sulfatides might play a role in the trafficking or the stabilisation

of NF-155 at paranodes. NF-155 is in close contact with axonal Caspr/contactin and its localisation in lipid nanodomains might be important to stabilize these protein complexes[60]. Regarding structural properties, GalCer forms tightly packed bilayers via intermolecular hydrogen bonds and *trans* interactions between GalCer and sulfatide which play a role in the attachment of the extracellular faces of the myelin membrane[61]. Together with the highly hydrophobic PLP, intermolecular hydrophobic forces lead to membrane "zippering", bringing myelin membranes in close contact (Figure 2.5 B). Furthermore, GSLs are enriched in lipid nanodomains which are also in myelin suggested to promote cellular adhesion by facilitating the localisation of membrane and transmembrane proteins[29]. However, GalCer is not essential for myelin formation and their absence can be compensated by upregulation of other GSLs like GlcCer[62]. CGT knockout mice also partially compensate the lack of GSLs by increasing the synthesis of hydroxylated SM[21]. Hydroxylation is catalysed by the fatty acid 2-hydroxylase (FA2H). The increased stability via hydrogen bonding between lipids appears to be crucial for myelin maintenance in aged brain, as myelin is degenerated in FA2H knockout mice which are otherwise healthy[33].

Gangliosides are present on neuronal membranes in high quantities[21]. The sialoglycan part of gangliosides extends out of the axonal membrane and thereby participates in intermolecular axon to glia interactions[63]. MAG is localized at the adaxonal myelin membrane where myelin interacts with the axon via MAG and two major ganglioside species on the neuronal membrane[63].

As GSLs, plasmalogens structurally contribute to the packing density and stability of the membrane[21]. Loss of enzymes of the biosynthesis of plasmalogens leads to relatively normal myelin but in reduced amounts[64]. More severe phenotypes are described for Schwann cells in PNS[21]. Moreover, it appears that plasmalogens might protect unsaturated membrane lipids containing (poly)unsaturated fatty acids against oxidation[65] and it is assumed that plasmalogens are able to quench oxidative reactions as long as the scavenging products are not toxic to the cell[66].

In summary, the biosynthesis and cellular trafficking of myelin lipids appear to be essential for the assembly and especially maintenance of myelin in the nervous system. Nevertheless, the knowledge about myelin membrane dynamics, such as membrane fluidity, movement of proteins and lipids in the membrane and the specificity and role of distinct protein-lipid interactions, is limited.

2.1.4. Interactions of Lipids with Transmembrane Proteins

Little is known about the functional roles of lipids in cells. The tremendous complexity of lipids is not required for their roles in physical properties on membranes[3] and more and more distinct roles and functions of lipids are identified[67–72]. However, how lipids modulate protein functions and structure is still relatively poorly understood and the molecular biological function of only a few lipids are known so far[2,73].

Membrane proteins interact with lipids in different ways depending on the relative residence time of the particular lipid at the protein-lipid interface[74]. If a lipid has fast exchange rates with the protein, it is considered a “bulk” lipid (Figure 2.6 A)[68]. A stronger interaction, via the hydrophobic matching of hydrocarbon chains of the lipid with the hydrophobic transmembrane domain (TMD) or via polar head groups of lipids with charged amino acids of the membrane protein leads to the formation of an annulus of lipids (“annular” lipids, Figure 2.6 B)[68]. Lipids with very low exchanges rates are named ”non-annular” lipids which often reside within large membrane protein complexes (Figure 2.6 C)[68]. Between proteins, strong electrostatic forces lead to tight interactions[75]. However, the interaction of annular lipids and even non-annular lipids with proteins is difficult to assess due to the comparably quite fast exchange rates of lipids with the protein[70].

Annular lipids accumulate around the membrane protein due to their increased residence time compared to bulk lipids[68]. This shell is not necessarily homogenous, because individual lipids of the shell might vary in their residence time[76]. Different interactions and functions of annular lipids on proteins are described[68]. Most strikingly is the influence of annular lipids on the modulation of protein function via mechanical forces[77]. Mechanosensitive channels are regulated by alterations in their local lipid environment which exerts a lateral pressure leading to a conformation shift of the channel[77]. Prokaryotic and eukaryotic mechanosensitive channels are in closed state when reconstituted in PC bilayers[78]. As soon as “cone-shaped” lysophospholipids are added to the lipid mixture, the channels are shifted to an open state[78]. Bacteriorhodopsin is a light-driven ion pump which is crystallised including its 18 tightly bound specific set of annular lipids[79]. Specific lipid classes like phosphatidyl glycerophosphate methyl ester, glycolipid sulfates, phosphatidyl glycerol, phosphatidyl glycerosulfates and squalene are known to mediate the contact between the trimeric complex in the bilayer plane[79].

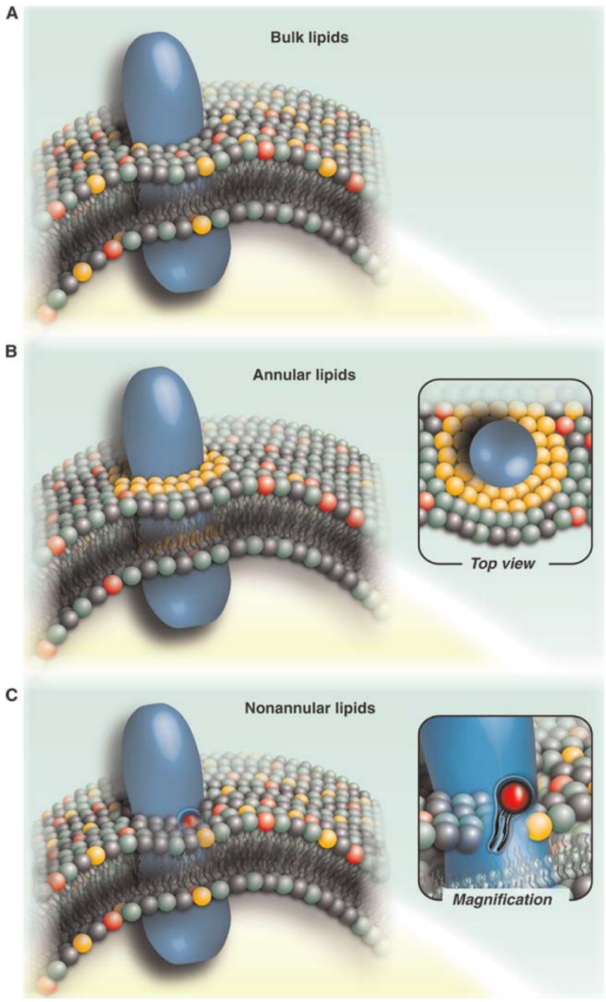

Figure 2.6 Schematic Representation of Intramembrane Protein-Lipid Interactions
A. Localisation of bulk lipids around a transmembrane protein**. B.** An annular lipid shell formed via transient interactions with the membrane protein**. C.** Non-annular lipid binding of a specific lipid with a membrane protein within the protein or protein complex. Adapted from[68].

Some non-annular lipid-protein interactions are identified by X-ray-crystallography[68]. The vacuolar-type (V-type) sodium ATPase of *Enterococcus hirae* contains lipids that reside within the large oligomeric membrane protein and thereby also act as "connecting lipids" that strengthen the contacts of the subunit[80]. Non-annular cholesterol is described to bind tightly to different proteins via a specific cholesterol-binding motif[81]. The β2-adrenergic receptor belongs to the G-protein-coupled receptors (GPCR)[82]. In a shallow groove of this receptor two bound cholesterol molecules are located which interact with four out of seven transmembrane helices via a relaxed version of the cholesterol motif (cholesterol-consensus motif, CCM)[82]. The molecular function of cholesterol as non-annular lipid in GPCRs is controversial[68]. It might either act via conformational change upon

binding to the receptor or indirectly by an alteration of membrane biophysical properties[68]. Thereby, the receptors are possibly targeted to distinct membrane domains or modulate the affinity for their ligands[83,84].

The ganglioside GM3 negatively regulates the epidermal growth factor (EGF) receptor (EGFR)[71]. EGF-stimulated phosphorylation of EGFR is significantly reduced upon addition of GM3[85]. Ligand binding is not affected, however in presence of GM3 the dimerization and thereby autophosphorylation of EGFR is strongly diminished[71]. The neuraminic acid of the GM3 is essential for this inhibition which indicates an interaction of this moiety with EGFR[71].

In summary, these and other examples emphasise the importance of non-annular lipids as well as annular lipids on protein functions by modulating their architecture, localisation or even their enzymatic functions. Nevertheless it is still challenging to analyse TMD-lipid complexes due to technical difficulties derived from the hydrophobic nature of TMD-containing proteins. It is still a matter of debate whether protein TMDs exist that are simply dissolved in the hydrophobic phase of the membrane or if there is a specificity in each TMD for one or several lipid species of the complex membrane[68].

2.1.5. Chain Length-Specific Protein-Lipid Interactions

Even though the knowledge of protein-lipid interactions is still limited, an increasing number of interactions are described (Section 2.1.4). Protein-lipid interactions were often not reported to depend on specific FA chain length of the lipids, however the FA chain length specificity was not addressed in detail in most of the cases. Lipids contain FAs of varying length, number of double bonds and saturation. FAs with C22-C24 are classified as VLCFAs, whereas lipids with ≥C26 are often termed ultra long chain FAs (ULCFAs). Long chain FAs (LCFAs) have chain lengths of C11-C20 of which C16 and C18 are the most abundant FA species in mammalian cells[15]. FAs without double bonds are saturated FAs. FAs containing one double bond are called monounsaturated fatty acids and FAs with more double bonds are called polyunsaturated FAs (PUFAs)[15]. The first and rate-liming step in the elongation of FAs is catalysed by ELOVLs. Seven isozymes (ELOVL1-7) are described in mammals, each owing a substrate specificity towards the FA length and degree of saturation[15]. Mutations or knockout of *ELVOL* genes result in

different diseases e.g. ichthyosis, insulin resistance, nervous system abnormalities like hypomyelination and lethal dermal permeability barrier defects[15,56,86]. The precise molecular mechanism of diseases and phenotypes in patient or mice with altered lipid composition is still subject of ongoing research and so far incompletely understood[86].

In SLs, most acyl moieties are saturated and monounsaturated VLCFAs[87]. Their synthesis is outlined in section 2.1.2. In most tissues, SLs with C16:0, C24:0 and C24:1 dominate, but the proportion of each FA varies considerably among tissues[88]. This is due to a varying expression of their catalysing enzymes in different tissues (Figure 2.7), such as CerS2 which is strongly expressed in liver, kidney, and actively myelinating OLGs (Section 2.1.2 and 2.1.3.2)[12,34]. The SL profile of tissues reflect the differential expression of CerSs[15]. E.g. C24 SLs constitute about 50% in liver and less than 20% in testis[15], indicating roles of SLs in tissue-specific processes. Indeed, mice lacking CerS2 show besides defects in myelin sheath stability (Section 2.1.3.3) also hepatocellular carcinomas[54,89]. Chain-length specific differences of ceramides and their pathological impact in Alzheimer's disease, inflammation, cystic fibrosis, diabetes, irritable bowel syndrome, multiple sclerosis, autophagy, apoptosis and cancer are already identified[11,46,90,91]. However, there are only a few firmly established examples of the interaction between endogenous ceramide and potential target proteins[91]. Furthermore, C24 SLs have different biophysical properties compared to C16 SLs such as effects on membrane fluidity, lipid nanodomain formation, and signalling across the membrane[92–95].

In neutrophils, C24 lactosylceramide (LacCer) is associated with the Src family kinase LYN in nanodomains which is necessary for its function[96]. The interdigitation of VLC LacCer fatty acyl side chains is proposed to allow direct hydrophobic interactions between the acyl chains of Lyn and those of LacCer[96]. In yeast, VLCFA SLs consist mainly of saturated C26 fatty acids which are essential for yeast viability[15]. Mutant yeast with limited VLCFA synthesis exhibit defects in vesicular transport mainly in the late endosome/multivesicular body[97], as well as vacuolar abnormalities, as recently suggested[98]. Vacuoles from mutant yeast cells displayed reduced levels of *in vitro* fusion which is possibly due to a block of tethering and docking based on mislocalisations of fusion markers. This is possibly originated in

affected lipid nanodomain localisation of fusion markers[98]. So far no precise protein-lipid interaction is described for this phenotype.

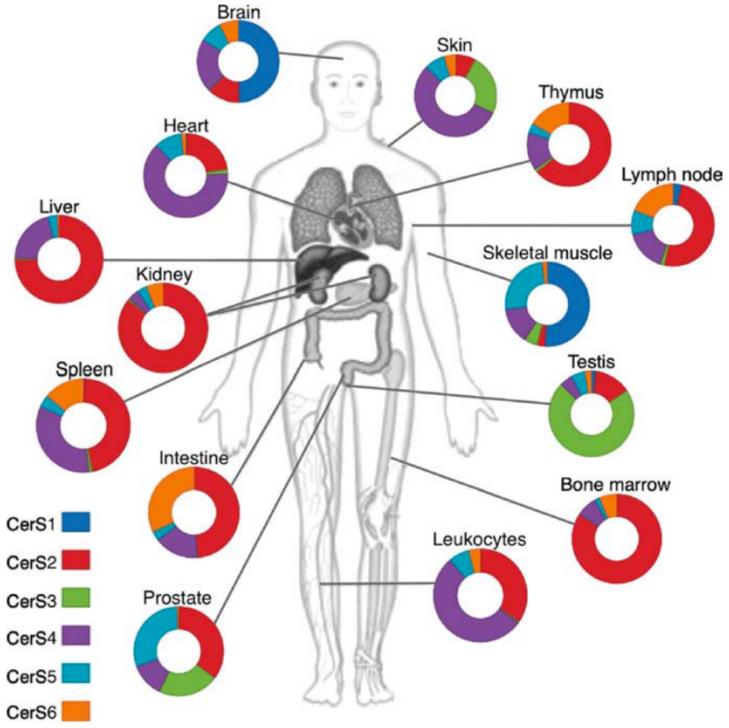

Figure 2.7 Ceramide Synthase mRNA Expression Profile in Human Tissues
The relative abundance of Ceramide Synthases (CerS) in each organ determines the amount of specific ceramide species that are produced. The pie chart for each organ represent the distribution of CerS, which are color-coded as in the Legend. Adapted from[13]

Mice lacking CerS6 exhibit diminished amounts of C16 Cer and are protected from high-fat-diet-induced obesity and glucose intolerance[99]. The mRNA expression of *CERS6* positively correlates with BMI and body fat content[99]. The interaction of the mitochondrial fission factor (Mff) with CerS6-dervied C16:0 SLs suggests a regulation of mitochondrial dynamics by the interaction[100]. CerS5 is redundant to CerS6 in the catalysis of C16 SLs[88], however a distinct intracellular pool of ceramide is regulated[100]. CerS6 is described to localise to mitochondria and mitochondria-associated membranes (MAM) and CerS6 deficiency leads to reduced C16 SLs in MAM and mitochondria fractions which was unaffected in CerS5 knockout mice[100]. Thus, different roles of SLs with varying chain-lengths are also present on a cellular scale depending on the localisation of metabolising enzymes[100–103].

On a cellular level, lipidomic analysis of Golgi-derived COPI vesicles revealed a partial segregation of cholesterol and SM 18:0 from the vesicle fraction[104]. SM18:0 interacts with p24, an abundant integral membrane protein of COPI vesicles. A point mutation within the identified binding site abolishes the interaction and is defective in normal COPI-mediated trafficking[72]. Several more intracellular target proteins of LCFA SLs are described. The direct interaction of C16:0 ceramide with Protein kinase ζ (PKCζ) and Protein phosphatase 2A (PP2A) activates their enzymatic activity, whereas the Inhibitor 2 of PP2A (IPP2A) preferentially interacts with C18 ceramide[11].

However to date, direct intracellular targets of especially VLCFA SLs are largely unknown[91].

2.1.6. Chemical Biology Tools to Study Protein-Lipid Interactions

Different methods have been developed to investigate short-lived protein-lipid interactions[73,105]. Photoactivatable groups are incorporated in lipids to allow for covalent bond formation between lipids and protein upon UV irradiation[105]. Diazirines are the smallest synthesised photoactivatable group to date[106]. Their small size is advantageous since bulky functionalised groups might interfere the interactions with proteins and change the localisation of the lipid of interest within the membrane[107]. Upon stimulation with UV light, a highly-reactive and short-lived carbene is formed that covalently links to carbo-hydrogen (CH), heteroatom-hydrogen (NH_2, SH or OH) or to a double bond. However, also a linear diazo isomer is generated that has a longer life-time and may react with nucleophiles as aspartyl- and glutamyl residues upon protonation[108,109]. Nevertheless, it remains the smallest known functional photoactivatable crosslinker. In combination with radiolabelling, the detection of protein-lipid crosslink-products is possible. [^{3}H]-photo-sphingosine was employed to probe for SL-protein interactions[67,105]. This validated the discovery of the first specific interaction of a protein with a single molecular lipid species, namely p24 and SM18:0[72] (Section 2.1.5). The development of click chemistry allowed the design of lipids that carry a small chemical group capable to couple a fluorophore for detection or an affinity tag for purification[110]. The application of a clickable lipid enables the detection of covalent protein lipidations (Figure 2.8 A) whereas the combination of a photoactivatable and a clickable functional group in “bifunctional lipids” is suitable for the

identification of short-lived protein-lipid interactions (Figure 2.8 B)[105]. A small alkyne group serves as clickable moiety at the terminus of the hydrocarbon chain of various lipids making it easily accessible for subsequent reactions[111]. Azide-containing reporters are coupled to the alkyne group via copper (I)-catalysed azide alkyne cycloaddition (CuAAC)[112].

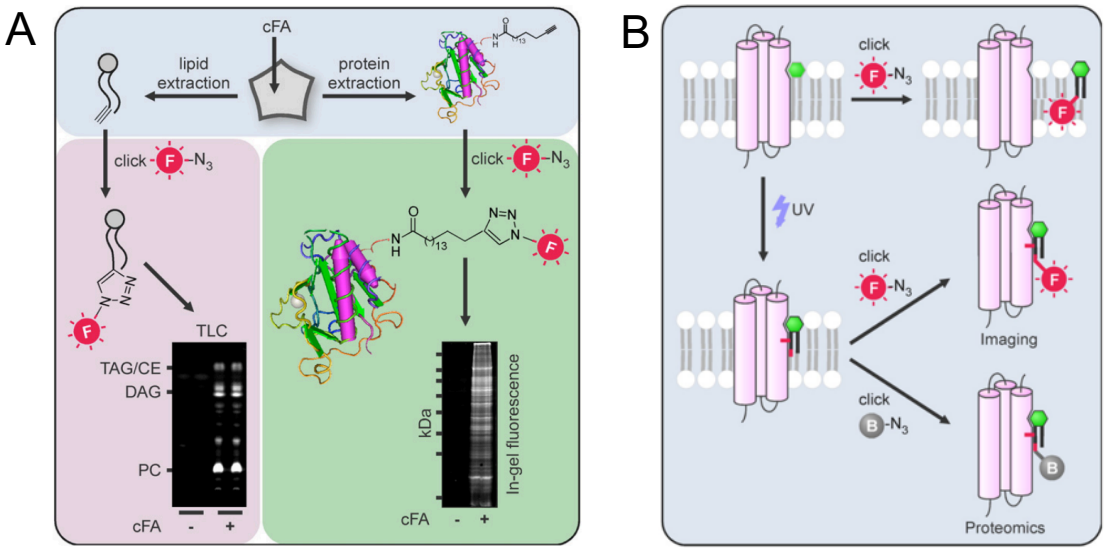

Figure 2.8 Applications of Clickable and Photo-Crosslinkable Lipid Analogues
A. Applications of clickable lipids. Clickable (c) lipids as clickable fatty acids (cFA) are fed to cells where they are further metabolised. The identification of lipid metabolism is achieved via click-reaction to a fluorophore (F) and subsequent thin-layer chromatography (TLC) analysis (left panel). The identification of lapidated proteins after click reaction to a fluorophore on a SDS-PAGE gel is shown on the right panel. **B. Applications of bifunctional lipids.** The photo-crosslinkable group leads to the formation of covalent protein-lipid complexes which can be localised within cells via the attachment of a fluorophore and confocal microscopy whereas the addition of an affinity tag allows for the identification of protein-lipid complexes on a proteome-wide scale. Adapted and modified from[105].

This chemical toolbox led to the identification of various lipidations and protein-lipid interactions[105]. Among those, a bifunctional sphingosine (photoactivatable and clickable sphingosine, pacSph) was developed to identify novel protein-SL interactions within membranes[113]. Cells readily take up the chemically modified SL and their metabolic fate and subcellular flux can be monitored by using fluorogenic coumarin-azide on thin-layer chromatography[114] and Alexa-azide dyes in confocal microscopy[113], respectively (Figure 2.8 B). Cross-linking by UV-irradiation allows the formation of a covalent linkage to adjacent proteins and by subsequent click-reaction to an affinity tag, 180 potential SL interacting proteins were identified[113]. To prevent the degradation of the bifunctional groups into the glycerolipid pathway

by the action of SGPL1 (Section 2.1.2), a knockout of this enzyme is required[115]. PacSph and novel chemically modified lipids have a great potential to discover novel roles of lipids.

Lipid diversity is partly based on chemical diversity of lipids themselves, however, lipids are not evenly distributed within the plane of the bilayer (Section 2.1.1). Cholesterol and SLs are able to self-associate into nanodomains in model membranes and those lipids are involved in the formation of highly dynamic nanoscale heterogeneities in the plasma membranes (Section 2.1.1)[7]. Lipid nanodomains are described to be cholesterol-depended except in some cases where an underlying actin cytoskeleton is required[116–118]. The assembly of lipid nanodomains is still controversially discussed due to the lack of knowledge about the physiochemical principles responsible for the compartmentalisation and the molecular mechanisms by which they are functionalised[119]. An increasing number of methods is available to manipulate the membrane cholesterol content, especially to study roles of cholesterol-enriched nanodomains[8]. Most commonly, cells are incubated with cyclodextrins which are cyclic oligosaccharides that exhibit a hydrophobic cavity which can extract cholesterol from cell membranes[8]. Heptameric cyclodextrins (β-cyclodextrins) have the highest affinity for inclusion of cholesterol[8]. The attachment of a methyl group strongly increases their water solubility[8]. Methyl-β-cyclodextrin (MβCD) are most widely used to deplete cells of cholesterol[8]. Multiple studies showed that cholesterol depletion results in the partitioning of proteins from L_O domains into L_D domains[120–123]. However, this does not imply that cholesterol is exclusively extracted from lipid nanodomains. Indeed, many studies show that cholesterol is depleted from different lipid domains as well as from different organelles[8]. Nevertheless, MβCD can be employed to dissociate lipid nanodomains.

2.2. Biological Functions of Dystroglycan

The identification of proteins interacting with VLCFA SLs revealed a possible interaction of these lipid species with dystroglycan (Section 2.3)[124]. Dystroglycan is a ubiquitously expressed heterodimeric adhesion receptor. It consists of two non-covalently interacting glycoproteins (αDG and βDG) that are post-translationally

cleaved from a single gene (*DAG1*) by an unknown enzyme in the ER[125]. The β-dystroglycan (βDG) subunit shows three N-linked glycosylation sites and is a type I transmembrane protein[126]. It binds to the carboxy-terminal domain of the extracellular peripheral membrane subunit α-dystroglycan (αDG) which also shows extensive N- and O-linked modifications[126]. The glycosylations are essential for the interaction with extracellular matrix (ECM) proteins (Figure 2.9)[126]. The central mucin-like region of αDG is important for the interaction to laminin G (LG) module containing extracellular matrix proteins including agrin, perlecan and laminin itself[126]. The intracellular carboxy-terminus of βDGs binds directly or indirectly to one of a number of actin binding proteins[126]. These proteins include most notably dystrophin which ensures the connection to the F-actin cytoskeleton[125]. The dystrophin-containing complex (DGC) is the core functional unit of the dystrophin-glycoprotein complex which physically links the ECM with cytoskeletal elements. Thereby it provides the major part of sarcolemma and fibre stability in skeletal muscle[127]. This complex further has an important role in mechanical stability of multiple mammalian tissues including neuromuscular junctions, neurons and myelinating Schwann cells[128]. Mutations in dystrophin resulting in a complete absence of the protein lead to the fatal X-linked condition called Duchenne muscular dystrophy (DMD)[126]. DMD suffering patients show sarcolemmal damage and necrosis[126] as well as cognitive impairments[129]. DMD mouse models (*mdx* mouse) display a delayed myelination during postnatal brain development[130]. Later studies discovered roles of dystroglycan in OLG myelination[130]. The loss of dystroglycan's ligand laminin also leads to myelination deficits or delays[131–133]. The selective loss of dystroglyan in OLGs reduces their ability to differentiate[134–136] and delays myelination in brain[137]. In glia and neurons, a DGC-like complex anchors membrane-associated proteins such as the water-channel aquaporin-4 to specialized sites since loss of dystrophin leads to their mislocalisation[138]. A loss of the Schwann cell sarcoglycan complex belonging to the DCG complex (Figure 2.9), leads to an altered myelin sheath and disorganised Schmidt-Lanterman incisures which is indicative for myelin instability[139]. The severity increases with age suggesting an important role of sarcoglyans in the stability of peripheral nerve myelin[139]. In OPCs, the cleavage of dystroglycan by metalloproteinases releases dystroglycan from its interaction to laminin-211, thereby leading to OLG cell proliferation[140].

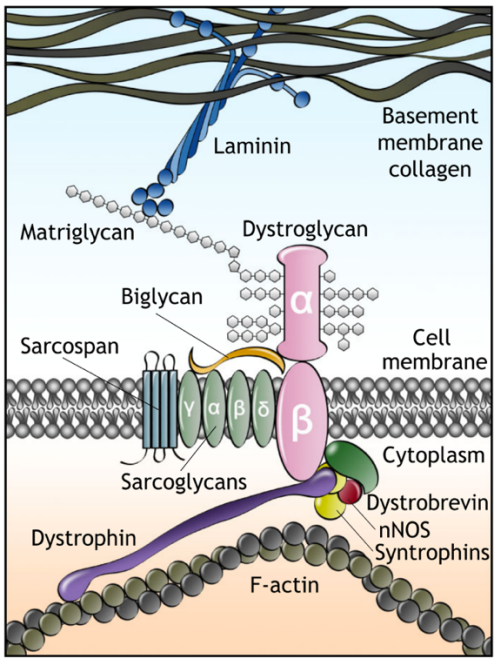

Figure 2.9 Schematic of Dystroglycan Protein Interactions Based on Biochemical and Functional Evidences
Matriglycan chains on the central mucin domain of α-Dystroglycan bind directly to laminin in the overlying basement membrane, while β-Dystroglycan is linked to the intracellular actin cytoskeleton through dystrophin. Adapted and modified from[141].

Mutations in glycosyltransferase genes that are responsible for the post-translational modifications of αDG lead to a disability of binding to the ECM. This results in severe diseases affecting muscles and brain such as in Fukuyama and congenital muscular dystrophy 1D, muscle eye brain disease or the Walker Warburg syndrome[142]. This again points to possible roles of dystroglycan in the neuronal system including functions in neuronal cell migration and patterning as well as neuronal cell adhesion, brain architecture and signalling[126]. Likely, this is partly due to the disrupted basement membrane in both muscle and brain[141]. The formation of the basement membrane begins with soluble extracellular laminin which binds to GalCer of the cell membrane[143]. As high concentrations of laminin are present, it polymerises to form a network at the cell surface which leads to the recruitment of basement proteins such as αDG to strengthen the nascent matrix[141]. Thus, αDG is not required for initial basement membrane formation, but likely participates in its maintenance[141].

Further clinical conditions, experimental and model systems, revealed functions of dystroglycan in neuronal migration, the blood brain barrier, retinal layering, Schwann cell wrapping and in the architecture of the nodes of Ranvier[144,145].

A number of studies found Y892 (in humans) of dystroglycan as a target for phosphorylation by Src and other Src family kinases that regulate the interaction between βDGs and cellular binding partners like the mentioned dystrophin[146–148]. Besides dystroglycan, also integrins are known laminin-receptors[126]. Binding of ECM proteins to integrins leads to allosteric changes across the plasma membrane[149]. This results in binding of integrins to signalling adapter proteins leading to tyrosine phosphorylation and the establishment of a multiprotein signalling complex (outside-in signalling)[150]. However, differently to integrins, dystroglycan has no variety in the combination of heterodimers as there is only one ubiquitously expressed α-/βDG heterodimer[126]. Nevertheless, the α-/βDG heterodimer is still capable to mediate multiple functions[126]. The interaction with laminins results in the formation of pY892 which is located in the cytoplasmic tail of βDG[146]. Whereas the phosphorylation results in a disruption of the C-terminal WW domain and thus the interaction of dystrophin to this domain is disabled[126], binding of Caveolin-3 (Cav3) the same site appeared insensitive to this phosphorylation[148]. Biochemically, the binding site of plectin overlaps with the one of dystrophin[151]. In the absence of dystrophin in *mdx* mice, the organisation of plectin and dystroglycan in the sarcolemma is altered and thereby being partially compensatory and protective[151]. Also, the signalling adapter Grb2 competes with the interaction to dystrophin as it binds to a SH3 domain which overlaps with the WW domain binding motif in dystroglycan. In OLGs, the interaction between dystroglycan, the adapter Grb2 and the insulin receptor subtrate-1 (IRS-1) is associated in a protein complex which comprise a positive regulatory effect of laminin on OLG differentiation via the insulin-like growth factor-1 (IGF-1)[136].

Dystroglycan appears to be localised in adhesion structures and plays a role in regulating the type and abundance of such structures within a cell[126]. Overexpressing dystroglycan increases the abundance of focal complexes while its knockdown causes the reverse effect[152]. The underlying molecular mechanism of action is not known, however vinexin, which is an interaction partner of vinculin known to reside in focal adhesions, may be recruited [152]. The binding occurs via a SH3 domain of vinexin and the proline rich C-terminal region of βDG[152]. Knockdown of dystroglycan in myoblasts results in a strongly diminished cell spreading on E3 laminin which cannot be rescued with the overexpressing of a construct mutated in the vinexin-binding site of dysroglycan[152]. This interaction was

also prevented by pY892[152]. Thus, vinexin competes with the dystrophin-homolog utrophin for the non-phosphorylated binding site[147] which might be partly regulated by expression of either proteins. Analyses of the required domain that drives filopodia formation reveal that the C-terminal cytoplasmic domain of βDG is necessary and sufficient for filopodia formation[126]. The cytoplasmic domain of βDG could be targeted to the plasma membrane by either secreted alkaline phosphatase-tags or by myristoylation sequences resulting in the location to the inner membrane leaflet[153,154].

Upon tyrosine phosphorylation, βDG undergoes a profound change in its subcellular localisation[146]. The phosphorylation occurs at focal adhesion sites which with leads to its internalisation revealing that dystroglycan acts as a signal-transducing receptor as it is phosphorylated upon interaction with ECM proteins[146]. Multiple studies show a lipid nanodomain/caveolae-localisation of βDG[155]. Also pY892 βDG is localised within nanodomains suggesting that the tyrosine phosphorylation by Src tyrosine kinases takes places within these domains and does not affect the localisation of dystroglycan[146]. The pool of pY892 βDG in internal membranous vesicles also contains the internalized lipid nanodomain/caveolae-like domains[146].

It is clear that dystroglycan forms a range of multiprotein complexes within the cell[126]. However, how different roles of dystroglycan are spatially and temporally regulated remains to be elucidated. The phosphorylation is one mechanism to regulate the binding of different partners to control its function. The identification of other interactions and distinct dystroglycan complexes in other systems is likely. Especially in OLGs, the molecular mechanism that regulates myelination, filopodia formation and long-term stability is not known so far.

2.3. Uncovering Proteins Interacting with Very Long Chain Fatty Acid Containing-Sphingolipid Species

As introduced in section 2.1.3.3 and 2.1.4, various clinical phenotypes and mouse models with an aberrant lipid composition are described. Especially FA-chain length specific-phenotypes are incompletely understood so far and direct intracellular targets of VLCFA SLs are largely unknown[91]. Therefore, we previously

established a proteomic approach to identify direct interaction partners of VLCFA SLs in a cellular system (Figure 2.10 A)[124]. The difficulty of identifying short-lived protein-lipid interactions was circumvented by the utilisation of pacSph (Section 2.1.6)[113]. However, as pacSph is incorporated in all cellular SL species, including LCFA SLs and VLCFA SLs, another mutation was introduced. HeLa cells necessarily depleted in SGPL1[115] and in addition CerS2 was generated by CRISPR-Cas9 mediated knockout. This prevents the incorporation of the bifunctional sphingosine into VLCFA SLs (Figure 2.10 B). Also endogenous VLCFA SLs are strongly diminished in this cell line due to the lack of CerS2 function, responsible for their synthesis[124]. After labelling the cells with pacSph, the chemically modified lipid was taken up and metabolised to different SL classes such as ceramide, HexCer and SM (Figure 2.10 B). To monitor the incorporation, the lipids were extracted, clicked to a fluorophore and separated on a silica plate. This readily visualised the depletion of VLCFA SLs in CerS2 knockout cells. The proteomic approach compared two conditions by employing stable-isotope labelling in cell culture (SILAC)[156]. The parental HeLa *SGPL1*$^{-/-}$ cells (cultured in "light" media) and HeLa *SGPL1*$^{-/-}$ *CERS2*$^{-/-}$ (cultured in "heavy" media) were labelled with the bifunctional sphingosine and proteins localising with modified lipids in each cell line were covalently crosslinked upon UV-irradiation (Figure 2.10 A). Cells lacking VLCFA SLs would not cross-link to proteins that are usually interacting/co-localising in the original condition. To enrich protein-lipid complexes, the cells were lysed and an affinity tag was clicked to the alkyne-moiety of the bifunctional lipid (described in section 2.1.6). After enrichment on beads, the protein-lipid complexes were eluted and subjected to mass spectrometric analysis. This led to the identification of 53 proteins that are potentially interacting with VLCFA SLs (Figure 2.10, Table 7.1)[124].

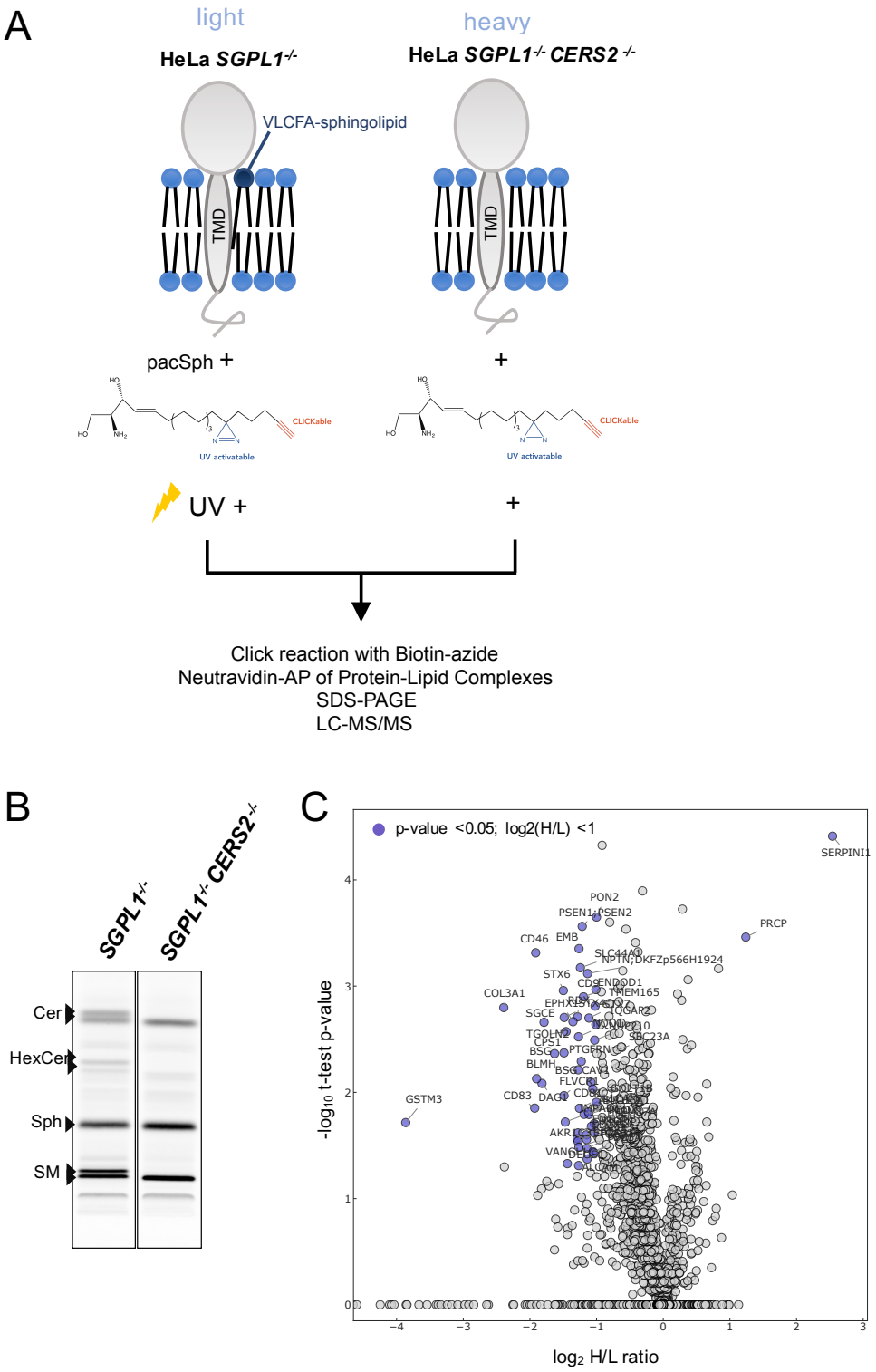

Figure 2.10 Proteomic Approach Identifying Proteins Interacting with Very Long Chain Fatty Acid Sphingolipid Species

A. Workflow of the proteomic approach that led to the identification of specific protein-sphingolipid interactions. HeLa *SGPL1*$^{-/-}$ and HeLa *SGPL1*$^{-/-}$ *CERS2*$^{-/-}$ cells were cultured in light and heavy SILAC media, respectively. HeLa *SGPL1*$^{-/-}$ *CERS2*$^{-/-}$ cells were deprived in endogenous VLCFA SL species. After feeding with pacSph, protein-lipid complexes were formed upon UV-irradiation. Click reaction to Biotin-azide and subsequent enrichment on affinity beads led to their enrichment. Proteins were identified with LC-MS/MS. **B. HPTLC analysis of pacSph metabolism**. HeLa *SGPL1*$^{-/-}$ and HeLa *SGPL1*$^{-/-}$ *CERS2*$^{-/-}$ cells were labelled with pacSph. Extracted lipids were subjected to click-reaction to a fluorogenic molecule. After lipid separation on a HPTLC separated

fluorescent lipids were detected. **C. Volcano plot of hits from the proteomic approach**. The log_2 H/L is plotted versus the negative log_{10} of the t-test p-value. TMD, transmembrane domain; Cer, Ceramide; HexCer, Hexosylceramide; Sph, Sphingosine; SM, Sphingomyelin; VLCFA SL, Very Long-Chain Fatty Acid-containing Sphingolipid, H, Heavy; L, Light.

2.4. Aim of the Thesis

The tissue- and organelle-specific expression and localisation of CerS enzymes and the highly diverse lipid compositions, including the proportion of each FA, varies among tissues, organelles and within the plane of the bilayer. This points to various functions of these lipids. The influences of the different acyl chain lengths of SLs is not yet understood and direct intracellular targets of VLCFA SLs are largely unknown. To discover novel roles of VLCFA SLs, a proteomic approach has been performed that identified proteins potentially interacting with VLCFA SLs. To follow up on this, this thesis aims at the further validation of several protein hits and the characterisation of a specific novel protein-VLCFA SL interactions. The characterisation includes the specification of the precise interacting SL species, their localisation in microdomains, the involvement of the TMD in lipid binding and their possible functional roles of the interaction. In terms of the function, the role of dystroglycan-VLCFA SL interactions in OLGs was investigated.

3. Results

3.1. *In silico* Analysis of 53 VLCFA-Sphingolipid Interacting Proteins

The previously performed proteomic approach identified proteins interacting with VLCFA SLs (Figure 2.10 and Table 7.1)[124]. Here, the bioinformatic analysis of the 53 identified protein hits was extended to define novel roles of VLCFA SLs. Protein-lipid interactions occur either with TMD-containing membrane proteins, peripheral membrane proteins or in hydrophobic cavities of soluble proteins[68]. For this reason, the distribution of TMD and non-TMD containing proteins of the hit list was analysed. 89% of the identified protein hits obtained from the proteomic approach comprised a TMD, and thus were localised within membranes (Figure 3.1 A). The majority of the proteins had one TMD (55%) whereas 34% were multi-spanning proteins. A detailed overview of the TMD count is visualized in figure 3.1 B. Different organelles are described to be enriched in specific lengths of TMDs[157]. Here, most of VLCFA SL interacting proteins comprised 21 amino acid-long TMDs followed by 23 amino acids as shown in figure 3.1 C. 60% of all proteins were localised in the plasma membrane followed by 20% localised in the Golgi (Figure 3.1 D). As protein interactions with a specific subset of SL species were analysed there may be a common motif present being responsible for the interaction with these structurally similar lipids. However, no motif could be identified within the TMDs of the 53 identified proteins (Figure 3.1 E). Merely, four proteins showed a somehow similar motif but spread over the length of the TMD. In neuroplasin (NPTN), basigin (BSG) and embigin (EMB) the possible motif was localised at the terminal site of the TMD. However, in ST3 beta-galactoside alpha-2,3-sialytransferase 1 (ST3GAL1) the same motif appeared to be localised in the centre of the TMD thus between two membrane leaflets.

VLCFA SLs may act by interacting with proteins in similar biological processes or molecular functions. Furthermore, proteins interacting with VLCFA SLs may be localised to specific cellular compartments. A gene ontology (GO) enrichment analysis was performed to investigate these possibilities. Identified proteins were mostly found to be enriched in different cellular compartments including autolysosome, secondary lysosome, Golgi cisterna membrane, trans-Golgi network membrane (Figure 3.2 A) and immunological synapse compared to the whole proteome.

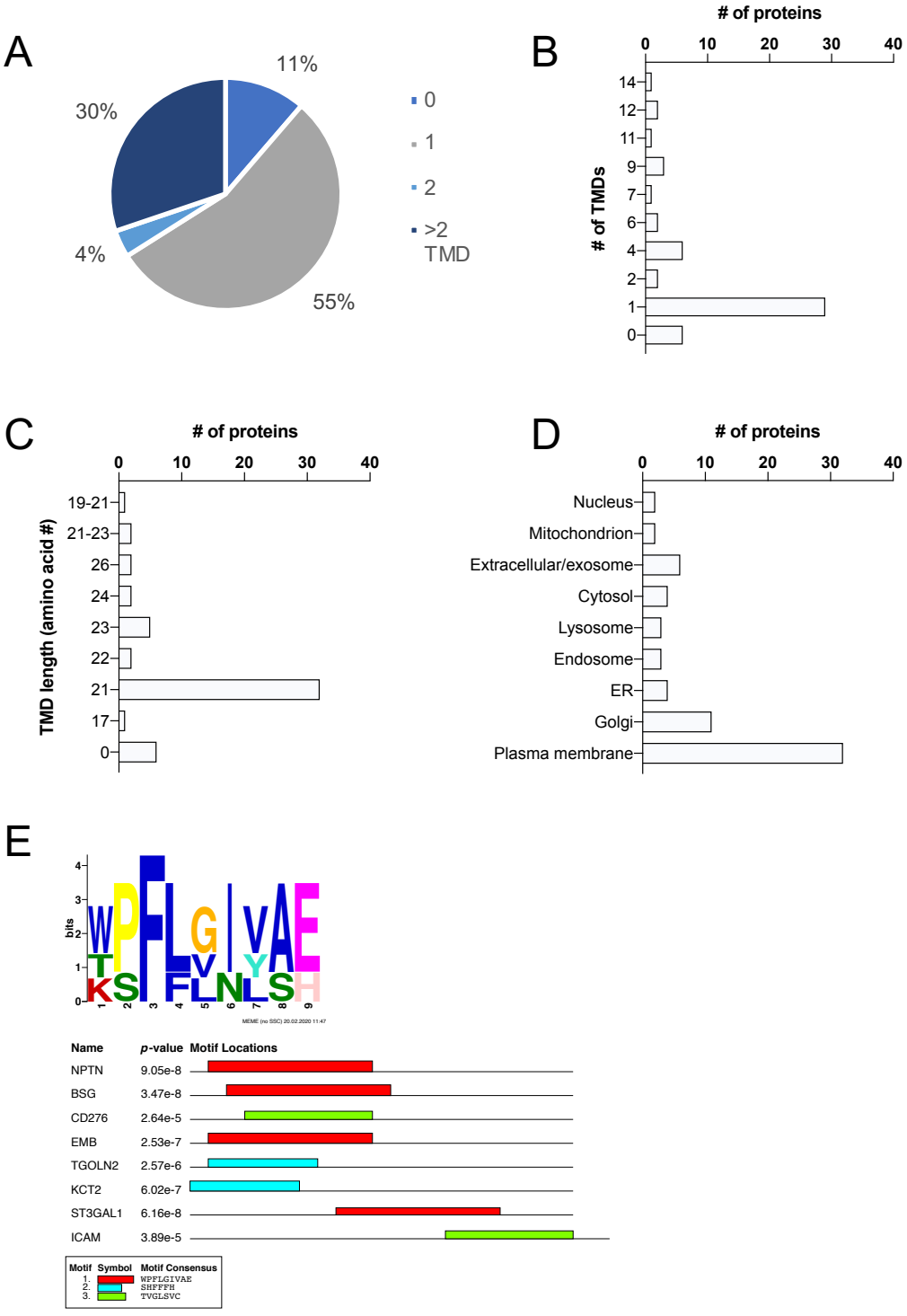

Figure 3.1 Transmembrane Domain Analysis of the 53 Identified VLCFA SL-Interacting Proteins

A. Pie chart visualizing the proportion of TMDs between hits. Percentages are shown for 0, 1, 2 or >2 TMDs. **B. Detailed overview of the TMD distribution in the dataset of 53 identified proteins. C. TMD length count of VLCFA-SL interacting proteins. D. Subcellular localisation of hits.** Multiple localisations per protein are shown and therefore exceeding the sum of 53 localisations. **E. Motif search within TMDs of 53 hits.** TMD sequence of dataset was subjected to motif analysis with MEME Suite[158]. The upper figure visualizes one identified motif, 9 amino acids in length, discovered in 4 out of 53 hits. The lower figure shows the localisation of this motif along the TMD sequence (in red) as well as two more discovered motifs, present in 2 out of 53 hits each. TMD, transmembrane domain.

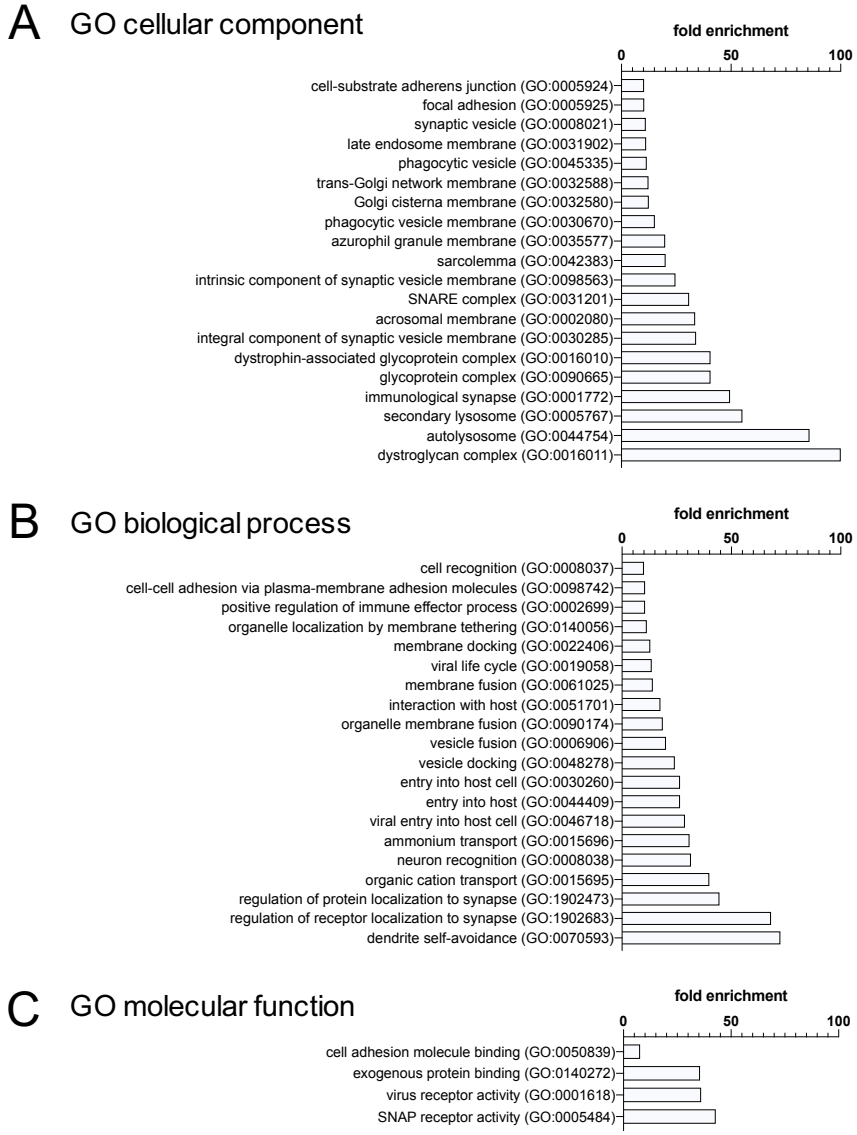

Figure 3.2 Gene Ontology Enrichment Analysis
Gene ontology (GO) term analysis was performed using the PANTHER Overrepresentation Test. Enrichment of certain GO terms in the dataset of 53 proteins in comparison to a reference dataset is depicted. **A. GO of cellular localisations B. GO of biological processes C. GO of molecular functions.** A-C. Shown are the top 20 of identified significantly (< p=0.001) enriched GO terms.

VLCFA SL interacting proteins appeared to play a role in dendrite self-avoidance, regulation of receptor/protein localisation to synapses, cell-cell adhesion via plasma membrane adhesion molecules, vesicle- or in general membrane fusion, and viral infections via entry into host cells (Figure 3.2 B).

The enriched cellular localisations and biological processes were reflecting the enriched molecular functions and cellular localisations. Roles in cell adhesion molecule binding, viral receptor activity and SNAP (Soluble N-ethylmaleimide-

sensitive-factor attachment) receptor activity were enriched among the VLCFA SL interacting proteins (Figure 3.2 C).

To identify possible functional associations between VLCFA SL interacting proteins by acting in functionally interacting modules or by the presence in the same signalling pathways, a STRING network analysis[159] was performed. The STRING network analysis is a precomputed global resource for exploration and analysis of functional associations[159]. Proteins may not simply interact by physical interactions. Indirect interactions by sharing a substrate in a metabolic pathway, by regulating each other transcriptionally or by participating in larger multi-protein assemblies are further possible interactions between proteins[159]. Therefore, the obtained hit list of 53 proteins was subjected to this network analysis and several proteins appeared functionally connected, as visualized in figure 3.3 by pink coloured lines.

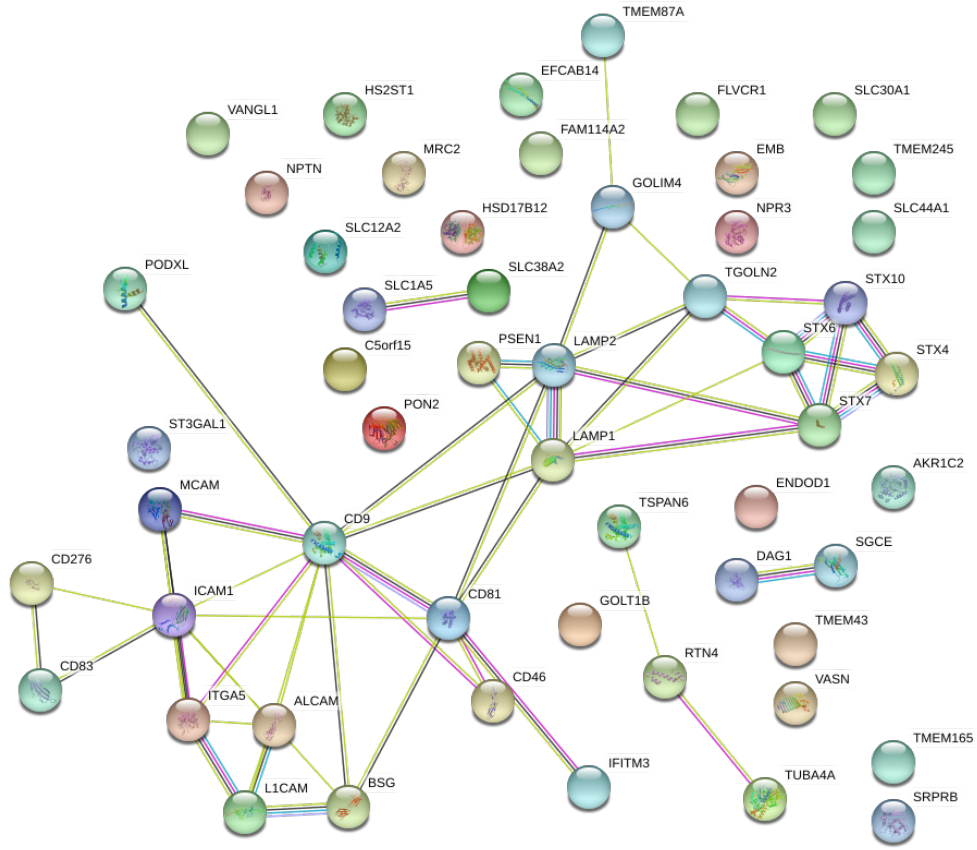

Figure 3.3 STRING Network Analysis
The hitlist of 53 identified proteins was subjected to a STRING network analysis[159]. Known interactions are shown as pink (experimentally determined) or blue (from curated databases) lines. Predicted interactions are visualised as green (gene neighbourhood), red (gene fusions) or blue (gene co-occurrence) lines. Other lines represent: text mining (light green), co-expression (black) and protein homology (violet). Filled nodes show if some structure is known or predicted.

These involved the functional relationship of identified Syntaxins (STXs), comprising STX4, STX6, STX7, STX10 which serve as SNAP receptors in membrane fusion[160]. Then plasma membrane-localised proteins with roles in cell adhesion and cellular-recognition processes appeared functionally connected. The central node among them was CD9 antigen (CD9) which is connected to CD81 antigen (CD81), Integrin alpha-5 (ITGA5) and Cell surface glycoprotein MUC18 (MCAM). Further sub- connections to Intracellular adhesion molecule 1 (ICAM1), Neural cell adhesion molecule 1 (L1CAM) and Membrane cofactor protein (CD46) were found. Two identified transporter proteins, Neutral amino acid transporter B(0) (SLC1A5) and the Sodium-coupled neutral amino acid transporter 2 (SLC38A2) were connected as well as the lysosome-localised proteins Lysosome-associated membrane glycoprotein 1 (LAMP1) and Lysosome-associated membrane glycoprotein 2 (LAMP2). Lastly, DAG1 was functionally connected with Epsilon-sarcoglycan (SGCE) while many other proteins remained unconnected.

3.2. Validation of novel Protein-VLCFA Interactions in Cellular Systems

The proteomic approach identified proteins possibly interacting with VLCFA SLs (introduced in section 2.3)[124]. To validate the data obtained from this proteomic approach, different assays were performed. These included protein-lipid pulldown assays with pacSph in the HeLa *SGPL1*$^{-/-}$ *CERS2*$^{-/-}$ cells and the parental HeLa *SGPL1*$^{-/-}$ cells as well as assays to study the influence of microdomains on the identified protein-SL interactions. Additionally, analyses to test the ability to rescue the reduced protein-lipid interactions in HeLa *SGPL1*$^{-/-}$ *CERS2*$^{-/-}$ cells and finally assays to validate the interaction to SLs in HeLa *SGPL1*$^{-/-}$ cells by inhibiting pacSph SL metabolism were performed.

3.2.1. Validation of the Proteomic Approach Using Overexpressed Proteins Versus Endogenous Protein Levels

To validate the protein-VLCFA SL interactions of the proteomic approach, an overexpression of FLAG-tagged versions of the selected proteins was performed. HeLa *SGPL1*$^{-/-}$ *CERS2*$^{-/-}$ cells and the parental HeLa *SGPL1*$^{-/-}$ cells were

transfected with DAG1-FLAG constructs. The following day, cells were labelled with pacSph, or as a control with pacFA, subjected to UV-crosslinking, cell lysis, click-reaction of the protein-lipid complexes to Biotin and enrichment of protein-SL-Biotin products on Neutravidin beads. Input and protein-lipid pulldown (PL-PD) samples were loaded on an SDS-PAGE gel, blotted and FLAG-tagged proteins were detected using an anti-FLAG antibody. FLAG-tagged βDG was pulled down in both cell lines with pacSph (Figure 3.4 A), however comparable expression levels in HeLa *SGPL1*$^{-/-}$ *CERS2*$^{-/-}$ cells and the parental HeLa *SGPL1*$^{-/-}$ cells could not be established. In addition, the amount of recovered βDG in PL-PDs varied strongly among experiments even though a significant reduction of βDG in HeLa *SGPL1*$^{-/-}$ *CERS2*$^{-/-}$ cells compared to the parental cells could be identified (Figure 3.4 A, C). The amount of endogenous βDG in PL-PDs was significantly reduced in HeLa *SGPL1*$^{-/-}$ *CERS2*$^{-/-}$ cells compared to the parental cells (Figure 3.4 B, C).

In parallel to PL-PD experiments, the intracellular localisation of overexpressed FLAG-tagged proteins was investigated by confocal microscopy. As before, FLAG-tagged DAG1-contructs were transfected into both cell lines. The control cells remained untransfected to monitor endogenous βDG localisation. The following day cells were fixed and stained with anti-FLAG or anti-βDG antibodies and processed for immunofluorescence microscopy. Overexpressed FLAG-tagged βDG appeared to be localised in ER and vesicles (Figure 3.4 E) whereas endogenous βDG appeared to be localised at specific sites at the plasma membrane in both cell lines (Figure 3.4 F). In HeLa *SGPL1*$^{-/-}$ *CERS2*$^{-/-}$ cells the localisation of overexpressed FLAG-tagged βDG appeared even more localised to intra-(or extra-) cellular vesicles compared to the parental cells (Figure 3.4 D).

To investigate if βDG is also localising with GPL lipid species, cells were labelled with pacFA instead of pacSph. PacFA is described to be mainly incorporated into pacPC species[161] therefore the pulldown experiment was also performed with pacFA (Figure 3.4 A, B). Interestingly, FLAG-tagged overexpressed βDG was also strongly pulled down with pacFA labelling in HeLa *SGPL1*$^{-/-}$ cells. Furthermore, a significantly lower interaction to pacFA-derived lipids in HeLa *SGPL1*$^{-/-}$ *CERS2*$^{-/-}$ cells compared to the parental cells was observed (Figure 3.4 D). The pulldown experiment employing pacFA was also performed without overexpressing the protein of interest. More cells were used for the experiment and endogenous proteins were detected. Figure 3.4 B and D show that the previously detected

interaction of βDG with pacFA-derived lipids was no longer present. The quantification of the proteomic approach validation with endogenous proteins is described in the next section.

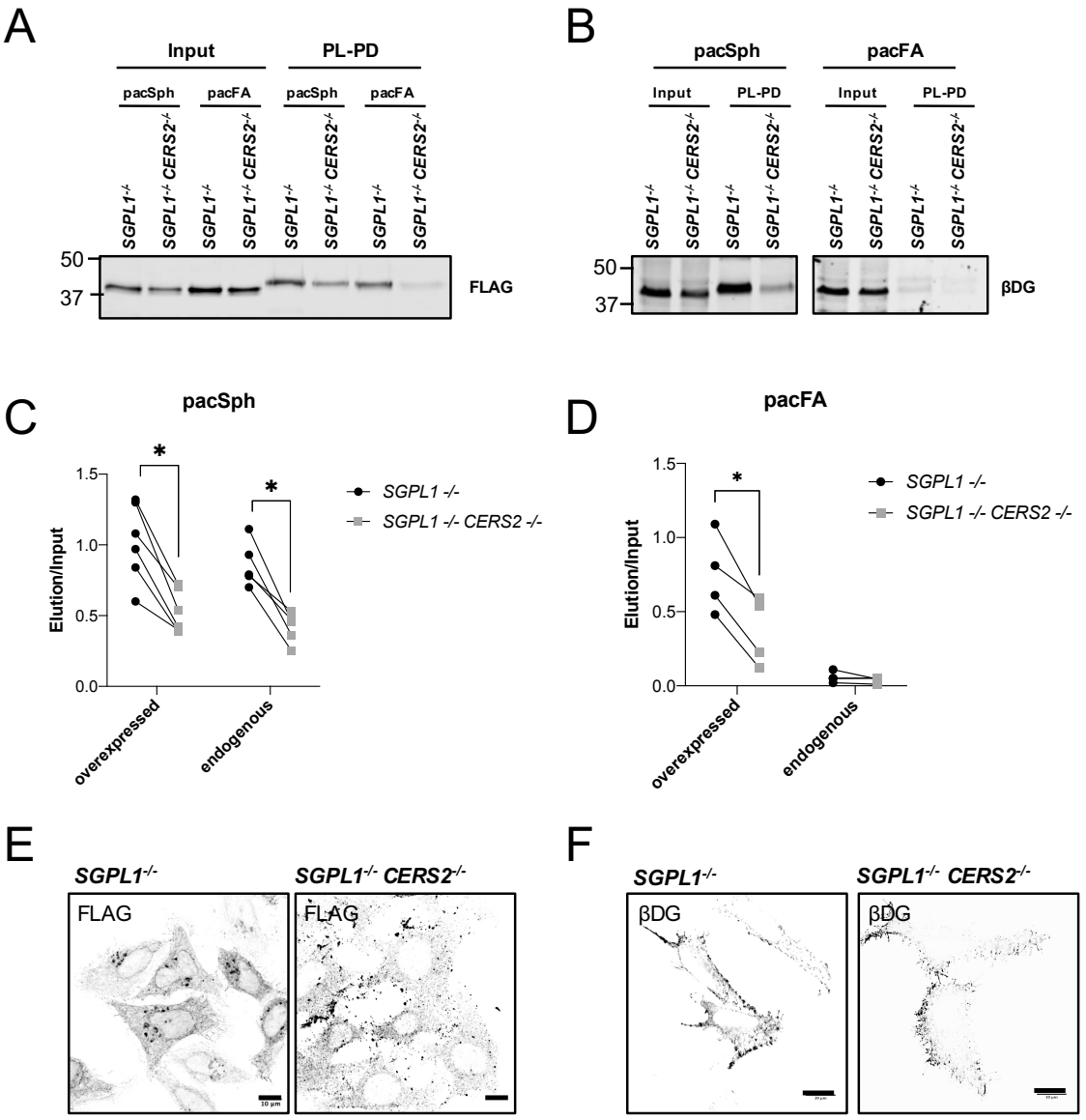

Figure 3.4 Validation of Protein-VLCFA SL Interactions Using Overexpression of FLAG-tagged Proteins Versus Endogenous Proteins

A. Protein-lipid pulldown analysis of overexpressed proteins. HeLa *SGPL1*$^{-/-}$ and HeLa *SGPL1*$^{-/-}$ *CERS2*$^{-/-}$ cells were transiently transfected with pCMV3-DAG1-FLAG for 24 h. The last 4 h, media was removed and replaced with media containing 6 µM pacSph or 50 µM pacFA. After subsequent UV-crosslinking, cell lysis, CuAAC-based click-reaction to Biotin-azide and enrichment of protein-lipid pulldown (PL-PD) on Neutravidin beads, elution (95%) and input (5%) samples were loaded on an SDS-PAGE gel, blotted and FLAG proteins were detected with an anti-FLAG antibody. **B. PL-PD of endogenous proteins.** HeLa *SGPL1*$^{-/-}$ and HeLa *SGPL1*$^{-/-}$*CERS2*$^{-/-}$ cells were labelled for 4 hours with 6 µM pacSph or 50 µM pacFA. After subsequent UV-crosslinking, cell lysis, CuAAC-based click-reaction to Biotin-azide, enrichment of PL-PD on Neutravidin beads, elution (95%) and input (5%) samples were loaded on SDS-PAGE gel, blotted and endogenous proteins were detected with an anti-βDG antibody. **C, D. Quantification of protein-lipid complexes in pacSph (C) and pacFA (D) labelled samples**. The protein amount in elution fractions was compared to input values. Shown are individual data points that are connected within one experiment. Two-sided

paired t-tests were performed. * = p<0.05, ** = p<0.001. **E. Confocal microscopy analysis of overexpressed proteins.** HeLa *SGPL1*$^{-/-}$ and HeLa *SGPL1*$^{-/-}$ *CERS2*$^{-/-}$ cells were transiently transfected with pCMV3-DAG1-FLAG for 24 h. After fixation and blocking, cells were stained with anti-FLAG and anti-mouse Alexa488 and prepared for confocal microscopy. **F. Confocal microscopy analysis of endogenous proteins.** HeLa *SGPL1*$^{-/-}$ and HeLa *SGPL1*$^{-/-}$ *CERS2*$^{-/-}$ cells were fixed and blocked, to stain cells with anti-βDG and anti-mouse Alexa488. After preparation for confocal microscopy, slides were imaged with a Zeiss LSM 800. Scale bar: 10 µm.

3.2.2. Validation of Identified Protein-VLCFA Sphingolipid Interactions Investigating Endogenous Proteins

To validate proteins that were identified by the proteomic approach to interact with VLCFA SLs[124], pacSph labelling and protein-lipid pulldown assays were performed. Three proteins were selected for validation based on the obtained ratio of the proteomic approach. The ratio reflects the degree of diminished interaction to SLs in VLCFA SL-deprived cells[124]. Among the proteins with the strongest reductions in the proteomic approach were βDG, Syntaxin 6 (STX6) and Trans Golgi network protein 2 (TGOLN2) which were chosen for validation. As controls, a protein with an unaffected SL-interaction in both cell lines and a protein that was interacting with more instead of fewer pac-derived lipids in the VLCFA SL-deprived cells were examined, namely Transferrin receptor (TFR) and Integrin beta 1 (ITGB1), respectively (see values in Supplementary Table 7.1).

As described in section 3.2.1, HeLa *SGPL1*$^{-/-}$ *CERS2*$^{-/-}$ cells and the parental HeLa *SGPL1*$^{-/-}$ cells were labelled with pacSph, subjected to UV-crosslinking (or as a control, without UV-crosslinking), cell lysis, click-reaction of the protein-lipid complexes to Biotin and enrichment of protein-SL-Biotin products on Neutravidin beads. Input and PL-PD samples were loaded on an SDS-PAGE gel, blotted and endogenous proteins were detected using respective antibodies. One blotting membrane was scanned for multiple proteins as elution samples contain all PL-PD complexes formed. Figure 3.5 A-C shows the validation of three protein hits of the proteomic approach. βDG, STX6 and TGOLN2 showed a significantly lower amount in PL-PD compared to input in cells lacking VLCFA SLs compared to the parental cells. Without UV-crosslinking, no protein was detected in the elution samples. The PL-PD with pacSph of TFR was identical in both cell lines (Figure 3.5 D). For ITGB1 two distinct bands were observed (Figure 3.5 E). When quantifying both bands, the amount of ITGB1 appeared to be enriched in HeLa *SGPL1*$^{-/-}$ *CERS2*$^{-/-}$ cells as found by the proteomic approach. However, the upper

band of ITGB1 is almost missing in the PL-PD of HeLa *SGPL1*$^{-/-}$ *CERS2*$^{-/-}$ cells. The quantification revealed a possible interaction of the upper band with VLCFA SLs, however more replicates would be required to test for statistical significance of this interaction.

The results of section 3.2.1 showed that the intracellular localisation of transiently expressed βDG did not match the one of the endogenous protein. To further exclude that changes in the localisation of endogenous proteins were present in HeLa *SGPL1*$^{-/-}$ *CERS2*$^{-/-}$ cells compared to the parental cells, an immunofluorescence analysis with confocal microscopy was performed. Both cell lines were seeded and fixed the following day, blocked and stained with antibodies against endogenous proteins. βDG seemed to be mainly localised to specific regions at the plasma membrane (Figure 3.6 A), as already shown in figure 3.4 F. In both cell lines STX6 and TGOLN2 appeared to be localised in the Golgi (Figure 3.6 B,C). TGOLN2 was furthermore appearing to localise to the nucleoplasm. TFR localisation appeared to be in intracellular endosomes (Figure 3.6 D) whereas ITGB1 showed an ER and plasma membrane localisation (Figure 3.6 E). For none of the investigated proteins, an altered localisation in HeLa *SGPL1*$^{-/-}$ *CERS2*$^{-/-}$ cells compared to the parental HeLa *SGPL1*$^{-/-}$ cells was observed.

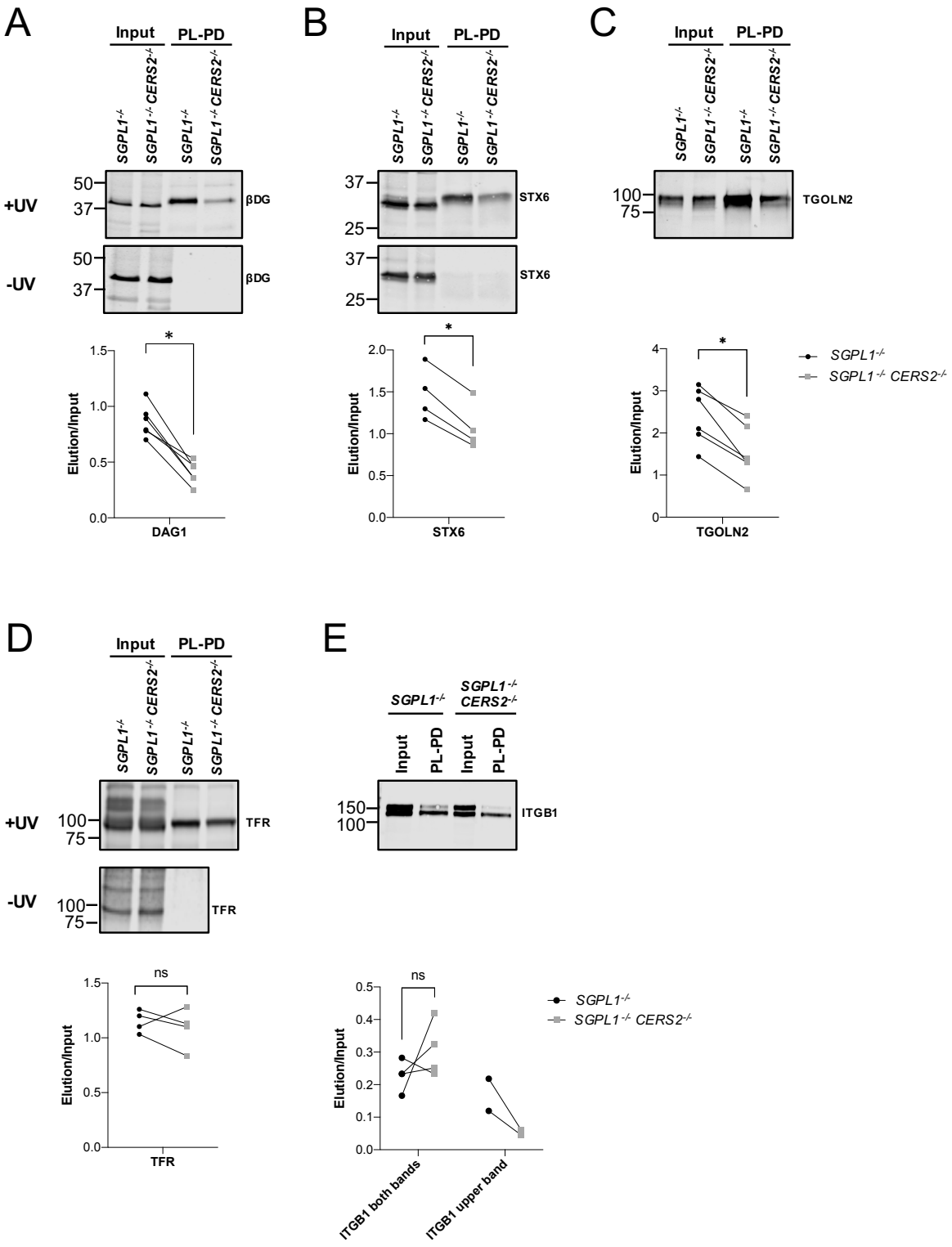

Figure 3.5 Validation of Selected Proteins Interacting with VLCFA SLs Detecting Endogenous Proteins

A-E. Validation assay of STX6, TGOLN2 and dystroglyan. HeLa *SGPL1*$^{-/-}$ and HeLa *SGPL1*$^{-/-}$ *CERS2*$^{-/-}$ cells were labelled with 6 µM pacSph for 4 h. After subsequent UV-crosslinking (or without as indicated), cell lysis, CuAAC-based click-reaction to Biotin-azide, enrichment of protein-lipid pulldowns (PL-PD) on Neutravidin beads, elution (95%) and input (5%) samples were loaded on SDS-PAGE gel, blotted and endogenous proteins were detected with specific antibodies against endogenous proteins. The upper panel shows the blots and the lower panel visualises the quantification of protein amounts in PL-PD versus input samples for +UV samples. A. β-dystroglycan (βDG) B. Synthaxin-6 (STX6) C. Trans-Golgi-network protein 2 (TGOLN2) D.

Transferrin-Receptor (TFR) E. Integrin beta-1 (ITGB1). For quantification protein amount in the elution was compared to input values. Shown are individual data points that are connected within one experiment. Data were obtained from six independent experiments (DAG1, TGOLN2), or four independent experiments (STX6, TFR, ITGB1 both bands), or two independent experiments (ITGB1 upper band). Two-sided paired t-tests were performed. * = $p<0.05$, ** = $p<0.001$. Fluorescence of secondary antibodies was detected using a LiCor and quantification was done with the Image Studio Software.

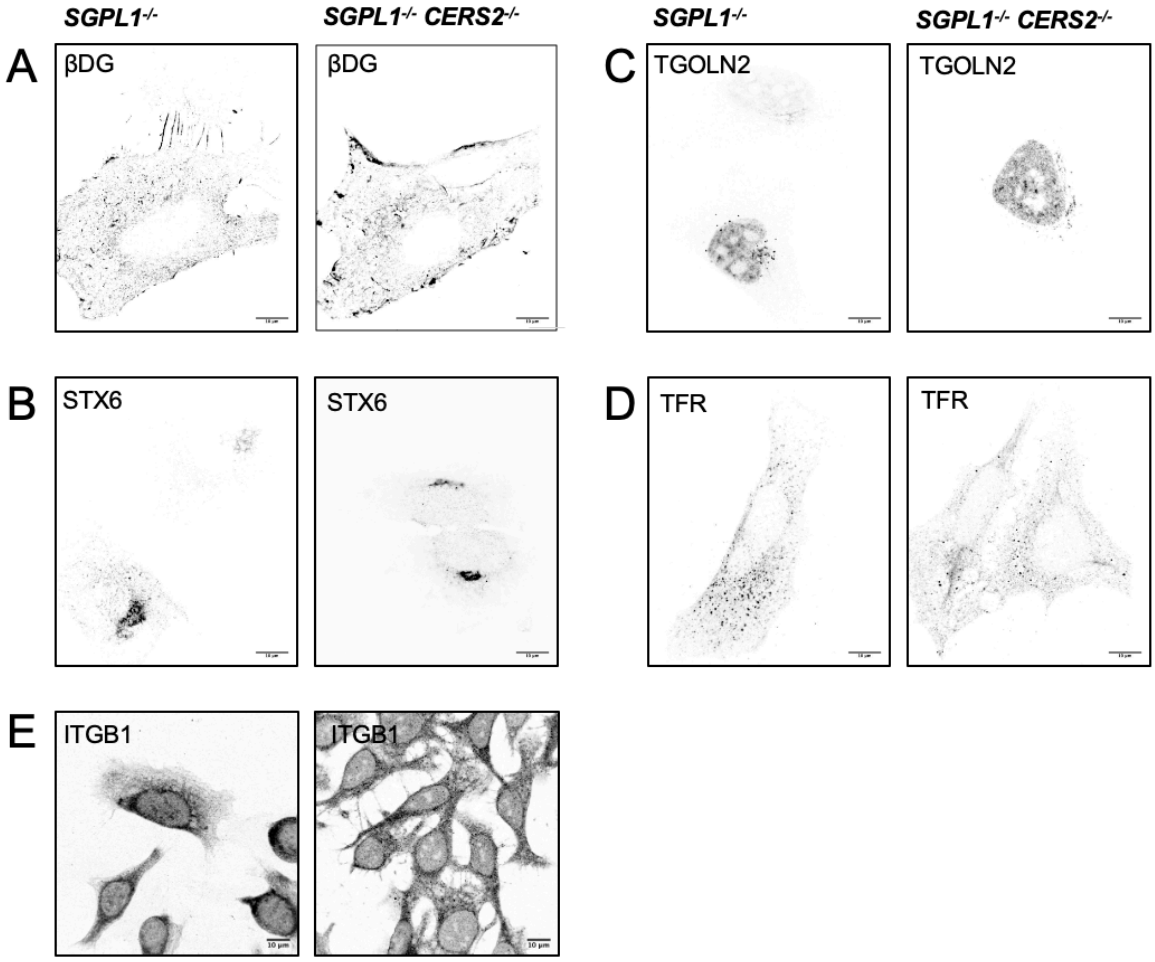

Figure 3.6 Confocal Microscopy Analysis of Endogenous Localisation of Selected Proteins
HeLa *SGPL1*$^{-/-}$ and HeLa *SGPL1*$^{-/-}$ *CERS2*$^{-/-}$ cells were fixed and blocked. Cells were stained with specific antibodies against endogenous proteins and with anti-primary species Alexa488. After preparation for confocal microscopy, slides were imaged with a Zeiss LSM 800. Scale bar: 10 µm.

3.2.3. Influence of Cholesterol on VLCFA SL-Interactions

The plasma membrane is not a structurally passive solvent, SLs and cholesterol are preferentially associated together in 'nanodomains' (Section 2.1.1)[5]. Especially VLCFA SLs are described to be enriched in lipids[6,19]. Therefore, it was of interest to investigate the influence of microdomain localisation on protein-VLCFA-SL

interaction of the identified proteins. For this purpose, MβCD was employed which was described to deplete cholesterol from the plasma membrane and thus to disrupt microdomains[8]. To exclude effects of MβCD treatment on pacSph metabolism in HeLa *SGPL1*$^{-/-}$ cells, cells were labelled with 6 µM pacSph and treated with MβCD. Untreated cells were used as controls. Lipids were extracted, clicked to Coumarin-azide, separated on a HPTLC-silica plate and the resulting fluorescent paclipids were detected. No significant difference in the pacSph labelling between untreated and treated cells was detectable (Figure 3.7 A). The HPTLC plate was stained for total lipids using sulfuric acid to visualize cholesterol. The chosen treatment reduced the cholesterol amount by 29% (Figure 3.7 B, C). With this condition, pulldown experiments were performed. HeLa *SGPL1*$^{-/-}$ cells were labelled with 6 µM pacSph and treated or not-treated with MβCD, subjected to UV-crosslinking, cell lysis, click-reaction of the protein-lipid complexes to Biotin and enrichment of protein-SL-Biotin products on Neutravidin beads. Input and PL-PD samples were loaded on an SDS-PAGE gel, blotted and endogenous proteins were detected using the respective antibodies. The treatment with MβCD significantly reduced the amount of crosslinked βDG (Figure 3.7 D, E). In comparison STX6 was not reduced by this treatment (Figure 3.7 D, E).

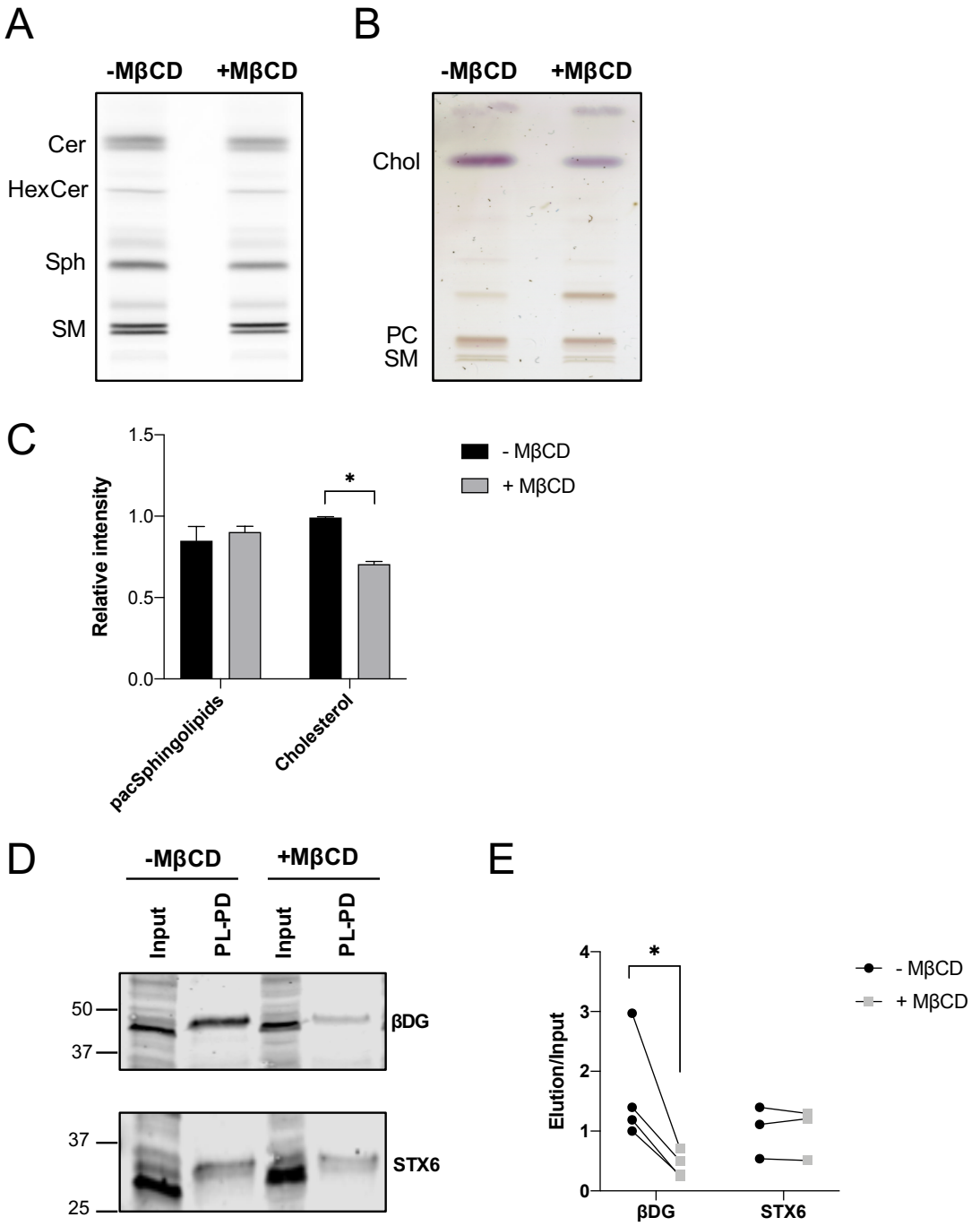

Figure 3.7 Effect of MβCD Treatment on Interaction of Selected Proteins with Sphingolipids A. HPTLC analysis to monitor pacSph metabolism. HeLa *SGPL1*$^{-/-}$ and HeLa *SGPL1*$^{-/-}$ *CERS2*$^{-/-}$ cells were labelled with 6 µM pacSph for 4 h. If indicated, 5 mM MβCD was added to the media for the last hour of pacSph labelling. Cells were collected, lipids were extracted and subjected to click-reaction to Coumarin-azide. Lipids were separated on a HPTLC silica plate and separated fluorescent lipids were detected using an Amersham Imager 600 with excitation at 460 nm and a Cy2 Emission Filter (525BP20). **B. Total lipid stain.** HTPLC plate from A. was sprayed with 20% sulfuric acid and incubated for 10 min at 125°C to visualise total lipids. **C. Quantification of detected pacSph-derived lipid species and total cholesterol.** PacSph-derived sphingolipid species were quantified using Fiji and normalised to total PC from the total lipid stain. Cholesterol was quantified using Fiji and was normalised to total PC. Shown is the mean ± SEM of three independent experiments. Multiple t-tests (two-sided, unpaired) were performed and corrected for multiple comparisons using the Holm-Sidak method. * = $p<0.05$, ** = $p<0.001$. **D. Protein-lipid pulldown analysis of endogenous proteins with and without MβCD treatment.** HeLa *SGPL1*$^{-}$

$^{-/-}$ and HeLa *SGPL1*$^{-/-}$ *CERS2*$^{-/-}$ cells were labelled with 6 µM pacSph for 4 h. If indicated, 5 mM MβCD was added to the media for the last hour of pacSph labelling. After subsequent UV-crosslinking, cell lysis, CuAAC-based click-reaction to Biotin-azide, enrichment of protein-lipid pulldown (PL-PD) on Neutravidin beads, elution (95%) and input (5%) samples were loaded on an SDS-PAGE gel, blotted and endogenous proteins were detected with an anti-βDG and anti-STX6 antibody. **E. Quantification of protein-lipid complexes in pacSph labelled samples.** The protein amount in elutions was compared to input values. Shown are individual data points that are connected within one experiment. Three independent experiments for DAG1 and two experiments for STX6 were performed. Two-tailed, paired t-tests were performed. * = $p<0.05$, ** = $p<0.001$. MβCD, methyl-β-cyclodextrin; Cer, ceramide; HexCer, hexosylceramide; Sph, sphingosine; SM, sphingomyelin; Chol, cholesterol; PC, phosphatidylcholine.

3.2.4. Rescue of Protein-VLCFA SL Interactions with CerS2 Overexpression

The proteomic approach identified proteins as candidates for specific interactions with VLCFA SLs[124]. The validation approach revealed a significant interaction of βDG, TGOLN2, STX6 and ITB1 with VLCFA SLs (Section 3.2.2). As the employed HeLa *SGPL1*$^{-/-}$ *CERS2*$^{-/-}$ cells are lacking the synthesis of VLCFA SLs and showed a reduced interaction with identified proteins, it was of interest to rescue this synthesis and observe the influence on protein-lipid interactions. This would allow a further validation of the identified specific protein-VLCFA SL interactions.

For this purpose, the depleted CerS2 protein was overexpressed in HeLa *SGPL1*$^{-/-}$ *CERS2*$^{-/-}$ cells. The CerS2 enzyme is responsible for the synthesis of SLs with C22-C24 fatty acids, whereas CerS1 generates SLs with N-linked C18 FAs[162]. The majority of LCFA-pacSM and other LCFA-SLs visible in HPTLC analysis were supposed to be C16 pacSLs, and not C18, as these are the most abundant SLs in HeLa cells besides C24 SLs[115]. However, a mass spectrometric analysis of the pac-derived SL species in these cells was not performed so far. The influence on the pacSph metabolism in HeLa *SGPL1*$^{-/-}$ *CERS2*$^{-/-}$ cells overexpressing CerS1 was of interest, since it could support to discriminate between protein-interactions with LCFA versus VLCFA SLs. In an initial experiment, a HPTLC analysis of pacSph metabolism in CerS2 and CerS1 overexpressing HeLa *SGPL1*$^{-/-}$ *CERS2*$^{-/-}$ cells was analysed (Figure 3.8 A). A significant rescue of the Cers2 depletion in HeLa *SGPL1*$^{-/-}$ *CERS2*$^{-/-}$ cells was observed as the band for VLCFA SL was re-appearing when comparing the pacSph metabolism to parental HeLa *SGPL1*$^{-/-}$ cells (Figure 3.8 A, B). For CerS1 overexpressing cells, a single band was detected for

each lipid class, however the precise FA chain length could not be analysed by HTPLC.

The same samples were prepared for mass spectrometric analysis of endogenous lipids and paclipids. SM and pacSM species were detected in precursor ion scanning of 184 m/z, with the selected fragment ion corresponding to the choline head group. Ceramide was detected by precursor ion scanning of 264.3 m/z to selectively monitor the C18-sphingosine backbone of ceramide species. For pacCer detection, the scan was changed to 300 m/z, to account for the C18-backbone containing the diazirine and alkyne functionalities of pacSph. CerS2 overexpression resulted, as suggested by HPTLC analysis (Figure 3.8 A), in the re-synthesis of C24-containing ceramide and SM lipids as well as corresponding C24-pacSLs (Figure 3.8 C, D). Furthermore, when overexpressing CerS1 in HeLa *SGPL1*$^{-/-}$ *CERS2*$^{-/-}$ cells an 8-fold relative increase of endogenous C18-containing ceramide (Cer 36:1;2) and a 5-fold increase in endogenous C18-containing SM (SM 36:1;2) was observed (Figure 3.8 C, D).

The overexpression of CerS2 in HeLa *SGPL1*$^{-/-}$ *CERS2*$^{-/-}$ cells led to the re-synthesis of VLCFA SLs in these cells. Furthermore, the overexpression of CerS1 in HeLa *SGPL1*$^{-/-}$ *CERS2*$^{-/-}$ cells resulted in the generation of majorly C18-pacSLs. Also in CerS2-overexpressing cells, a large proportion of pac-Cer36:1;2 could be detected but appeared lower compared to CerS1 overexpressing cells. To elucidate the influence of the modified pacSph-labelling in these conditions, the protein-lipid pulldown assay was performed. The samples were prepared as for the HTPLC and lipidomic analysis described above, but instead of lipid extraction, cells were subjected to UV-crosslinking, cell lysis, click-reaction of the protein-lipid complexes to Biotin and enrichment of protein-SL-Biotin products on Neutravidin beads. Input and PL-PD samples were loaded on an SDS-PAGE gel, blotted and endogenous proteins were detected using specific antibodies. When overexpressing CerS2 in knockout cells, the interaction of βDG to pacSLs was significantly increasing and was even more pronounced compared to HeLa *SGPL1*$^{-/-}$ cells (Figure 3.9 A, B). When comparing the amount of βDG in PL-PD of CerS1 versus CerS2 overexpressing cells, the amount was non-significantly lower in CerS1 overexpressing cells (Figure 3.9 A, B), however a trend may be observed. The diminished amount of STX6 in HeLa *SGPL1*$^{-/-}$ *CERS2*$^{-/-}$ protein-lipid pulldowns was rescued when overexpressing CerS2 in knockout cells. Differently to βDG, the

pulldown of STX6 in CerS1 overexpressing samples was comparable to PL-PDs of CerS2 knockout cells (Figure 3.9 A, B).

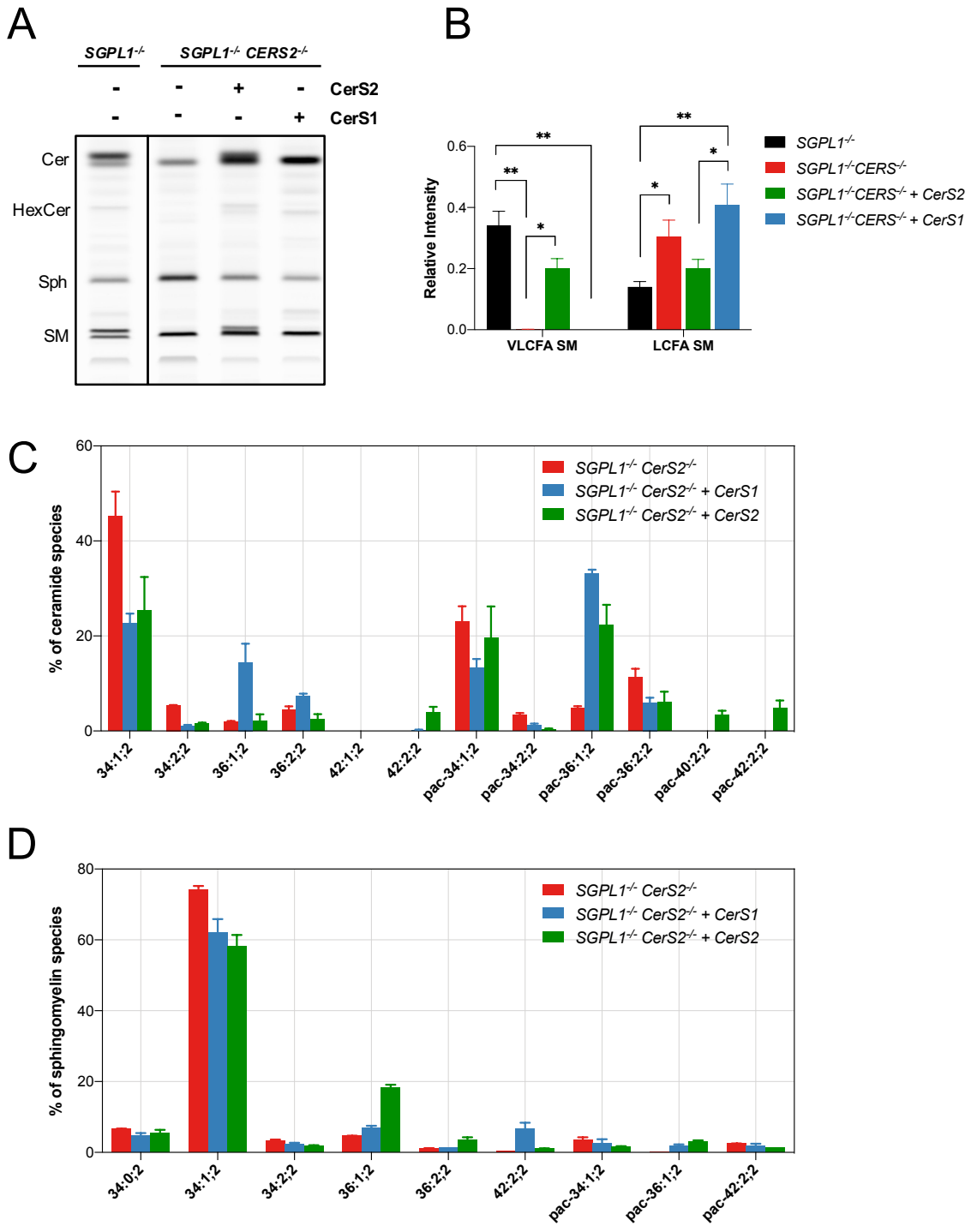

Figure 3.8 Effect of CerS2 and CerS1 Overexpression on pacSph Metabolism.
A. HPTLC analysis of pacSph metabolism. HeLa *SGPL1*$^{-/-}$ *CERS2*$^{-/-}$ cells were transfected with pCMV6-CERS2 or pCMV6-CERS1 for 48 h. Labelling was done with 6 µM pacSph for 4 h also in HeLa *SGPL1*$^{-/-}$ cells. Cells were collected, lipids were extracted and subjected to click-reaction to Coumarin-Azide. Lipids were separated on a HPTLC silica plate and separated fluorescent lipids were detected using an Amersham Imager 600 with excitation at 460 nm and a Cy2 Emission Filter (525BP20). **B. Quantification of detected pacSph-derived lipid species.** PacSph-derived sphingolipid species were quantified using Fiji and shown as relative intensity per species to total paclipids. Only LCFA vs VLCFA SM species are visualized. Shown is mean ± SEM of four

independent experiments. Multiple t-tests were performed and corrected for multiple comparisons using the Holm-Sidak method. * = p<0.05, ** = p<0.001. **C-D. Lipidomic analysis of ceramide and sphingomyelin lipid species.** Samples were prepared as described for A. SM and pacSM was scanned by PIC 184 m/z; Ceramide by PREC 264.3 m/z; pacCeramide by PREC 300 m/z. Measurements were done with an QTRAP 6500+, quantification was performed by comparing to internal standards. Shown is mean ± SEM of two independent experiments. Lipidomic measurement was performed by Timo Sachsenheimer and Christian Lüchtenborg. Cer, ceramide; HexCer, hexosylceramide; Sph, sphingosine; SM, sphingomyelin; VLCFA, very long chain fatty acid containing sphingolipid species; LCFA, long chain fatty acid containing sphingolipid species; FA, fatty acid. Lipid species were annotated according to their molecular composition as follows: sum of carbon atoms in the FAs:sum of double bonds in the FAs;sum of hydroxyl groups in the long-chain base and the FA moiety.

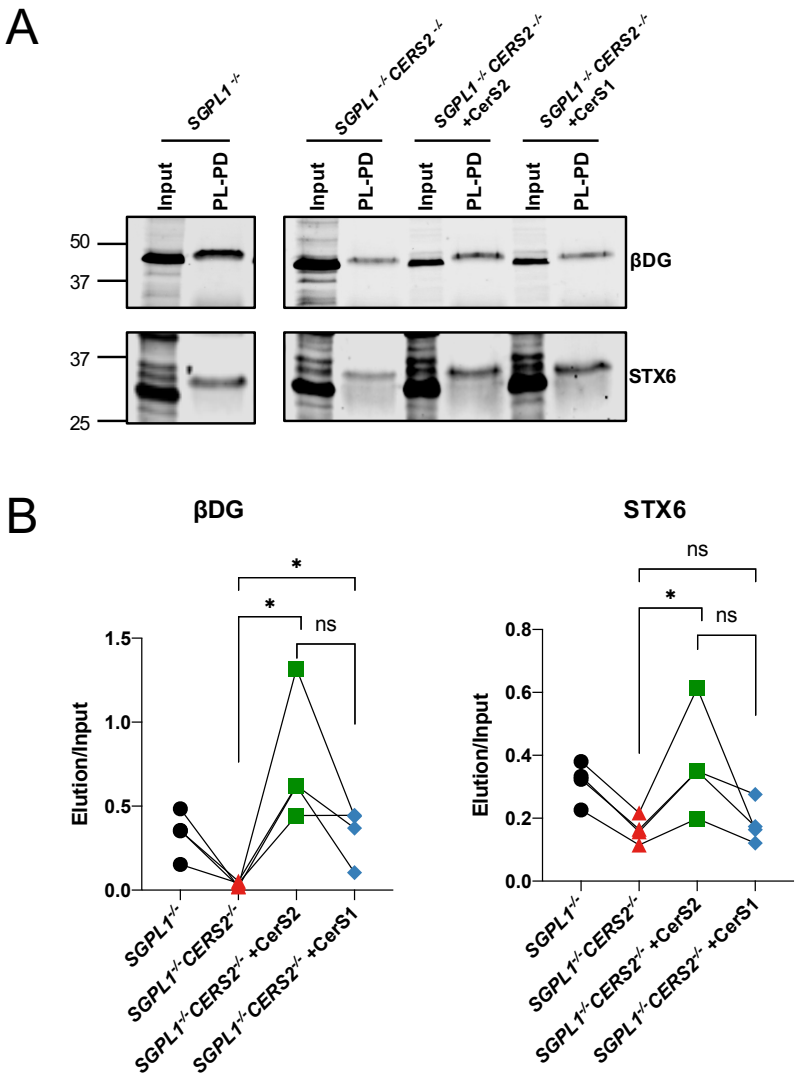

Figure 3.9 Pulldown Analysis of CerS2 and CerS1 Overexpressing Cells
A. Protein-lipid pulldown analysis of endogenous proteins comparing CerS1 and CerS2 overexpressing HeLa *SGPL1*$^{-/-}$ *CERS2*$^{-/-}$ cells. HeLa *SGPL1*$^{-/-}$ *CERS2*$^{-/-}$ cells were transfected with pCMV6-CERS2 or pCMV6-CERS1 or mock for 48 h. Labelling was done with 0.5 µM pacSph for 4 h also in HeLa SGPL1$^{-/-}$ cells. After subsequent UV-crosslinking, cell lysis, CuAAC-based click-reaction to Biotin-azide, enrichment of protein-lipid pulldown (PL-PD) on Neutravidin beads, elution (95%) and input (5%) samples were loaded on SDS-PAGE gel, blotted and endogenous proteins were detected with an anti-βDG/STX6 antibodies. **B. Quantification of Western blot signals.** Protein amount in elution was compared to input values. Shown are individual data points that are connected within one experiment. Two-tailed paired t-tests were performed. * = p<0.05, ** = p<0.001.

3.2.5. Inhibition of pacSph Metabolism

The first reaction of pacSph metabolism in cells is catalysed by CerS enzymes to form ceramide from the sphingosine precursor and a fatty acyl-CoA[13]. Fumonisin B1 (FB1) is a unspecific CerS inhibitor[163] which was employed to further validate the interaction of proteins with pacSph-derived SL species from the proteomic approach. First, a HPTLC analysis was performed to confirm the ability of FB1 to inhibit CerS and thus, the pacSph metabolism in HeLa *SGPL1*$^{-/-}$ cells. Treated and mock-treated cells were labelled with 0.5 µM pacSph, samples were collected, lipids were extracted, pacSph-derived lipids were clicked to Coumarin-azide, separated on a HPTLC-Silica plate and the resulting fluorescent paclipids were detected. FB1 reduced the synthesis of pacSM and pacCer, whereas the amount of not-utilized pacSph was significantly elevated (Figure 3.10 A, B). For SM, two bands are visible on the TLC, corresponding to the abundant LCFA and VLCFA SM species (Section 3.2.4). Surprisingly, the upper band, corresponding to the VLCFA SM species, appeared significantly more diminished compared to the lower LC-SM band (Figure 3.10 A, C).

Being able to diminish the pacSph metabolism, this treatment was applied to protein-lipid pulldown analysis. HeLa *SGPL1*$^{-/-}$ cells were treated and mock-treated with FB1, cells were labelled with pacSph, subjected to UV-crosslinking, cell lysis, click-reaction of the protein-lipid complexes to Biotin and enrichment of protein-SL-Biotin products on Neutravidin beads. Input and PL-PD samples were loaded on an SDS-PAGE gel, blotted and endogenous proteins were detected using specific antibodies. βDG-pacSL interaction was reduced by 92% whereas for STX6 a minor, non-significant reduction was observed in PL-PD of FB1 treated cells. More replicates are required to finally conclude about ITGB1, however a minor reduction could be suggested. Also, the upper band of ITGB1 seemed to be stronger diminished by this treatment.

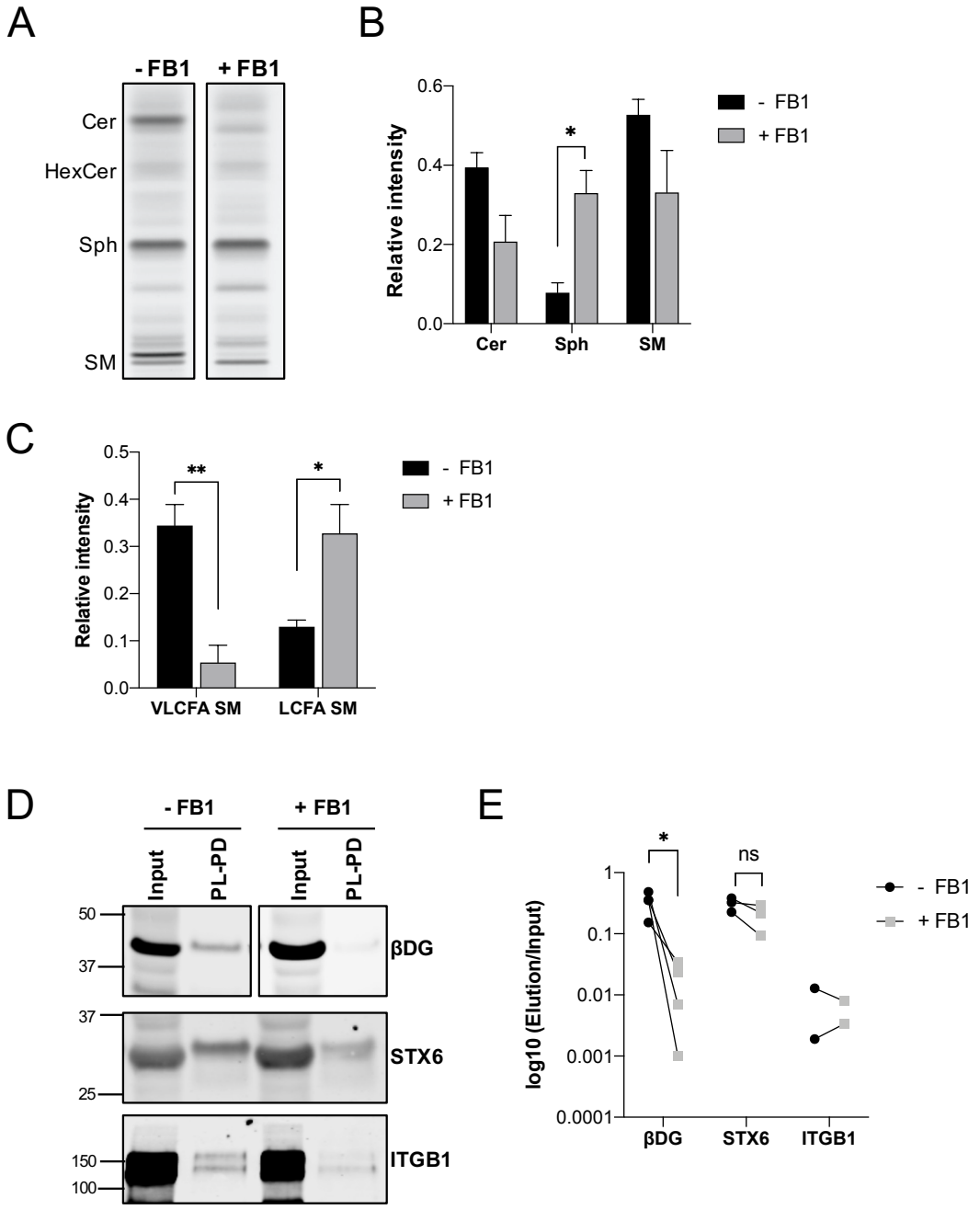

Figure 3.10 Effect of Fumonisin B1 Treatment on pacSph Metabolism and Protein-Lipid Pulldown Analysis

A. HPTLC analysis of pacSph metabolism with FB1 treatment. HeLa *SGPL1*$^{-/-}$ cells were treated with 50 µM FB1 for 20 h prior labelling. Labelling was done with 0.5 µM pacSph for 4 h. Cells were collected, lipids extracted and subjected to click-reaction to Coumarin-azide. Lipids were separated on a HPTLC silica plate and separated fluorescent lipids were detected using an Amersham Imager 600 with excitation at 460 nm and a Cy2 Emission Filter (525BP20). **B. Quantification of detected pacSph-derived lipid species.** PacSph-derived sphingolipid species were quantified using Fiji and are shown as relative intensity per species to total paclipids. Shown is the mean ± SEM of four independent experiments. Multiple t-tests were performed and corrected for multiple comparisons with the Holm-Sidak method. **C. Quantification of VLCFA SM and LCFA SM.** PacSph-derived sphingolipid species were quantified using Fiji and are shown as relative intensity per species to total paclipids. Shown is mean ± SEM of four independent experiments. **D. Protein-lipid pulldown analysis of endogenous proteins with and without FB1 treatment.** HeLa *SGPL1*$^{-/-}$ cells were treated with 50 µM FB1 for 20 h prior labelling. Labelling was done with 0.5 µM pacSph for 4 h. After subsequent UV-crosslinking, cell lysis, CuAAC-based click-reaction to Biotin-azide,

enrichment of PL-PD on Neutravidin beads, elution (95%) and input (5%) samples were loaded on an SDS-PAGE gel, blotted and endogenous proteins were detected with specific antibodies. **E. Quantification of Western blot signals.** Protein amount in elution compared to input values. Shown are individual data points that are connected within one experiment. Data represent four (DAG1), three (STX6) or two (ITGB1) independent experiments. Two-sided paired t-tests were performed. * = p<0.05, ** = p<0.001. VLCFA, very-long chain fatty acid; LCFA, long chain fatty acid; Cer, ceramide; HexCer, hexosylceramide; Sph, sphingosine; SM, sphingomyelin; FB1, Fumonisin B1

3.3. Investigation of Class-Specific Protein-Sphingolipid Interactions

The metabolism of pacSph results in the synthesis of different pacSL classes[113]. Therefore, it was not possible to delineate the specific lipid class that was interacting with the identified proteins from the proteomic approach. To investigate the class-specific protein-lipid interactions different strategies like inhibiting pathways in the pacSph metabolism as well as labelling with a combination of clickable sugar analogues and photo-crosslinkable sphingosine were employed.

3.3.1. Modifying pacSph Metabolism with siRNAs

The metabolism of lipids can be modulated by different methods. Section 3.2.5 describes the application of FB1 to diminish the metabolism of pacSph. To inhibit specific pathways of the SL metabolism, siRNA-mediated knockdowns were applied. SiRNAs against Phosphatidylcholine: ceramide cholinephospho-transferase (SGMS1) which is catalysing the formation of SM through transfer of the phosphatidyl head group from phosphatidylcholine to the primary hydroxyl of ceramide[91] was used. In addition, siRNAs against Ceramide Glucosyltransferase (UGCG), catalysing the transfer of glucose from UDP-glucose to ceramide[91], were deployed. To investigate the successful inhibition of selected pathways in pacSph metabolism, a HPTLC analysis was performed. HeLa *SGPL1*$^{-/-}$ cells were treated with siUGCG and siSGMS1 and after 48 h, cells were labelled with 6 µM pacSph for 4 hours. Samples were collected, lipids were extracted, pacSph-derived lipids were clicked to Coumarin-azide, separated on a HPTLC-Silica plate and the resulting fluorescent paclipids were detected. A significant reduction of pacHexCer lipids in siUGCG treated cells was achieved (-67%; Figure 3.11 A, B) whereas for SM only a minor non-significant reduction was observed (-21%; Figure 3.11 A, B).

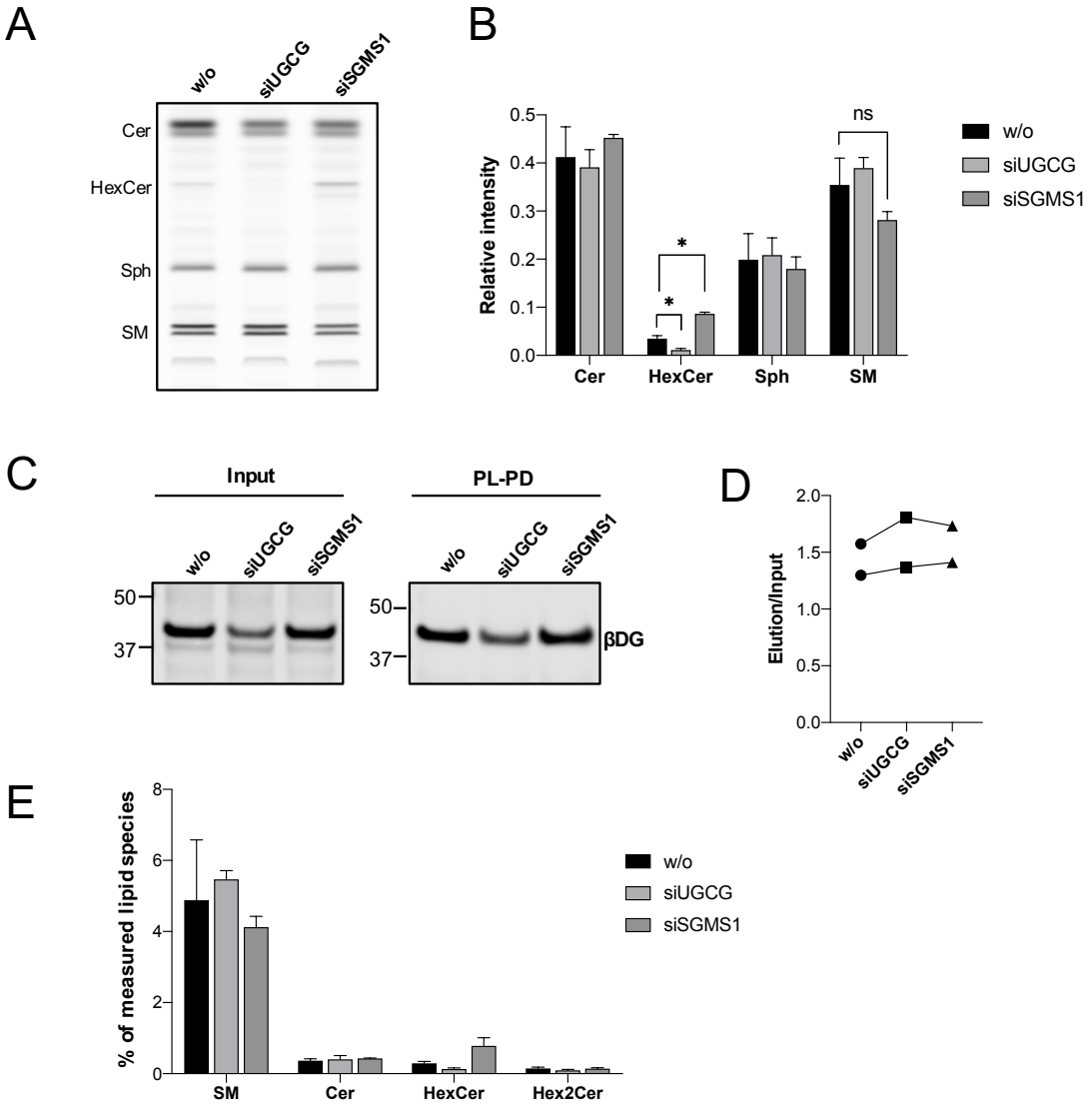

Figure 3.11 Influence of siRNA Treatment on pacSph Metabolism and Protein-Lipid Pulldown A. HPTLC analysis of pacSph metabolism with siRNA treatment. HeLa *SGPL1*$^{-/-}$ cells were transfected with 50 nM siRNA for 48 h. Labelling was done with 6 µM pacSph for 4 h. Cells were collected, lipids were extracted and subjected to click-reaction to Coumarin-azide. Lipids were separated on a HPTLC silica plate and separated fluorescent lipids were detected using an Amersham Imager 600 with excitation at 460 nm and a Cy2 Emission Filter (525BP20). **B. Quantification of detected pacSph-derived lipid classes.** PacSph-derived sphingolipid species were quantified using Fiji and are shown as relative intensity per species to total paclipids. Shown is the mean ± SEM of four independent experiments. Two-sided unpaired t-tests were performed. * = p<0.05, ** = p<0.001. **C. Protein-lipid pulldown analysis of endogenous proteins with and without siRNA treatment.** HeLa SGPL1$^{-/-}$ cells were transfected with 50 nM siRNA for 48 h. Labelling was done with 0.5 µM pacSph for 4 h. After subsequent UV-crosslinking, cell lysis, CuAAC-based click-reaction to Biotin-azide, enrichment of PL-PD on Neutravidin beads, elution (95%) and input (5%) samples were loaded on an SDS-PAGE gel, blotted and endogenous proteins were detected with an specific antibody. **D. Protein amount in elution compared to input values**. Shown are individual data points that are connected within one experiment. Two replicates for each treatment were performed. **E. Lipidomic analysis of sphingolipid species.** Samples were prepared as described for A. Measurements were done with an QTRAP 6500+, quantification by comparing to internal standards. Shown is the class distribution of sphingolipids. Data are represented as mean ± SD of two independent experiments. Lipidomic measurement was performed by Christian Lüchtenborg. SM, sphingomyelin, Cer, ceramide; HexCer, hexosylceramide; Hex2Cer, Lactosylceramide; Sph, Sphingosine.

Even though only a minor inhibition of the SGMS1 synthesis was detectable, the synthesis of HexCer was strongly elevated in the presence of siRNAs targeting SGMS1 (>2.5 fold; Figure 3.11 A-B). The same effect was observed for endogenous lipid classes monitored by mass spectrometric analysis (Figure 3.11 E). As HexCer was significantly reduced by this treatment, we decided to investigate how this treatment affects the interaction of selected proteins with pacSLs. HeLa *SGPL1*$^{-/-}$ cells were treated with siUGCG and siSGMS1 and were labelled with 0.5 µM pacSph. Cells were subjected to UV-crosslinking, cell lysis, click-reaction of the protein-lipid complexes to Biotin and enrichment of protein-SL-Biotin products on Neutravidin beads. Input and PL-PD samples were loaded on an SDS-PAGE gel, blotted and endogenous proteins were detected using specific antibodies. βDG-SL interactions appeared not altered when modifying the pacSph metabolism with siRNAs (Figure 3.11 C, D).

3.3.2. Application of Knockout Cells to Investigate Class-Specific Lipid-Protein Interactions

As described in section 3.3.1, the usage of siRNAs already resulted in a strong reduction of HexCer species labelling. The inhibition of complete SL metabolism pathways was tested in which a possible background signal from the remaining lipid classes was circumvented. Since HeLa cells require SGMS1 for growth[18], it was not possible to target the SM metabolism in these cells by knocking out *SGMS1* or *SGMS2*. To target GlcCer and higher GSLs, a HEK *SGPL1*$^{-/-}$ *UGCG*$^{-/-}$ cells was established by P. Haberkant, EMBL, and these cells were provided for this study. UGCG is catalysing the formation of Glucosylceramide (GlcCer) and therefore this lipid and all downstream lipids are depleted in *UGCG* knockout cells[164]. The short labelling time of 4 h with pacSph resulted in only minor amounts of pacHexCer and presumably downstream GSLs (usually the amount of GlcCer was about 5% of total paclipids, see figure 3.11 B). Therefore, an extended labelling time with a lower concentration of pacSph was tested.

Initially, the difference between the short and long labelling time on the pacSph metabolism was analysed. HEK *SGPL1*$^{-/-}$ cells and HEK *SGPL1*$^{-/-}$ *UGCG*$^{-/-}$ cells were labelled with 6 µM pacSph for 4 h or 0.5 µM for 24 h. Lipids were extracted, clicked to Coumarin-azide, separated on a HPTLC-Silica plate and the resulting fluorescent paclipids were detected. The paclipid profile of labelling with 6 µM

pacSph revealed a complete lack of HexCer paclipids in HEK *SGPL1*$^{-/-}$ *UGCG*$^{-/-}$ cells (Figure 3.12 A-B). Labelling with 0.5 µM pacSph resulted in a different pacSph labelling behaviour compared to 6 µM pacSph (Figure 3.12 A). The added pacSph was almost completely metabolised. Ceramide and HexCer appeared to be strongly metabolised to downstream lipids (Figure 3.12 A, C). Higher GSLs could not be detected by HTPLC analysis but were synthesised as shown by mass spectrometric analysis (Master thesis, Timo Sachsenheimer, AG Brügger[165]). The longer incubation with 0.5 µM pacSph yielded 6 times as much pacGM3 compared to shorter incubation times with higher concentrations[165]. Interestingly, both cell lines showed differences in the incorporation rate of pacSph into LCFA and VLCFA SM (Figure 3.12 C). Strikingly, HEK *SGPL1*$^{-/-}$ cells synthesized significantly more VLCFA SM than LCFA SM with 0.5 µM pacSph for 24 h, which was not observed for HEK *SGPL1*$^{-/-}$ *UGCG*$^{-/-}$ cells and for the short labelling time in both cell lines (Figure 3.12 C).

To subsequently analyse an interaction of selected proteins with GlcCer and also higher GSLs, HEK *SGPL1*$^{-/-}$ cells and HEK *SGPL1*$^{-/-}$ *UGCG*$^{-/-}$ cells were labelled with the lower pacSph concentration for a longer incubation time. The cells were subjected to UV-crosslinking, cell lysis, click-reaction of the protein-lipid complexes to Biotin and enrichment of protein-SL-Biotin products on Neutravidin beads. Input and PL-PD samples were loaded on an SDS-PAGE gel, blotted and endogenous proteins were detected using specific antibodies. Solely the upper band of ITGB1 was pulled down as protein-lipid complex when labelling for 24 h with pacSph (Figure 3.12 D). HEK *SGPL1*$^{-/-}$ *UGCG*$^{-/-}$ cells showed a significantly reduced interaction of ITGB1 with pacSph-derived SLs, whereas STX6 and βDG were not altered in their protein-lipid interaction (Figure 3.12 D, E).

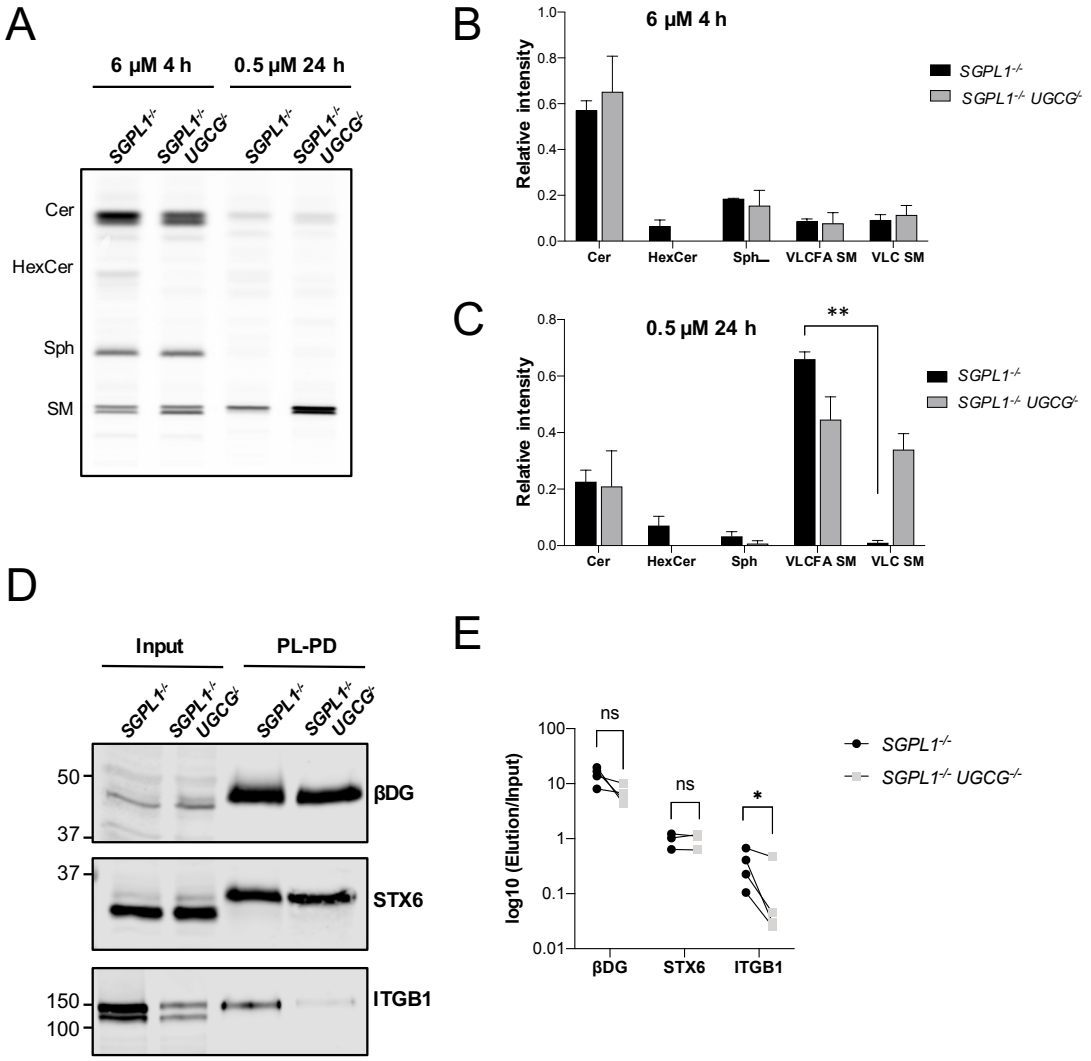

Figure 3.12 Analysis of Class Specific Protein-Lipid Interactions using UGCG knockout cells A. HPTLC analysis of pacSph metabolism in UGCG knockout cells. HEK *SGPL1*$^{-/-}$ cells and HEK *SGPL1*$^{-/-}$ *UGCG*$^{-/-}$cells were labelled with 6 µM pacSph for 4 h or 0.5 µM pacSph for 24 h. Cells were collected, lipids were extracted and subjected to click-reaction to Coumarin-azide. Lipids were separated on a HPTLC silica plate and separated fluorescent lipids were detected using an Amersham Imager 600 with excitation at 460 nm and a Cy2 Emission Filter (525BP20). **B-C. Quantification of detected pacSph-derived lipid classes.** PacSph-derived sphingolipid species were quantified using Fiji and are shown as relative intensity per species to total paclipids. Shown is mean ± SEM of two (B) or three (C) independent experiments. Multiple t-tests were performed and corrected for multiple comparisons using the Holm-Sidak method. **D. Protein-lipid pulldown analysis of endogenous proteins in UGCG knockout cells**. HEK *SGPL1*$^{-/-}$ cells and HEK *SGPL1*$^{-/-}$ *UGCG*$^{-/-}$ cells were labelled with 0.5 µM pacSph for 24 h After subsequent UV-crosslinking, cell lysis, CuAAC-based click-reaction to Biotin-azide, enrichment of PL-PD on Neutravidin beads, elution (95%) and input (5%) samples were loaded on an SDS-PAGE gel, blotted and endogenous proteins were detected with specific antibodies. For ITGB1, only the upper band was quantified. **E. Protein amount in elution compared to input values**. Shown are individual data points that are connected within one experiment. Four (βDG) three (STX6) or four (ITGB1) independent experiments were performed. Two-tailed paired t-tests were performed. * = p<0.05, ** = p<0.001. SM, sphingomyelin, Cer, ceramide; HexCer, hexosylceramide; Sph, Sphingosine; VLCFA, very-long chain fatty acid; LCFA, long chain fatty acid.

To exclude an influence of the knockout on the endogenous localisation of the analysed proteins, an immunofluorescence staining and confocal microscopy was performed. Differently to HeLa cells (Figure 3.6), βDG localisation in HEK cells looked like being in endosomal vesicles. There was no difference in the βDG localisation between HEK *SGPL1*$^{-/-}$ cells and HEK *SGPL1*$^{-/-}$ *UGCG*$^{-/-}$ knockout cells (Figure 3.13).

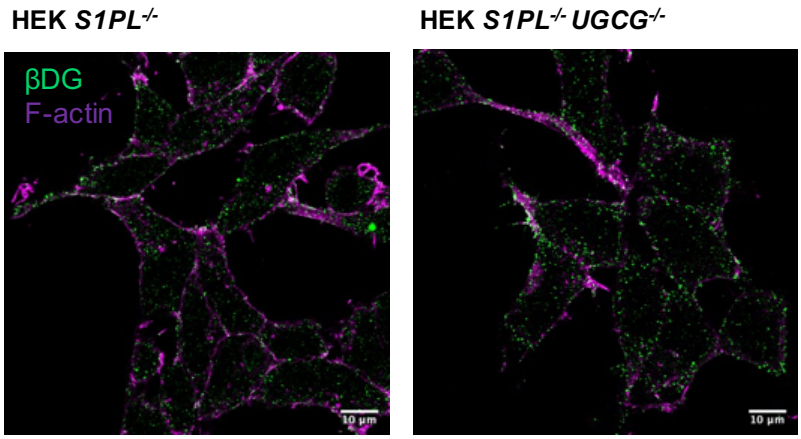

Figure 3.13 Confocal Microscopy of β-Dystroglycan Localisation in HEK Cells
HEK *SGPL1*$^{-/-}$ and HEK *SGPL1*$^{-/-}$ *UGCG*$^{-/-}$ cells were seeded on collagen, fixed and blocked. Cells were stained with specific antibodies against endogenous proteins and with anti-primary species Alexa488 as well as with F-actin using Phalloidin-Alexa647 to localise the cells. After preparation for confocal microscopy, slides were imaged with a Zeiss LSM 800. Scale bar: 10 µm.

3.4. Influence of the Transmembrane Domain of β-Dystroglycan in the Interaction with Sphingolipids

There are a few examples where proteins are described to interact with lipids specifically with amino acids of the transmembrane domain (TMD)[72,166]. The performed proteomic approach identified proteins interacting with SLs with a specific fatty acid lengths[124]. The TMD-length analysis of identified proteins did not reveal an enrichment of particularly long TMDs, nor was a specific interaction motif discovered (Section 3.1). Therefore, specific amino acids were considered to be important for individual protein-SL interactions. As βDG has been successfully validated as a SL-interacting protein, its TMD was subjected to further analysis. As a first step towards the investigation of individual amino acids in protein-lipid interactions, the complete TMD of βDG was exchanged with TMDs of other proteins that are described to not interact with SLs or are likewise localised to the

plasma membrane. Furthermore, HeLa DAG1 knockout cells were generated to test if the overexpression of DAG1 shows an improved endogenous localisation.

3.4.1. Protein-Lipid Interaction Analysis of Transmembrane Domain-Swapped β-Dystroglycan Constructs

βDG was identified and successfully validated to interact with VLCFA SLs. TOPCONS[167] analysis predicted a TMD length of 21 amino acids (Supplementary Figure 7.1). These 21 amino acids were replaced with 21 amino acids of the TMDs from CD63 TMD3, Cd8a, and ASGR1 as depicted in figure 3.14 A. To get first insights into the role of the TMD in protein-VLCFA SL interactions, the overexpression of FLAG-tagged constructs in HeLa *SGPL1*$^{-/-}$ *CERS2*$^{-/-}$ cells and the parental HeLa *SGPL1*$^{-/-}$ cells was performed although overexpression artefacts were previously described (Section 3.2.1).

Plasmids with FLAG-tagged TMD-swapped DAG1 constructs were transfected for 24 h prior labelling with pacSph. The samples were subjected to UV-crosslinking, cell lysis, click-reaction of the protein-lipid complexes to Biotin and enrichment of protein-SL-Biotin products on Neutravidin beads. Input and protein-lipid pulldown (PL-PD) samples were loaded on an SDS-PAGE gel, blotted and FLAG-tagged proteins were detected using anti-FLAG antibodies. Strikingly, instead of a reduced interaction of TMD-swapped constructs with SLs, all swap-mutants showed a stronger interaction (Figure 3.14 B-C) in HeLa *SGPL1*$^{-/-}$ cells compared to wild-type DAG1. Noticeable, the protein-lipid pulldown of swapped DAG1 constructs was varying stronger than wild-type DAG1 as visualized by individual data points in the bar chart of figure 3.14 C. Interestingly, for all mutants, a reduced binding of DAG1 to pacSLs in HeLa *SGPL1*$^{-/-}$ *CERS2*$^{-/-}$ cells could still be suggested, expect for the CD63TMD3swap mutant.

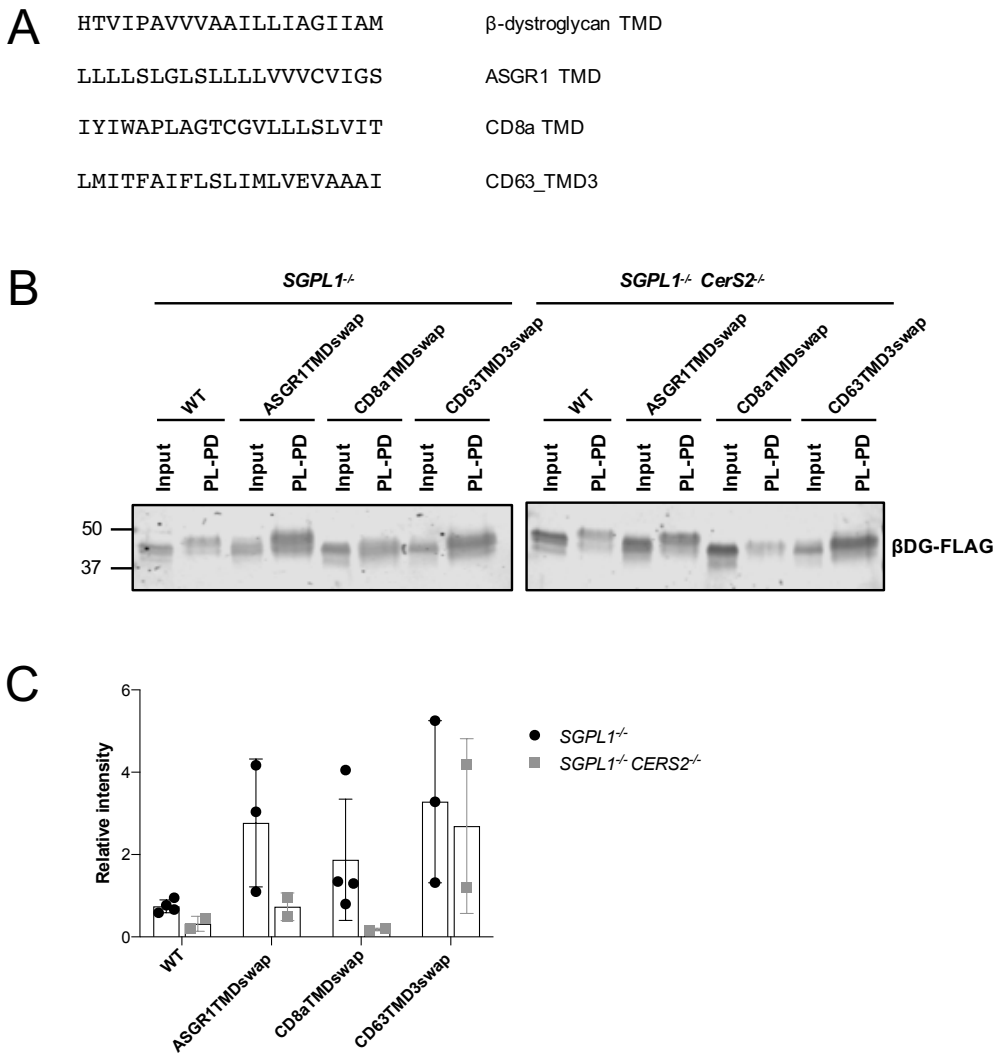

Figure 3.14 Influence of the TMD in Dystroglycan-Sphingolipid Interactions
A. Design of β-dystroglycan TMD swap mutants. Depicted are the 21 TMD amino acids that were replaced with 21 amino acids of the TMDs from ASGR1, CD8a and CD63 TMD3. **B. Protein-lipid pulldown analysis of overexpressed proteins.** HeLa *SGPL1*$^{-/-}$ and HeLa *SGPL1*$^{-/-}$ *CERS2*$^{-/-}$ cells were transiently transfected with pBJ5-DAG1 (wild-type or swap)-FLAG plasmids for 24 h. The last 4 h, the media was removed and replaced with media containing 6 µM pacSph. After subsequent UV-crosslinking, cell lysis, CuAAC-based click-reaction to Biotin-azide, enrichment of PL-PD on Neutravidin beads, elution (95%) and input (5%) samples were loaded on SDS-PAGE gel, blotted and FLAG proteins were detected with an anti-FLAG antibody. **C. Quantification of Western blot signals.** Protein amount in elution compared to input values. Shown is the mean ± SD of at three independent experiments for HeLa *SGPL1*$^{-/-}$ and two independent experiments for HeLa *SGPL1*$^{-/-}$ *CERS2*$^{-/-}$ cells including individual data points.

3.4.2. Generation of HeLa DAG1 Knockout Cells to Study Lipid-Protein Interactions of Overexpressed Swap Mutants

As the overexpression of DAG1-FLAG in HeLa SGPL1$^{-/-}$ cells resulted in mislocalisations (Section 3.2.1), a knockout of endogenous DAG1 in HeLa SGPL1$^{-/-}$ cells was designed to possibly obtain an improved localisation for protein-lipid

pulldown studies. To knockout DAG1 with CRISPR-Cas9, a sgRNA with very few off-target sites was designed using CCTop[168]. The sgRNA target sequence and localisation on DAG1 gene and CDS are displayed in figure 3.15 A. Oligos were designed, and cloned into a Cas9-GFP containing plasmid[169]. HeLa wild-type and HeLa *SGPL1*$^{-/-}$ cells were transiently transfected and sorted for GFP positive cells. Single cell-derived cell populations were analysed by Western blot analysis. For each cell type, a clone that did not show any βDG signal was obtained (Figure 3.15 B). The expression of plasmids from section 3.4.1 were used for overexpression in the newly established *DAG1* knockout cells. HeLa *SGPL1*$^{-/-}$ and HeLa *SGPL1*$^{-/-}$ *DAG1*$^{-/-}$ cells were transfected with wild-type FLAG-tagged DAG1 and CD8a-TMD swapped FLAG-tagged DAG1 constructs. After labelling with pacSph, cells were subjected to UV-crosslinking, cell lysis, click-reaction of the protein-lipid complexes to Biotin and enrichment of protein-SL-Biotin products on Neutravidin beads. Input and PL-PD samples were loaded on an SDS-PAGE gel, blotted and FLAG-tagged proteins were detected using anti-FLAG antibodies. HeLa *SGPL1*$^{-/-}$ *DAG1*$^{-/-}$ cells showed lower signals compared to HeLa SGPL1$^{-/-}$cells (Figure 3.15 C). So far, there was no striking difference in protein-SL interactions between the wild-type and swap mutant detectable in HeLa *SGPL1*$^{-/-}$ *DAG1*$^{-/-}$ cells (Figure 3.15 D). However, it appeared that the protein-lipid pulldown of the swap-construct in HeLa *SGPL1*$^{-/-}$ *DAG1*$^{-/-}$ cells is now comparable to the protein-lipid pulldown of the wild-type construct. Before, the swap constructs showed an increased protein-lipid interaction in HeLa *SGPL1*$^{-/-}$ cells compared to wild-type constructs (Section 3.4.1, figure 3.14 C).

To compare the localisation of overexpressed DAG1 between HeLa *SGPL1*$^{-/-}$ and HeLa *SGPL1*$^{-/-}$ *DAG1*$^{-/-}$ cells, transfected cell samples for immunofluorescence analysis and confocal microscopy analysis were generated. More FLAG-tagged βDG appeared to be in vesicular compartments of HeLa *SGPL1*$^{-/-}$ cells compared to HeLa *SGPL1*$^{-/-}$ *DAG1*$^{-/-}$ cells, whereas HeLa *SGPL1*$^{-/-}$ *DAG1*$^{-/-}$ cells seemed to show a rather strong Golgi and ER-localisation (Figure 3.14 E). Again, both protein variants appeared to be located at the plasma membrane. Summarizing, even though DAG1 was knocked out, the overexpression was still exceeding the amount of tolerable protein levels to mostly obtain a plasma membrane localisation, as for the endogenous protein.

Conclusively, it appeared that the DAG1 knockout may had an improved cellular localisation as seen in protein-lipid pulldown assays and confocal microscopy analysis. However, the influence of the TMD on the interaction of DAG1 with SLs is either not influenced by the TMD or the performed assay is not suitable to delineate this question.

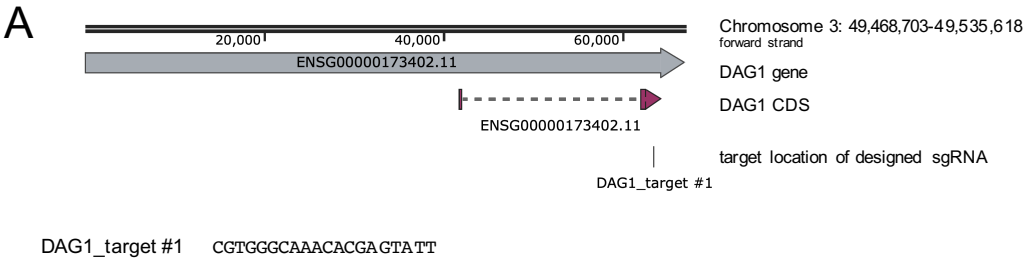

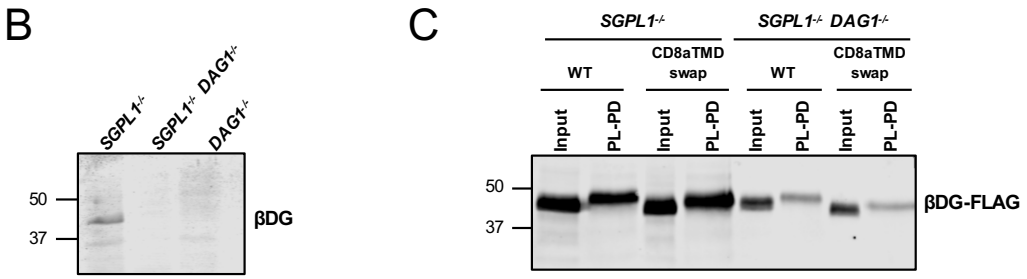

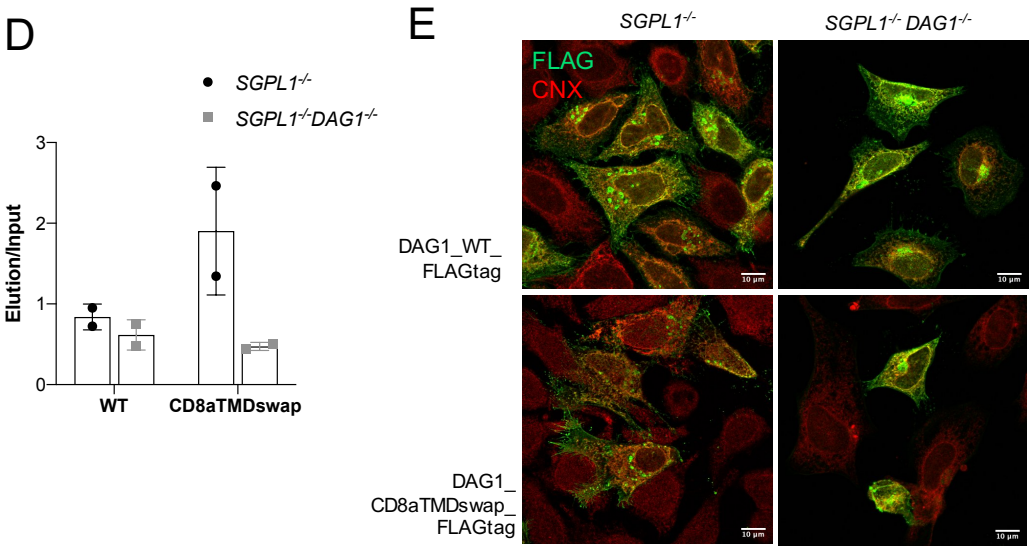

Figure 3.15 CRISPR-Cas9 Knockout of DAG1 in HeLa Cells to Investigate Lipid-DAG1 Interactions with Overexpression
A. SgRNA sequence and localisation on human *DAG1* gene. **B. Western blot analysis of total cell lysates**. HeLa *SGPL1*$^{-/-}$, HeLa *SGPL1*$^{-/-}$ *DAG1*$^{-/-}$ and HeLa *DAG1*$^{-/-}$ cells were seeded, collected, lysed and 50 µg total protein was loaded on an SDS-PAGE gel, blotted and endogenous

βDG was detected. **C. Protein-lipid pulldown analysis of overexpressed proteins.** HeLa *SGPL1*$^{-/-}$ and HeLa *SGPL1*$^{-/-}$ *DAG1*$^{-/-}$ cells were transiently transfected with pBJ5-DAG1 (wild-type or swap)-FLAG plasmids for 24 h. The last 4 h, the media was removed and replaced with media containing 6 µM pacSph. After subsequent UV-crosslinking, cell lysis, CuAAC-based click-reaction to Biotin-azide, enrichment of PL-PD on Neutravidin beads, elution (95%) and input (5%) samples were loaded on an SDS-PAGE gel, blotted and FLAG proteins were detected with an anti-FLAG antibody. Shown is a representative blot of two independent replicates. **D. Quantification of Western blot signals.** Protein amount in elution compared to input values. Shown is mean ± SD of at two independent experiments including individual data points. **E. Confocal microscopy analysis of overexpressed DAG1 swap constructs.** HeLa *SGPL1*$^{-/-}$ and HeLa *SGPL1*$^{-/-}$ *DAG1*$^{-/-}$ cells were transiently transfected with pBJ5-DAG1 (wild-type or swap)-FLAG plasmids for 24 h. Cells were fixed and blocked, to stain the cells with specific antibodies against FLAG-tag and anti-CNX (to visualise ER). After preparation for confocal microscopy, slides were imaged with a Zeiss LSM 800. Scale bar: 10 µm. CNX, Calnexin.

3.5. Role of Dystroglycan and VLCFA-SLs in Oligodendrocytes

Out of 53 identified putative very long chain fatty acid interacting proteins, four protein-SL interactions were successfully validated (Section 3.2). STX6 and βDG and were further characterised with respect to their association in lipid nanodomains (Section 3.2). For βDG, STX6 and ITGB1 first attempts to identify the class of the interacting lipid were made (Section 3.3). For βDG the involvement of the TMD in lipid interactions was investigated (Section 3.4). To further elucidate a novel role of a herein identified protein-SL interaction, βDG was chosen for functional studies. The selection was based on literature research and the successful validation.

VLCFA SLs are synthesized by CerS2 which is strongly expressed in brain during active myelination[34]. Resulting VLCFA SLs are described to be important for myelin stability, however, the underlining molecular mechanism promoting this stability remain unknown so far[54]. The expression of dystroglycan is increasing during active myelination in OLGs and a role of dystroglycan in myelin stability is suggested[134]. Thus, the possible role of a VLCFA SL-βDG interaction in OLGs was investigated. Oli-*neu* cells, an immortalized mouse OLG cell line, were provided for this work (E. Krämer, University Mainz)[170]. Firstly, phenotypic changes of differentiating Oli-*neu* cells upon the addition of cAMP analogues as well as lipidomic changes were investigated. Secondly, knockout cells were generated to study protein-lipid interactions and potential phenotypic alterations.

3.5.1. Oli-*neu* cells are Forming Sheets and Show Increasing VLCFA Sphingolipid Levels upon Differentiation

OLGs synthesize a specialized membrane which enwraps axons to provide a fast conduction of action potentials and axonal integrity[33]. To study roles of lipids in their ability to regulate the cellular localisation of proteins, Oli-*neu* cells were chosen. For this purpose the changes between differentiated and undifferentiated Oli-*neu* cells was analysed with respect to their phenotype in immunofluorescence staining with confocal microscopy as well as their lipidomic profile changes. Oli-*neu* cell differentiation is initiated by the addition of a dibutyryl cAMP (dbcAMP) *in vitro*[170].

During the formation of myelin membranes, OLGs change from a mostly bipolar or multipolar shape to a highly arborized structure of pre-myelinating OLGs[171]. The newly established protrusions are developing membranous sheets of mature OLGs *in vitro*[172]. To investigate the morphological changes of Oli-*neu* cells during differentiation, Oli-n*eu* cells were seeded and treated with dbcAMP for differentiation *in vitro*. After 0, 3 or 5 days of treatment, the cells were prepared for immunofluorescence analysis and confocal microscopy. The localisation of actin was visualised as the cytoskeleton is crucial for extension of protrusions[173] and therefore able to clearly visualise processes. Upon stimulation of differentiation with dbcAMP, Oli-*neu* cells were forming highly arborized protrusions (after 3 days) which were finally developing membranous sheets (after 5 days, figure 3.16).

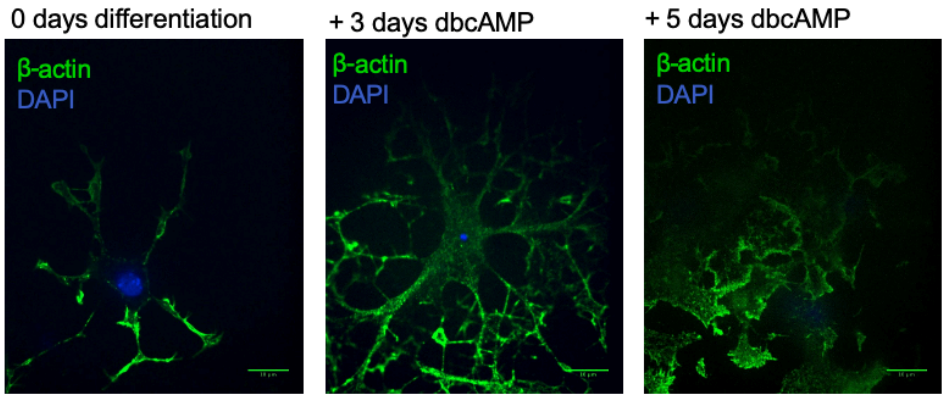

Figure 3.16 Confocal Microscopy of Differentiating Oli-*neu* cells
Oli-*neu* cells were treated as indicated with 100 mM dbcAMP for 0/3/5 days. Cells were fixed and blocked, to stain cells with specific antibodies against β-actin and DAPI to visualize nuclei. After preparation for confocal microscopy, the slides were imaged with a Zeiss LSM 800. Scale bar: 10 µm.

Quantitative differences of lipid species between undifferentiated OLGs and mature myelin are partly described[174,175], however, especially the initial changes during myelination are not addressed so far. Therefore Oli-*neu* cells were seeded and treated or not-treated with dbcAMP to investigate the lipidomic changes during the first phase of myelination *in vitro*. The lipid distribution of differentiated versus undifferentiated Oli-*neu* cells revealed a significant increase of ether-linked phosphatidylcholine (ePC) upon treatment. Furthermore, a trend of an accumulation of HexCer, sulfatide (SGalCer), and ethanolamine plasmalogen (pl-PE) with 18:0 fatty acids was detectable, whereas cholesterol was reduced by initiation of differentiation with dbcAMP (Figure 3.17 A). The most abundant lipid classes are PC (41 %), aPE, PS, and PI (about 10 %) and cholesterol (17 to 10 %, in undifferentiated and differentiated samples, respectively). GSLs were present in minor amounts (about 0.4% to 1 %, in undifferentiated and differentiated samples, respectively). A minor elevation of sulfatide by differentiation could be suggested, whereas the ganglioside species GD3 and GM3 appeared to be diminished upon differentiation (Figure 3.17 B). Focussing on the double bond distribution of all measured lipids, mono-unsaturated lipids and lipids with two double bonds were increasing while lipids with 5, 6, 7 or more double bonds were significantly decreasing (Figure 3.17 C).

The species distribution within PC and ethanolamine plasmalogen (pl-PE) revealed an enrichment of lipids with especially C18 FAs (Figure 3.18 A, B). PC 34:1 was most likely representing of C16 and C18 FAs and increased strongly upon differentiation. PC 36:1 and PC 36:2 also increased strongly, which likely consist of two FAs with C18 and varying double bond number (Figure 3.18 A). The pl-PE analysis allowed the direct analysis of FA chain composition. Here, the elevation of C18 FAs became decisive as P-18:0/18:1, P-18:0/20:1 and P-18:0/20:3 were significantly increasing. Again, The strong decrease of polyunsaturated lipids with more than two double bonds is detectable (Figure 3.18 B).

Examining the distribution of individual SL species, elevated VLCFA SL species were observed (Figure 3.19 A-C). These included HexCer 40:1;2, HexCer 42:1;2 and SM 42:1;2. Also C18 FA-containing SLs were enriched, like HexCer 36:1;2 and SM 36:1;2. However, as the bars show high errors, not all strong changes were significant.

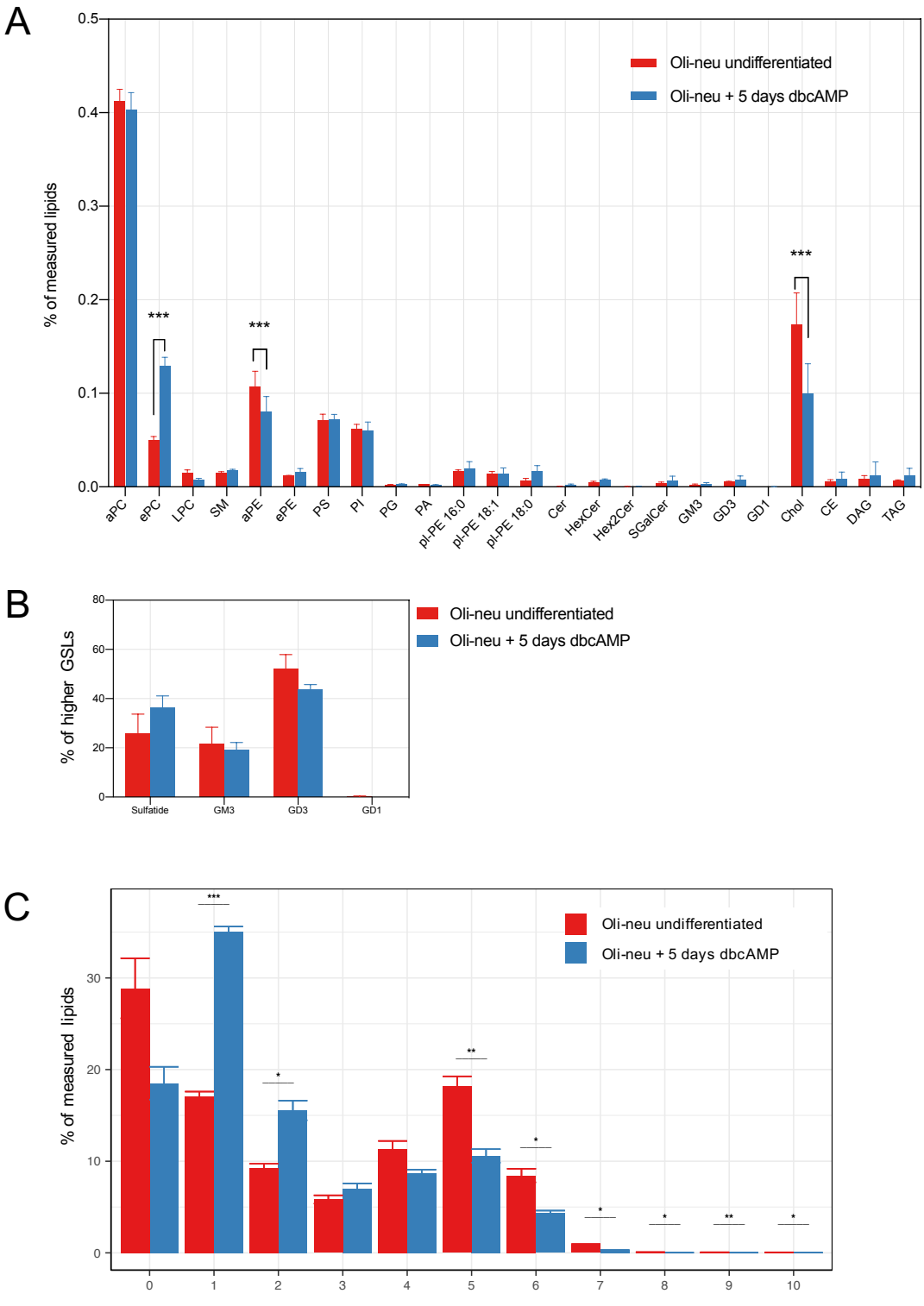

Figure 3.17 Lipidomic Analysis of Differentiating Oli-*neu* Cells
Oli-*neu* cells were treated with 100 mM dbcAMP for 0 or 5 days and lipids were extracted with internal standards for lipidomic analysis. **A. Distribution of all measured lipids. B. Distribution of higher GSL species. C. Distribution of double bond frequency of all measured lipids.** X-axis*:* double bond number in fatty acid of lipids. Data represent mean ± SEM of three independent experiments. Two-tailed unpaired t-tests were performed. * = p<0.05, ** = p<0.002, ***<0.001. aPC, phosphatidylcholine, ePC, ether-linked phosphatidylcholine; LPC, lyso-phosphatidylcholine; SM, sphingomyelin; aPE, ester-linked phosphatidylethanolamine; ePE, ether-linked phosphatidylethanolamine; PS, phosphatidylserine; PI, phosphatidylinositol; PG, phosphatidyl-

glycerol; PA, phosphatidic acid; pl-PE, ethanolamine plasmalogen; Cer, ceramide; HexCer, hexosylceramide; Hex2Cer, lactosylceramide; SGalCer, sulfatide; GM3, monosialodihexosylganglioside; GD1 and GD2, disialodihexosylganglioside; Chol, cholesterol; CE, cholesterol ester; DAG, triacylglycerol; TAG, triacylglycerol. Lipid species were annotated according to their molecular composition as follows: sum of carbon atoms in the FAs:sum of double bonds in the FAs. Lipidomic measurements were performed by Christian Lüchtenborg and Timo Sachsenheimer.

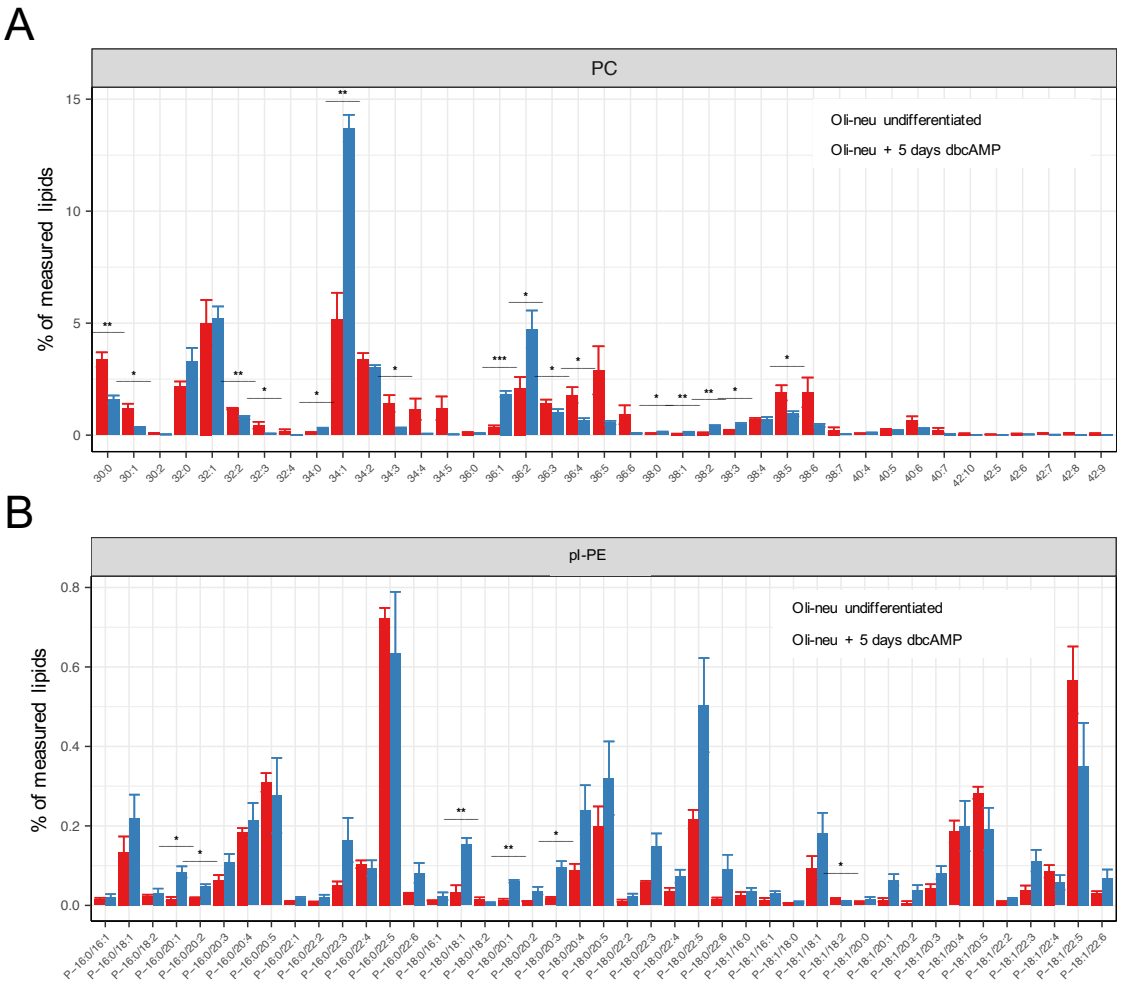

Figure 3.18 Glycerophospholipid Species Profiles of Differentiating Oli-*neu* Cells
Oli-*neu* cells were treated with 100 mM dbcAMP for 0 or 5 days and lipids were extracted with internal standards for lipidomic analysis. **A. Distribution of phosphatidylcholine species B. Distribution of ethanolamine plasmalogen species.** Data represent the mean ± SEM of three independent experiments. Two-tailed unpaired t-tests were performed. * = p<0.05, ** = p<0.002, ***<0.001. pl-PE, ethanolamine plasmalogen; PC, phosphatidylcholine. Lipid species were annotated according to their molecular composition as follows: sum of carbon atoms in the FAs:sum of double bonds in the FAs. Lipidomic measurements were performed by Christian Lüchtenborg.

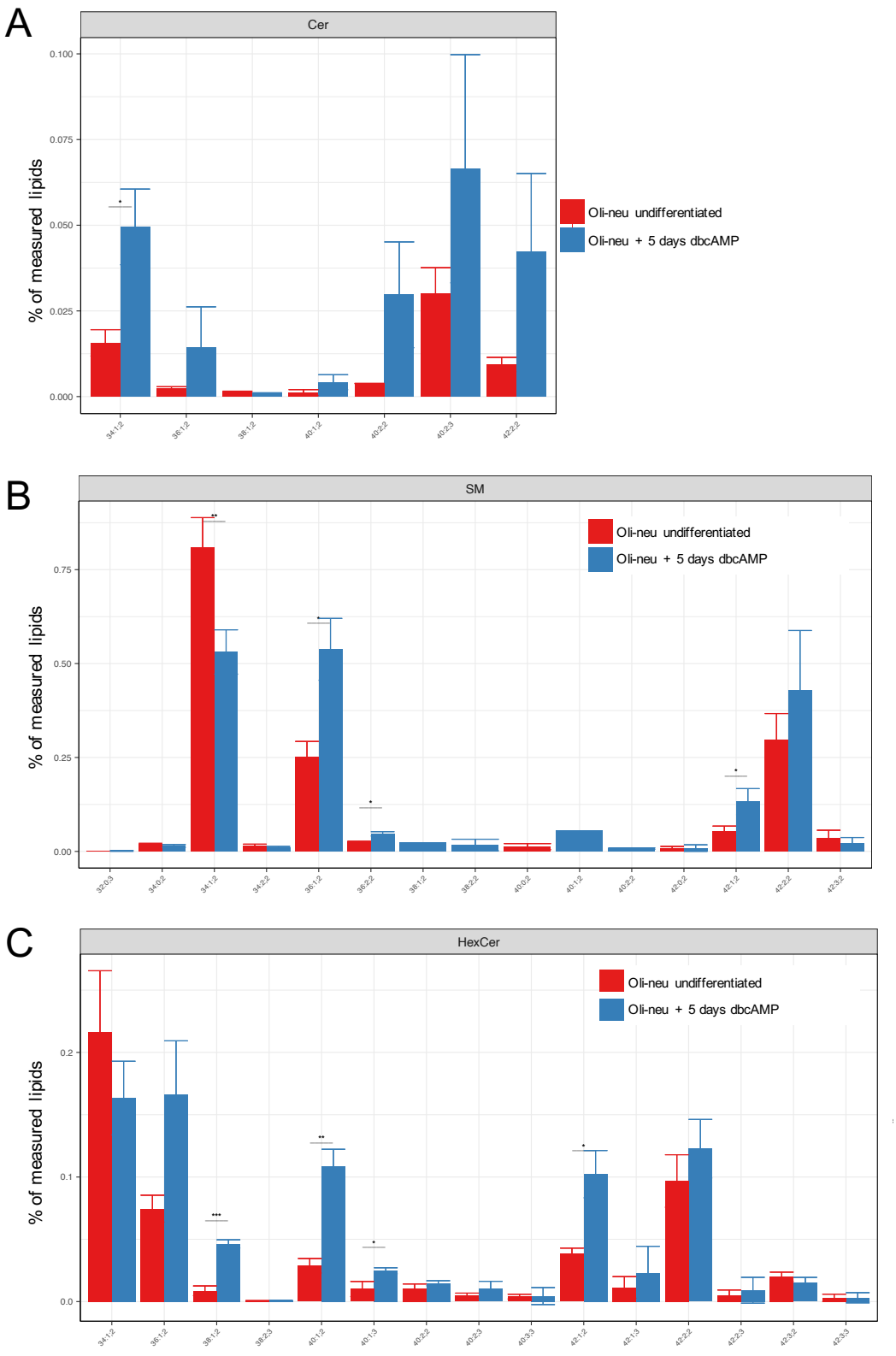

Figure 3.19 Sphingolipid Species Profiles of Differentiating Oli-*neu* Cells
Oli-*neu* cells were treated with 100 mM dbcAMP for 0 or 5 days and lipids were extracted with internal standards for lipidomic analysis. **A. Distribution of ceramide species compared to all measured lipids B. distribution of SM species compared to all measured lipids C. Distribution of HexCer species compared to all measured lipids.** Data represent mean ± SEM of three independent experiments. Two-tailed unpaired t-tests were performed. * = $p<0.05$, ** = $p<0.002$, ***<0.001. Cer, ceramide; HexCer, hexosylceramide; SM, sphingomyelin. Lipid species

were annotated according to their molecular composition as follows: sum of carbon atoms in the FAs:sum of double bonds in the FAs;sum of hydroxyl groups in the long-chain base and the FA moiety. Lipidomic measurements were performed by Christian Lüchtenborg.

3.5.2. CRISPR-Cas9 Knockout of SGPL1, CERS2 and DAG1

In order to investigate protein-SL interactions in Oli-*neu* cells by employing the bifunctional sphingosine, as for HeLa cells (Section 3.2)[115], a SGPL1 knockout was required. This knockout should prevent the degradation of sphingoid bases at the C2-C3 position and thereby the loss of the functionalised groups into the GPL pathway[115]. To knockout SGPL1 with CRISPR-Cas9, two sgRNAs with very few off-target sites were designed using CCTop[168]. The sgRNA target sequences and localisations on the mouse *SGPL1* gene and CDS are displayed in figure 3.20 A. Oligos were designed, and cloned into a Cas9-GFP containing plasmid[169]. Oli-*neu* cells were transiently transfected and sorted for GFP positive cells. Single cell-derived cell populations were analysed by sequencing the genomic DNA of targeted locus as well as HPTLC analysis. For both sgRNAs, a cell population showing two different genomic sequences at the sgRNA target loci was identified (Figure 3.20 B). SGPL1 S2 contained 6 and 7 nucleotide deletions whereas SGPL1 S6 showed one very long deletion (98 bp) and one insertion (124 bp). The metabolism of pacSph was tested in both cell lines by HPTLC analysis. Oli-*neu* wild-type and *SGPL1*$^{-/-}$ (S2 and S6) cells were labelled with 1.5 µM pacSph. Lipids were extracted, clicked to Coumarin-azide, separated on a HPTLC-Silica plate and the resulting fluorescent paclipids were detected. Compared to wild-type Oli-*neu* cells, no PC band was detected in SGPL1 knockout cells (Figure 3.20 C). Therefore, cells were applicable for initial protein-SL interaction studies using pacSph.

Oli-*neu SGPL1*$^{-/-}$ S6 were seeded, labelled with 1.5 µM pacSph, subjected to UV-crosslinking, cell lysis, click-reaction of the protein-lipid complexes to Biotin and enrichment of protein-SL-Biotin products on Neutravidin beads. Input and PL-PD samples were loaded on an SDS-PAGE gel, blotted and endogenous proteins were detected using specific antibodies. βDG and ITGB1 were identified to interact with VLCFA SLs in HeLa cells (Section 3.2) and were also interacting with pacSph-derived SL species in Oli-*neu* cells as signals of βDG and ITGB1 were detected in PL-PD samples (Figure 3.20 D).

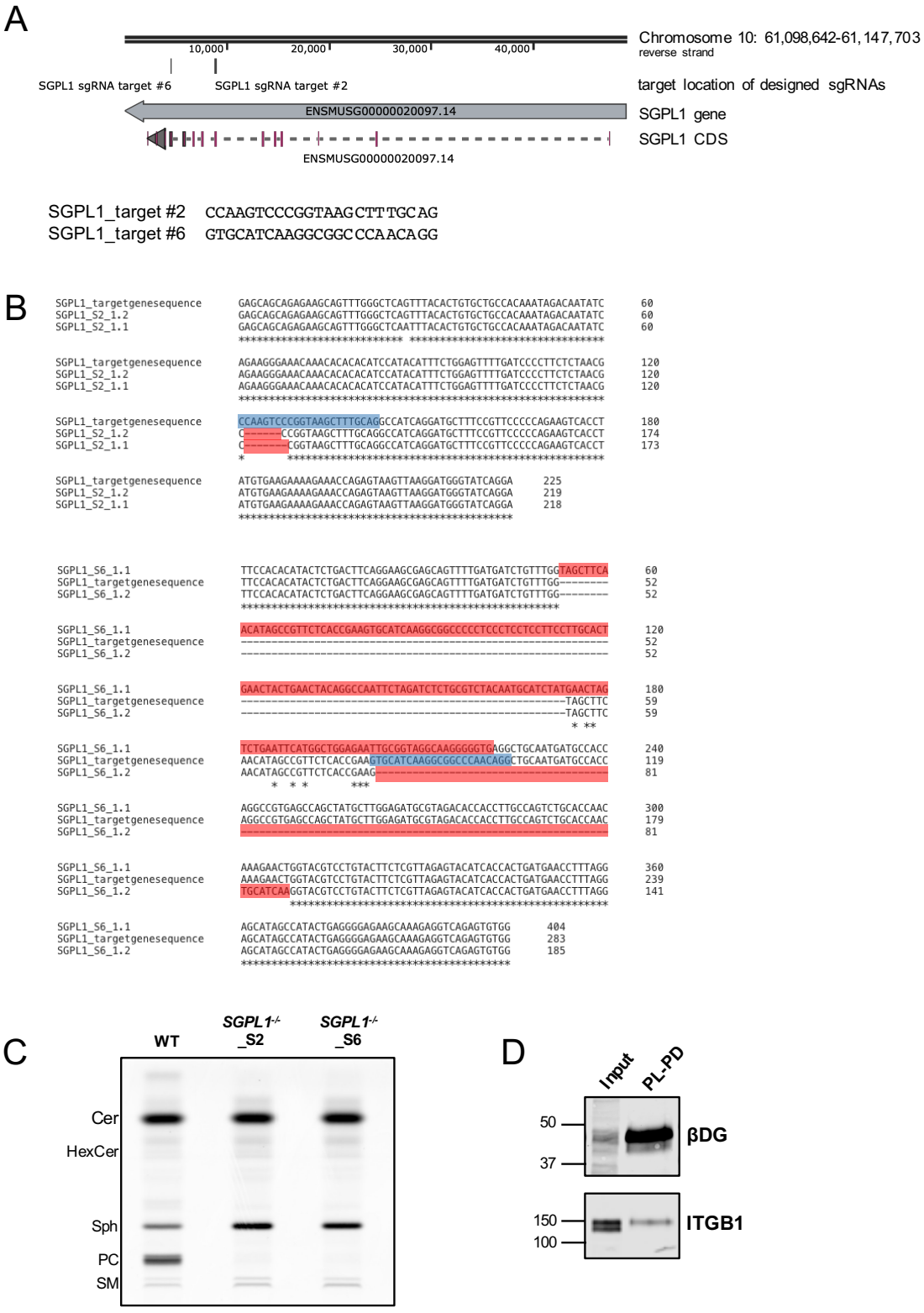

Figure 3.20 SGPL1 Knockout in Oli-*neu* cells

A. Structure of the mouse *SGPL1* gene. Localisation of sgRNAs on *SGPL1* gene and SGPL1 CDS. **B. Sequencing of the genomic locus.** Alignment of sequencing results of wild-type and mutant gDNA. In red: mismatches. In blue: sgRNA target. **C. HPTLC analysis of Oli-*neu* SGPL1 knockout cells.** Oli-*neu* *SGPL1*$^{-/-}$ cells (S2 and S6) were labelled with 1.5 µM pacSph for 4 h. Cells were collected, lipids extracted and subjected to click-reaction to Coumarin-azide. Lipids were separated on a HPTLC silica plate and separated fluorescent lipids were detected using an Amersham Imager 600 with excitation at 460 nm and a Cy2 Emission Filter (525BP20). **D. Protein-**

lipid pulldown analysis of endogenous proteins. Oli-*neu SGPL1*$^{-/-}$ S6 cells were labelled with 0.5 µM pacSph for 24 h. After subsequent UV-crosslinking, cell lysis, CuAAC-based click-reaction to Biotin-azide, enrichment of PL-PD on Neutravidin beads, elution (95%) and input (5%) samples were loaded on an SDS-PAGE gel, blotted and endogenous proteins were detected with specific antibodies. Shown is a representative blot of three replicates.

In order to investigate influences in protein trafficking in Oli-*neu* cells, CerS2 knockout cells were generated by the same approach as described for the SGPL1 knockout in Oli-*neu* cells. A sgRNA with very few off-target sites was designed using CCTop[168]. The sgRNA target sequences and localisations on the mouse *CERS2* gene and CDS are displayed in figure 3.21 A. Oligos were designed and cloned into a Cas9-GFP containing plasmid[169]. Oli-*neu* cells were transiently transfected and sorted for GFP positive cells. Single cell-derived cell populations were analysed by HPTLC and lipidomic analysis. For HPTLC analysis Oli-*neu CERS2*$^{-/-}$ (C7_2 clone) cells were labelled with 1.5 µM pacSph. Lipids were extracted, clicked to Coumarin-azide, separated on a HPTLC-Silica plate and the resulting fluorescent paclipids were detected. Compared to wild-type cells, a lack of VLCFA SM could be observed (Figure 3.21 B, indicated with a red arrow). Additional verification by lipidomic analysis was performed. The SM species distribution showed that VLCFA SM lipids were depleted, whereas C16-FA containing SM was elevated (Figure 3.21 C). Both results indicate a complete knockout of CerS2.

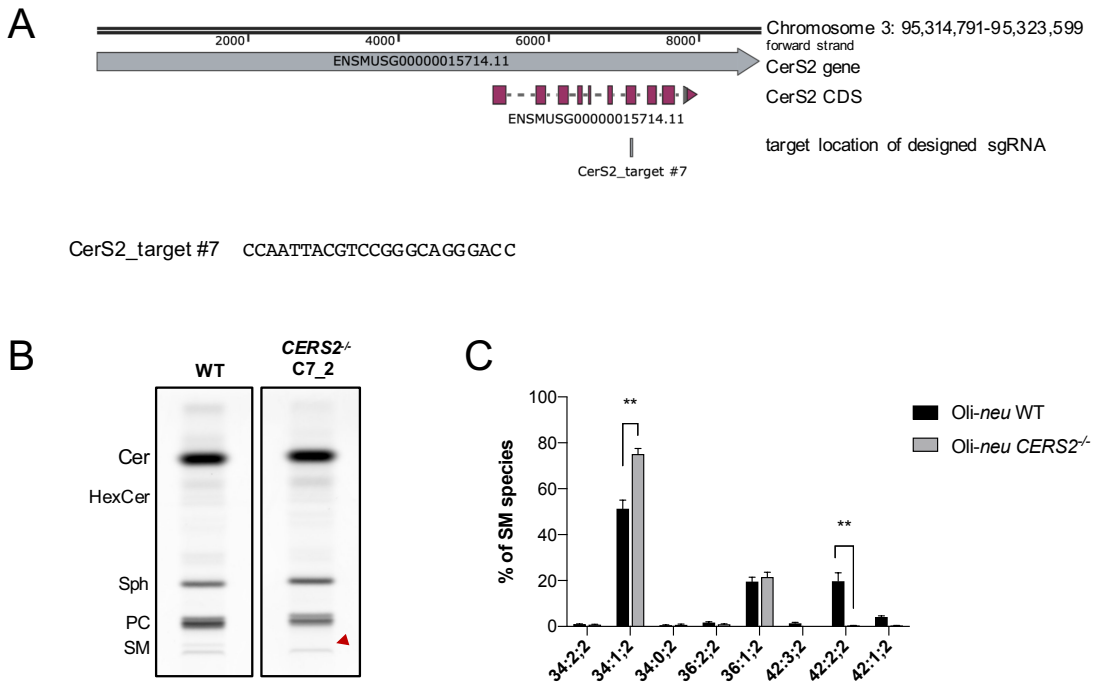

Figure 3.21 CerS2 Knockout in Oli-*neu* cells
A. Structure of the mouse *CERS2* gene. Localisation of sgRNA on *CERS2* gene and CERS2 CDS. **B. HPTLC analysis of Oli-*neu* CerS2 knockout cells.** Oli-*neu* *CERS2*$^{-/-}$ cells (C7_2) were labelled with 1.5 µM pacSph for 4 h. Cells were collected, lipids extracted and subjected to click-reaction to Coumarin-azide. Lipids were separated on a HPTLC silica plate and separated fluorescent lipids were detected using an Amersham Imager 600 with excitation at 460 nm and a Cy2 Emission Filter (525BP20). Red-arrow points to a lacking very long chain fatty acid-containing SM lipid in CerS2 knockout of Oli-*neu*. **C. Lipidomic analysis of SM species.** Distribution within SM species is shown. Two-sided unpaired t-tests were performed correct for multiple comparisons using the Holm-Sidak method. Shown is mean ± SEM of three independent experiments. * = p<0.05, ** = p<0.001. Cer, ceramide; HexCer, hexosylceramide; Sph, sphingosine; PC, phosphatidylcholine; SM, sphingomyelin. Lipid species were annotated according to their molecular composition as follows: sum of carbon atoms in the FAs:sum of double bonds in the FAs;sum of hydroxyl groups in the long-chain base and the FA moiety. Lipidomic measurements were performed by Christian Lüchtenborg.

To further compare the obtained CerS2 knockout with phenotypes of dystroglycan knockout cells, Oli-*neu* DAG1 knockout cells were generated. A sgRNA with very few off-target sites was designed using CCTop[168]. The sgRNA target sequences and localisations on the mouse DAG1 gene and CDS are displayed in figure 3.22 A. Oligos were designed, and cloned into a Cas9-GFP containing plasmid[169]. Oli-*neu* cells were transiently transfected and sorted for GFP positive cells. Single cell-derived cell populations were analysed by sequencing the genomic DNA of targeted locus as well as Western blot and lipidomic analysis. A cell population showing two different genomic sequences at the sgRNA target loci was identified

(14 nt and 187 nt deletions, figure 3.22 B). Furthermore, endogenous βDG was not detected in Western blot analysis with 50 µg whole protein lysate.

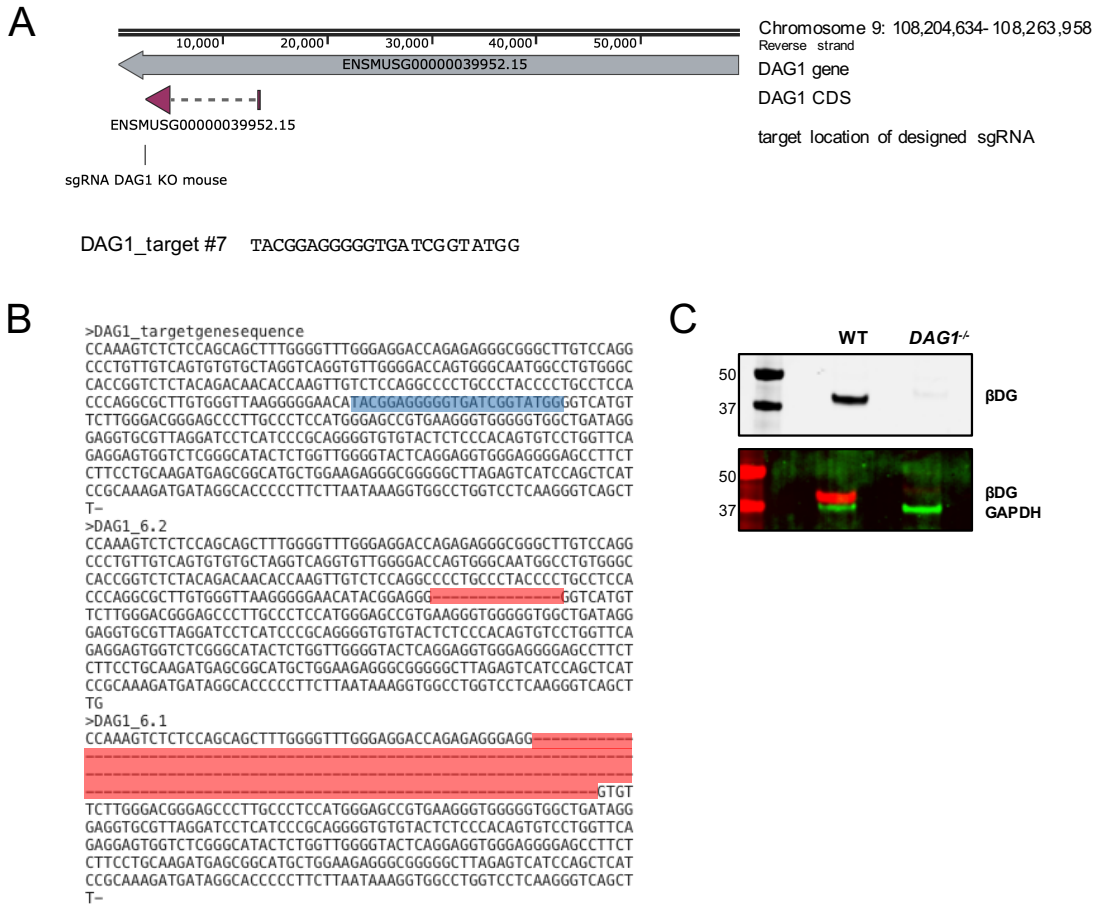

Figure 3.22 DAG1 Knockout in Oli-*neu* Cells
A. Structure of the mouse *DAG1* gene. Localisation of sgRNA on *DAG1* gene and DAG1 CDS. **B. Sequencing of the genomic locus.** Alignment of wild-type and results from gDNA sequencing are shown. In red: mismatches in blue: sgRNA target. **C. Western blot of DAG1 knockout cells.** 50 µg of total cell lysate was loaded on an SDS-PAGE gel and blotted. Endogenous βDG (grey in upper panel or red in lower panel) and GAPDH (green) as loading control were detected.

3.5.3. Endogenous Localisation of β-dystroglycan in Oli-*neu* Mutants

Dystroglycan (αDG) is described to localise at the cortical cell body and in leading edges of processes in newly formed OLGs[135]. During OLG differentiation dystroglycan is frequently found at process branch points[135]. The intracellular localisation of βDG in undifferentiated and differentiated Oli-*neu* cells and the generated mutants was analysed by immunofluorescence and confocal microscopy to elucidate the role of VLCFA SLs in protein localisation. In wild-type Oli-*neu* cells, a vesicular localisation of βDG was observed (Figure 3.23 A).

Strikingly, in differentiating Oli-*neu* cells, βDG immunoreactivity was found to be localized to the plasma membrane at branches (Figure 3.23 A). This localisation-change was not observed in Oli-*neu CERS2*$^{-/-}$ (C7_2) cells. In Oli-*neu DAG1*$^{-/-}$ cells no signal for βDG was detected.

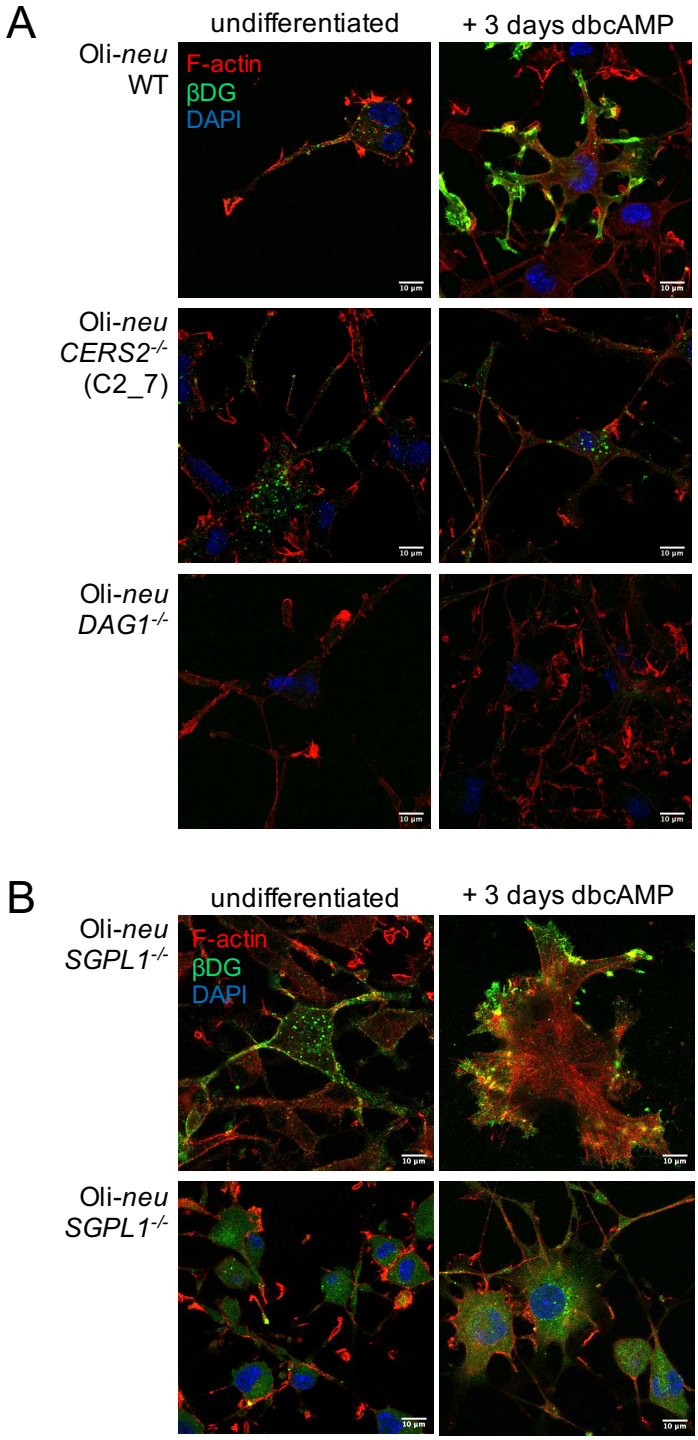

Figure 3.23 Confocal Microsopy of β-Dystroglycan Localisation in Oli-*neu* Mutant Cell Lines
Oli-*neu* wild-type, Oli-*neu SGPL1*$^{-/-}$ cells (S2 and S6), Oli-*neu CERS2*$^{-/-}$ cells and Oli-*neu DAG1*$^{-/-}$ cells were seeded and treated as indicated with dbcAMP. Cells were fixed and blocked. Afterwards,

cells were stained with specific antibodies against βDG. F-actin was stained with phalloidin-Alexa647 to visualise the cell processes and DAPI to visualize nuclei. After preparation for confocal microscopy, slides were imaged with a Zeiss LSM 800. Scale bar: 10 µm.

To exclude an influence of SGPL1 knockouts on βDG localisation, the two different SGPL1 knockout cell lines were also tested by confocal microscopy. The SGPL1 S6 knockout already showed an plasma membrane localisation of βDG in undifferentiated cells. In SGPL1 S2 knockouts, the signal for βDG appeared noisy and did not change upon differentiation.

Conclusively, the lipidomic analysis revealed an influence of the dbcAMP treatment on the lipid profile with an majorly decreasing overall unsaturation and an increase in ether-lipids. Three different Oli-*neu* knockout cells were established by CRISPR-Cas9 technology. The localisation of βDG was found to localise from vesicular structures to sheets during myelination of Oli-*neu* cells. The trafficking of βDG to sheets was abolished in the generated CerS2 knockouts in Oli-*neu* cells.

4. Discussion

In this thesis, interactions of proteins with VLCFA SLs were investigated. The obtained results are discussed in two separate sections. Firstly, the validation and biochemical characterisation of protein-VLCFA SL interactions are discussed (Section 4.1) and secondly, the possible biological function of dystroglycan-VLCFA SL interaction in oligodendrocytes is discussed (Section 4.2).

4.1. Characterisation of Protein-VLCFA SLs Interactions

Direct intracellular targets of very long chain fatty acid-containing SLs are largely unknown[11]. Therefore we previously established a proteomic approach to identify direct interaction partners of VLCFA SLs in a cellular system[124]. The previously identified protein-VLCFA SL interactions may occur in a non-annular or annular way and thereby are either regulating specific functions or are preferentially localising with the proteins. The novel interactions were examined to delineate possible functional roles of the identified protein-VLCFA SL interactions based on GO term and functional network analysis. Furthermore, selected candidate proteins were subjected to validation studies and the VLCFA SL interactions were characterised in terms of lipid class-specificity, nanodomain localisation and in case of dystroglycan, the involvement of the TMD in lipid binding.

4.1.1. Putative Interaction Motifs and Functional Roles of Proteins Interacting with VLCFA SL

4.1.1.1. TMD analysis

A previously performed proteomic approach identified novel proteins possibly interacting with VLCFA SLs[124]. The bioinformatic analysis of the identified proteins (Section 3.1) revealed special features and interactions of and between the protein hits. Most putative VLCFA-interacting proteins were membrane proteins localised in the plasma membrane and comprised one TMD with 21 amino acids. Different acyl chain lengths are described to sort proteins based on their similar hydrophobic thickness which varies within the plane of the bilayer and among organelle membranes[176]. Proteins localised to the plasma membrane comprise in average a TMD length of 25 amino acids[157]. However, the mentioned proteomic approach

identified mostly plasma membrane-localised proteins with 21 amino acid long-TMDs which implies that the hydrophobic sorting is not the reason for the interaction of identified hits with VLCFA SLs. VLCFA SLs are described to interdigitate into the opposing leaflet[177] and therefore are not necessarily increasing the hydrophobic thickness of the membrane[19]. The interdigitation of VLCFA SLs into the opposing leaflet possibly allows the formation of particularly strong interactions with a TMD due to the formation of large interaction sites with transmembrane segments. The formation of a particularly strong interaction due to the very long, interdigitating fatty acid chain is also suggested for C24 LacCer that is described to interact with the acyl-chains of LYN kinases in neutrophils[96]. Thus, the identified proteins may not localise with VLCFA SLs due to hydrophobic sorting but they rather interact with VLCFA SLs by forming a large interaction face, thereby reducing the dissociation time. Generally, transmembrane proteins interact with lipids via hydrophobic interactions between the hydrophobic transmembrane moieties of the protein and the hydrophobic lipid tail of the lipid[70]. In addition, electrostatic, hydrogen bonding and hydrophobic interactions between the lipid head groups and amino acid residues can be involved[176]. Non-annular lipid binding most often occurs within cavities of TM proteins[68,176]. Especially the non-annular interaction of lipids within cavities leads to decreasing dissociation times[68]. These cavities could be formed by different hydrophobic amino acids which would not lead to the emergence of a specific interaction motif. Among the VLCFA SLs-interacting proteins, no interaction motif was found within the TMD of the identified single-spanner proteins. The absence of a common motif points to specific interactions in the individual cases rather than a common interaction mode. The proteomic approach investigated in this thesis did not discriminate between different lipid classes and therefore the identified proteins could interact with any SL species, such as gangliosides, sulfatides or SM VLCFA SL species. Furthermore, the interacting VLCFA could either be a saturated or unsaturated, e.g. C24:0 FA or C24:1 FA, which further increases the number of lipid species candidates. Thus, the complexity of the possible interacting lipid species did not allow the identification of a general interaction motif among the identified proteins. Thus, in contrast to a previous study which was based on an bioinformatic approach[72], the aim of this work was not to decipher a novel SL interaction motif,

but to identify novel protein SL interactions as direct molecular targets of VLCFA SLs are largely unknown so far.

4.1.1.2. GO Term Analysis

Diverse enriched biological processes, molecular functions and cellular localisations were identified among the proteins-VLCFA SLs interactions. Among the enriched GO terms, putative roles of VLCFA SL protein interactions in membrane/vesicle fusion as part of a SNARE complex were discovered. Four syntaxins were identified that are assigned to these GO terms. Syntaxins are multidomain proteins that belong to the family of SNARE proteins with a globular amino terminal domain, a SNARE domain and a carboxy terminal transmembrane domain[160]. They are distributed throughout the cell and are required for a wide range of intracellular membrane fusion processes mediated by SNARE complexes[160].

Interestingly, unsaturated PS are described to change the orientation of the SNARE complex relative to a bilayer and thereby increases fusion for calcium-mediated exocytosis *in vitro*[178]. After calcium binding to synaptotagmin 1, its calcium-binding loops insert into the membrane, causing local acyl chain disorder and curvature in the bilayer near the fusion site[178]. Disordering the acyl chains leads to a conformational change in the juxta-membrane linker region of syntaxins, inducing the trans-cis conformation transition of the SNARE complex that pulls the two membranes[178].

In lipid vesicles, interdigitating C24:1 ceramide is enriched in tubular structures and thereby drives the formation of cochleate-type tubular structures[177]. Based on these data, the herein identified interaction of syntaxins with VLCFA SLs may occur with a C24:1 ceramide to jointly promote fusion by the formation of tubular structures. The interaction of syntaxins with an unsaturated C24:1 ceramide would increase membrane bending at fusion sites to promote fusion as described for unsaturated PS in calcium-mediated exocytosis for neurotransmitter release.

Furthermore, yeast cells with reduced levels of C26 lipids (corresponding to C24 SLs in mammalian cells[15]), show mislocalisation of fusion machinery proteins (including Rab- and Rho-family GTPases)[98] which leads to defects in tethering and docking steps of vacuole fusion[97]. Thus, it is suggested that the lack of C26 VLCFA prevents the specific clustering and enrichment of fusion proteins at fusion sites,

eventually due to disrupted lipid nanodomains that may be enriched in fusion proteins[98]. Concluding, the discovered VLCFA SLs-syntaxin interaction may directly promote fusion by localising with an unsaturated C24:1 SL or indirectly by promoting the localisation of syntaxins to fusion sites. The SL class and saturation of the identified VLCFA SL that interacts with syntaxins remains to be elucidated.

Furthermore, GO terms pointing to putative roles of VLCFA SL-protein interactions in cell adhesion were identified. The identified proteins BSG, L1CAM, ITGA5, MCAM and NPTN are assigned to GO terms involving cell adhesion. Membrane nanodomains are described to serve as regulators for numerous cellular events including the formation of platforms for ECM adhesion and intracellular cytoskeletal tethering to the plasma membrane[179]. Thus, already described lipid-interactions and localisations in lipid nanodomains of the identified VLCFA SL-interacting proteins was questioned.
Cell-matrix adhesion is mediated by the cell adhesion receptors integrins (including ITGA5, and the positively validated ITGB1, section 3.2.2) which are described to localise in lipid nanodomains, thereby promoting signaling[122].
Studies in knockout mice revealed the interaction of axonal adhesion molecule L1CAM with the α2,3-sialic acid on CD24 which plays a role in interactions of neuron with other cells[180]. Sialyated CD24 is excluded together with L1CAM from lipid nanodomains in dorsal root ganglions[180].
Concluding, roles of VLCFA SL in cell adhesion may partly occur in lipid nanodomains, but not for all discovered cell adhesion proteins, a nanodomain localisation is described so far.

Dendrite self-avoidance was among the strongly enriched GO terms. According to the GO database, EMB, BSG and NPTN are involved in this biological process[181]. Dendrite self-avoidance is a property of neurons, which makes established branch structures turn away from another[182]. This allows the dendrites to evenly spread over a territory. NPTN, BSG and EMB are structurally very similar and belong to the group of IgSF proteins[183]. Each family member comprises two laminin G-like domains (LG domains) that projects into the extracellular space[183]. All proteins contain a glutamate at exactly the same position in the TMD which could be important for molecular interactions within the membrane region[183]. Especially for

protein-SL interactions, a role of membrane embedded acidic residues is suggested[72,166] and could occupy a dominant role in the herein identified interaction with VLCFA SLs. For NPTN a functional link to the ganglioside composition of the neuronal membrane is described[183]. However, a specific interaction of these proteins with lipids has not been described to date, and it might be of interest to study whether VLCFA SL interactions of NPTN, EMG or BSG are involved in dendrite-self avoidance.

Biological processes associated with viral entry into host cells and proteins that are involved in viral interaction with host were discovered among the VLCFA SL interacting proteins. Interferon-induced transmembrane protein 3 (IFITM3) is a well-known antiviral effector of the influenza virus[184]. ITGA5 acts as a receptor for human metapneumovirus[185] and human parvovirus B19[186]. Finally dystroglycan acts as a receptor for lassa virus[187], lymphocytic choriomeningitis virus glycoprotein[188] and class C new-world arenaviruses[189]. The putative interaction of these proteins with VLCFA SLs may influence the interaction with viral proteins, e.g. by targeting them to the plasma membrane or by partitioning them into different signalling complexes where multiple proteins that are necessary for viral entry are localised. However, this hypothesis needs to be investigated in future studies.

The identified proteins DAG1 and SGCE were assigned to the enriched GO terms “dystroglycan complex”, “sarcolemma”, and “dystrophin-associated glycoprotein complex”. VLCFA SLs interactions with DAG1 and SGCE possibly play a role in linking the ECM to F-actin, which is described to be mediated by DAG1 and SGCE within in the DGC complex in different tissues[139] (see section 4.2.3 for further discussion).

Five proteins from the proteomic approach were assigned to localise to the immunological synapse. These included the Activated leukocyte cell adhesion molecule (ALCAM/CD166 antigen), CD81, NPTN, STX7 and ICAM1. The formation of the immunological synapse is a dynamic process in which a multi-molecular assembly of receptors and adhesion molecules accumulate at the interface of T-Cells and antigen-presenting cells[190]. The assembly of the immunological synapse is described to rely on clustering of lipid nanodomains

which are required for optimal T cell activation[191]. ALCAM plays an important role in the stabilisation of the immunological synapse of leukocytes and its function in cell adhesion is induced by CD9[192]. The identified interaction of CD9 and ALCAM with VLCFA SLs might support their interaction within the same lipid environment and thereby VLCFA SLs may stabilise their interaction in the immunological synapse. ICAM1 is required for the formation of the immunological synapse but is depleted from the synapse before calcium is released[190]. Thus, VLCFA SLs might play a specific role in the formation and stabilisation of the immunological synapse before calcium release. Future investigations of protein-SL interactions during T cell stimulation could help to substantiate interactions and functional roles.

4.1.1.3. Functional Network Analysis

The functional network analysis highlighted functional associations between identified VLCFA SL interacting proteins. Multiple studies showed a functional link between the discovered VLCFA SL interacting proteins (Section 3.1). For some of them, a regulation by lipids is described[193–196].

In fibroblasts, growth is dependent on fibroblast growth factor and its receptor (FGFR) which is stably associated with ganglioside GM3, CD9 and CD81[195]. Interestingly, the depletion of GM3 enhances the phosphorylation of FGFR and the interaction of FGFR with integrins and CD9/CD81 increases[195]. The acyl chain length of the associated GM3 was not investigated, however the previously performed proteomic approach suggests an interaction of the complex components CD9, CD81, ITGA5 as well as IGBT1 with VLCFA SLs[124] (discovery of the ITGB1-VLCFA SL interaction is discussed in section 4.1.2). The interaction of the complex components with VLCFA SLs implies that the negative regulatory role of GM3 on FGFR may specifically be mediated by a VLCFA GM3.

Generally, CD9 and CD81 are tetraspanins which are able to interact with each other thereby forming a “tetraspanin web”[194]. Through this web, tetraspanins are expected to play specific roles in membrane compartmentalisation, tetraspanin-dependent membrane fusion and vesicular trafficking[194]. Tetraspanins undergo palmitoylation and are described to associate with cholesterol and gangliosides[194]. The herein identified association of two tetraspanins with VLCFA SL most likely stabilises, promotes or inhibits the interaction of complex components within the

“web” of tetraspanins. Therefore, the interactions of CD9 and CD81 with VLCFA SLs might occur in an annular way within the “tetraspanin web”.

Notably, CD9 is also detected in myelin of mouse brain at postnatal day 16[196]. CD9 expression continuously increases with age, persists in adult brain and is localised to the outermost membrane of compact myelin[196]. The localisation to compact myelin and the described association of CD9 with ITGB1, suggests a role these proteins in transducing signals from the ECM into OLGs[196,197]. Loss of CD9 does not affect myelination of OLGs[197], however CD9 appears to play a role in the termination of myelination[198]. Later studies describe the involvement of CD9 in the formation of paranodal junctions which are disrupted in CST-deficient mice[198]. Thus, the discovered interaction of CD9 with a VLCFA SL, most likely VLCFA sulfatide, appears to stabilise the localisation of CD9 to paranodal regions. Also other proteins, such as NF-155, appear to be stabilised or trafficked to paranodes by sulfatides, which is mislocalising in CST knockout mice[199].

Concluding, CD9 and many of its diverse interaction partners in protein complexes were herein discovered to interact with VLCFA SL species. Further studies will help to decipher potential roles of VLCFA SLs in modulating the function of the proteins identified in the proteomic approach. CD9 is described to be regulated by a ganglioside in one complex[194–196], and by a sulfatide species in a different complex[193]. This fact suggests that the putative interaction of VLCFA SLs with CD9 occurs with the VLC acyl chain and/or the sphingosine backbone rather than the lipid head group. In general, the preference of diverse complex components for similar lipids might promote their combined regulation within a complex[119].

Furthermore, SLC1A5 and SLC38A2 appeared to be functionally linked. Both proteins are neutral amino acid transporters[200] and were identified to be interact with VLCFA SLs[124]. So far, no role of lipids in the glutamine transport by these proteins[201] has been described.

Lastly, the functionally redundant lysosomal proteins LAMP1 and LAMP2[202] were identified in the proteome-wide mapping to interact with VLCFA SLs[124]. Also for LAMP1 and LAMP2 no regulation in orchestration with a lipid has been described so far.

The functional link of DAG1 and SGCE is discussed in section 4.2.2.

Summarising, the functional network analysis suggested potential roles of VLCFA SL-protein interactions in a number of different cellular processes and pathways. A modulation of these processes by a direct protein-lipid interaction is only described in a few cases so far. Molecular dynamics simulations (MDS), biochemical and cellular approaches would allow a further characterisation and validation of the previously identified VLCFA SL interacting proteins and potentially substantiate novel functions of the respective lipid partners.

4.1.2. Biochemical Investigation and Validation of Chain-Length Specific Protein-Sphingolipid Interactions

To monitor protein-lipid interactions, HeLa SGPL1 knockout cells were cultivated in the presence of pacSph lipids, which were taken up and channelled into the cellular SL metabolism. As its endogenous counterpart, pacSph is mainly incorporated into C16:0, C24:0 and C24:1 SLs[113]. In comparison to wild-type cells, CerS2 knockout cells lacking VLCFA SL species allowed the identification of proteins interacting specifically with VLCFA SLs[124]. These data might help to understand a number of cellular phenotypes with aberrant lipid distributions that lack molecular explanations so far. The proteomic approach that led to the identification of VLCFA SL interactions was initially validated by overexpression of the respective candidate proteins[124]. However, the expression level differed between wild-type and CerS2 knockout cells and the recovered protein amount in protein-lipid pulldowns was varying strongly. Typically, the overexpression of proteins using viral vectors leads to an up to 100-fold enrichment compared to endogenous protein levels[203]. This likely increases the chance of weak, non-physiological interactions and leads to aberrant compartmentalisation of the overexpressed proteins[203]. Indeed, overexpression of dystroglycan led to a mislocalisation of the protein observed by immunofluorescence staining and confocal microscopy. This was also reflected by an elevated interaction of pacFA-derived lipid species with overexpressed but not endogenous dystroglycan, indicating that the overexpression led to non-physiological lipid interactions. The pulldown assay performed with pacFA-labelled cells further emphasised a difference in the localisation of dystroglycan in wild-type and CerS2 knockout cells. CerS2 knockout cells showed a much lower interaction of dystroglycan with pacFA-derived lipids compared to the parental cells indicating an different localisation. In

CerS2 knockout cells it appeared that dystroglycan is localised more prominently to endo/exosomes.

To avoid false positive validations of overexpressed protein candidates, a validation of protein-SL interactions was performed for the endogenous proteins. This allowed the successful validation of βDG, STX6 and TGOLN2 as VLCFA SL interacting proteins. The upper band of ITGB1 appeared as a candidate for VLCFA SL interaction, and will have to validated by including an higher number of experiments. The upper band represented the plasma membrane-localised and glycosylated form of ITGB1 (data from L. Förster, AG Brügger) which was specifically interacting with VLCFA SLs.

Localisation studies of the positively validated protein candidates did not reveal an altered localisation in CerS2 knockout cells compared to parental cells (generated by CRISPR-Cas9 knockout leading to premature Stop codons[124]). However, even though confocal microscopy did not reveal an altered subcellular localisation, candidate proteins might not be targeted to the correct site within the membrane. The CerS2 knockout, for example, might influence the number and composition of membrane lipid nanodomains and, thus, the assembly of signalling complexes therein. Indeed, an altered localisation of the insulin receptor is reported in CerS2 knockout mice based on the observation of the protein's inability to partition into detergent-resistant membranes (DRMs)[204], a biochemical method to investigate lipid nanodomains[205]. This mislocalisation prevents the successful phosphorylation of the Insulin receptor in CerS2 knockout mice[204]. Concluding, further experiments should be performed to exclude influences of the altered lipidome on the discovered protein-lipid interactions. This would imply that proteins which were identified in the proteomic approach might not specifically interact (non-annularly) with VLCFA SLs but instead localise within membrane nanodomains and interact with the lipid via bulk or annular interactions. However, not all discovered proteins were assigned to lipid nanodomains suggesting specific non-annular interactions in these cases. Future assays are required to distinguish the types of interaction.

The localisation of a protein within a lipid nanodomain is often investigated by analysing the composition of DRMs[205]. An alternative approach to study lipid nanodomains is the use of cyclodextrins, which extract cholesterol from membranes and thereby disrupt these domains[8]. To investigate whether

dystroglycan or STX6 is sensitive to SL interactions when these domains are disrupted, HeLa SGPL1 knockout cells were treated with cyclodextrin in combination with pacSph labelling (Section 3.2.2). Short cyclodextrin treatments did not influence the pacSph labelling behaviour but significantly reduced cholesterol levels within the cellular membranes. Hence, this condition was suitable for protein-SL interaction studies. The dystroglycan-SL interaction was sensitive to cholesterol depletion, implying that the interaction to SLs is cholesterol-dependent, e.g. by occurring within a lipid nanodomain. Proteins are crosslinked to bulk, annular or non-annular paclipids. If the cyclodextrin treatment changes the endogenous localisation of βDG to e.g. intracellular vesicles, and thereby alters the protein's lipid environment remains to be elucidated. Dystroglycan was recovered in the soluble fraction in DRM experiments in astrocytes [206], whereas dystroglycan was shown to interact with caveolin-1 within lipid nanodomains in smooth muscle cells[207]. In brain, dystroglycan was also reported to localise in lipid nanodomains[208]. However, the reduction of βDG-SL interactions due to cholesterol depletion does not exclude a specific protein-lipid interaction. The altered lipid environment of βDG in L_D domains might reduce the "background" signal derived from bulk pacSLs within lipid nanodomains. However, some βDG was still identified to interact with pacSLs in cyclodextrin-treated cells, indicating that there might be a remaining specific interaction. To further employ if the interaction of βDG with a SL is in fact non-annular or if βDG is simply localising in lipid nanodomains, further experiments are required.

In contrast, the Golgi-localised STX6-SL interaction was not affected by the cyclodextrin treatment. Since cyclodextrin is able to extract cholesterol from all organelle membranes independently of lipid nanodomains[8] it might also influence the lipid environment of STX6. If the short treatment time with cyclodextrin depleted cholesterol from endomembranes, and thereby was able to influence the lipid environment of STX6, remains to be elucidated. Syntaxins are described to be excluded from lipid nanodomains[209]. Thus, the independence to cyclodextrin treatment would coincide with the localisation in L_D domains.

Summarising, dystroglycan-SL interaction was sensitive to cholesterol depletion whereas STX6-SL interaction was unaffected. The analysis of microdomain association highlighted the importance of further studies focussing on the type of the identified lipid interactions.

The knockout of *CERS2* resulted in a loss of VLCFA SLs in HeLa cells and was used to identify proteins interacting with these lipids[124]. The rescue of CerS2 expression led to the re-synthesis of endogenous and pac-VLCFA SLs (Section 3.2.4). Also a strong increase in pacCer36:1;2 was detected in CerS2 overexpressing cells. Thus, overexpressed CerS2 influenced the activity of CerS1, thereby increasing the synthesis of pacC18 SLs. As endogenous C18 SLs were not upregulated, the addition of pacSph might have enhanced the synthesis of pacC18 SLs. An influence of CerS2 on CerS1 activity has been suggested earlier[210]. The overexpression of CerS1 in CerS2 knockout cells strongly elevated the synthesis of endogenous C18 SLs and pacC18 SLs, whereas C24 SLs remained absent. Applying the overexpression to protein-lipid pulldown assays, the diminished amount of βDG- and STX6-SL interactions in CerS2 knockout cells were recovered, whereas in CerS1 overexpressing samples the protein amounts appeared lower compared to CerS2 overexpression. This indicates a preference of βDG and STX6 for VLCFA SLs. For βDG more replicates are necessary to confirm this observation. Moreover, the (re-)formation of lipid nanodomains was likely differently affected when CerS1 or CerS2 expression is upregulated in CerS2 knockout cells.

The amount of dystroglycan was elevated in protein-lipid pulldowns of CerS1 overexpressing cells compared to CerS2 knockout cells, indicating a localisation also to C18 SLs even though it appeared less compared to C24 SLs. For STX6, an overexpression of CerS1 did not lead to an elevated protein-lipid pulldown compared to CerS2 knockout cells indicating a strong preference for C24 SLs. The influence of the overexpression of CerS2 versus CerS1 on protein localisation will further substantiate the results from the protein-lipid pulldown assay. To validate the specificity of the identified proteins for VLCFA SLs, proteins like TFR that were not identified to interact with VLCFA SLs should be included in further analyses. The amount of TFR in the protein-lipid pulldown should remain unaffected by the overexpression of CerS2. Additionally, p24 should be included in the analysis, as it is a specific C18 SL interacting protein[72]. This will further demonstrate the feasibility of the overexpression of CerS1 to detect specific proteome-wide C18 SL interacting proteins compared to non-overexpressing cells.

To further investigate whether the obtained protein signals in protein-lipid pulldown assays were indeed derived from the photo-crosslinking of a paclipid to a protein, a small molecule inhibitor of CerS, FB1, was used (Section 3.2.5). The treatment with FB1 successfully diminished the overall metabolism of pacSph in HeLa cells. FB1 is a fungal toxin that is thought to inhibit ceramide synthase in a competitive manner due to structural similarities to LCBs[211]. It is currently unknown how FB1 binds and inhibits mammalian ceramide synthases since the order of substrate binding and the catalytic mechanisms are not well understood. Mammalian ceramide synthases were described to catalyse the N-acylation of FB1[212]. The formation of LC and VLC N-acyl-FB1 overall reflects the level of endogenous fatty acid distribution of the analysed tissues, however slightly higher values for VLC N-acyl-FB1 are detectable[212], thereby indicating a preference for CerS2 enzymes. In *Arabidopsis thaliana*, LAG one homologue 1 (LOH1) is catalysing the formation of VLCFA SLs[213]. The plant LOH1 is a ceramide synthase isoform which is described to be the most sensitive isoform to FB1 treatment[213]. The inhibition of the pacSph metabolism further indicated a preference of FB1 for the VLCFA SL-catalysing CerS2 enzyme in HeLa cells. This was clearly detectable for SM, however for ceramide, the chain length distribution could not be evaluated as the VLC and LC bands were not distinguishable by HPTLC analysis. Further lipidomic analysis of the pacSL profile can reveal the influence of FB1 on pacSL incorporation into ceramide. Additionally, the influence of FB1 treatment on endogenous SL lipid synthesis can be evaluated by mass spectrometry. So far, the obtained data revealed a successful inhibition of the SL metabolism most likely due to a competition between FB1 and pacSph for the binding pockets of CerS enzymes.
The reduced amount of βDG in protein-lipid pulldowns of FB1 treated cells indicates that a pacSph metabolite was interacting with βDG in untreated cells. For STX6 a trend in the reduction of protein-pacSL interaction by FB1 treatment was detected. More replicates may reveal a significant reduction of STX6 by FB1 treatment. Furthermore, ITGB1 did not appear to be diminished by the treatment when evaluating the amount of both glycosylated forms. Further replicates may reveal a selective inhibition of the protein-SL interaction of the upper band of ITGB1, which appeared to be diminished upon treatment with FB1. Concluding, the treatment with FB1 validated the specific interaction of βDG with a pacSL in

the performed assay. For the STX6 and ITGB1 proteins further assays are required to confirm the interaction to an SL.

Summarising, the proteomic approach that led to the identification of VLCFA SL-interacting proteins[124], was validated by employing a protein-lipid pulldown assay with a selected number of proteins (STX6, TGOLN2, βDG). These proteins were chosen based on the value obtained by the proteomic assay (Table 7.1). The three proteins were strongly diminished in the proteomic assay. Protein-lipid interactions reduced in the VLCFA SL deprived cells were specifically rescued by the overexpression of CerS2 which led to elevated amounts of candidate proteins co-purified with pacSLs. As lipid nanodomain identity might be modified in CerS2 knockout cells, the localisation of protein candidates might have been altered in these cells and thereby led to the identification in the proteomic approach. This could be the case for βDG and further experiments are required to distinguish between annular and non-annular lipid binding. E.g., the non-annular or annular lipid binding of the identified protein-lipid interactions can be addressed by observing the exchange rate of detergents with lipids in native mass spectrometry [214]. Biochemical assays not employing pacSph should further substantiate the interaction of the identified proteins with VLCFA SLs. Also, a simulation of protein-lipid interactions might be feasible, depending on the availability of secondary structure information of the transmembrane regions. This would furthermore facilitate the differentiation between annular and non-annular lipid binding.

4.1.3. Investigation of Lipid Class Specificity of Protein-Sphingolipid Interactions

The modification of pacSph metabolism by inhibiting enzymes downstream of ceramide synthesis is a possibility to investigate a lipid class specificity of protein-sphingolipid interactions. SiRNAs against UGCG effectively reduced the *de novo* synthesis of HexCer whereas SGMS1 knockdown led to a minor insignificant reduction of SM (Section 2.1.5). The knockdown was presumably at least partly successful as the majority of the remaining SM could be synthesised by the reductant function of SGMS2[102]. SGMS1-deficient KBM7 show reduced levels of SM, and the remaining proportion was likewise suggested to be synthesised by SGMS2[102]. Especially the growth of HeLa cells is known to depend on SGMS1 and

SGMS2[18], wherefore the activity of SGMS2 might be particularly elevated in HeLa cells while SGMS1 is diminished by the siRNA knockdown. The metabolism of pacSph and the endogenous lipid profile which showed a slight reduction of SM was accompanied by a strong elevation of HexCer indicating an interconnected regulation of the SL metabolism. The strong elevation of HexCer by siSGMS1 treatment in HeLa cells was in line with previous data[102]. The knockout of SGMS1 in KBM7 cells further results a strong increase in GlcCer and LacCer[102]. SGMS1 knockout mice show 4-7 fold elevated GlcCer and GM3 levels in plasma and tissues[215]. The formation of a complex between SGMS1 and UGCG increases the rate of SM and decrease the GlcCer synthesis[216], explaining the strong elevation of GlcCer in SGMS1 knockdown and knockout studies. Nevertheless, as HeLa cells require SM for growth[18], the reduction of SM to identify protein-SM interactions was not feasible in HeLa cells. However, the upregulation of pacHexCer might lead to an elevated signal of proteins interacting with HexCer species. For βDG, the treatment with both siRNAs did not show any influence on the protein-lipid pulldown. This result indicates that under these experimental conditions βDG was not interacting with a HexCer species. To further support this result, proteins known to interact with HexCer species should be included as a reference. A complete block of GlcCer synthesis could also be considered, which would also strongly affect lipid classes downstream of GlcCer.

To address the specifies-specificity of the identified protein-VLCFA SLs interactions, HEK cells lacking UGCG and were provided for this work (unpublished data, P. Haberkant, EMBL). The labelling with 6 µM pacSph for 4 hours generated about 5% pacHexCer species compared to other pacSph-labelled lipid classes. To obtain large quantities of pacGlcCer and higher pacGSL lipids and thereby large differences to UGCG knockout cells (lacking all lipids downstream GlcCer), longer labelling times were considered.

The elevated labelling time resulted in a strong increase of pacGM3 compared to shorter labelling times[165]. HEK UGCG knockout cells are lacking GM3 and show reduced levels of HexCer[165]. The remaining HexCer pool most likely represents GalCer lipids as these two HexCer lipid species could not be distinguished in the employed mass spectrometric analysis[165]. Furthermore, pacSM as well as endogenous SM are elevated in UGCG knockout cells[165]. The elevation of SM is

presumably the result of compensatory mechanisms due to the interconnected regulation of SL metabolism. The formation of a heterodimer between UGCG and SGMS1 leads to an increased synthesis of SM whereas GlcCer synthesis is diminished[216]. Based on this observation, the SM metabolism was not elevated in HEK UGCG knockout cells. However, this study did not investigate the endogenous lipid levels of HEK UGCG knockout cells[216].

The protein-lipid pulldown analysis in HEK UGCG knockout cells with long pacSph labelling times revealed significant differences in protein-lipid interactions of the glycosylated form of ITGB1, indicating an interaction of ITGB1 with an GSL species. βDG and STX6 did not seem to interact with an GSL species as their protein amount in protein-lipid pulldowns was not altered between both conditions. However, as analysis using confocal microscopy suggested, βDG showed a rather endosomal localisation in HEK cells compared to the plasma membrane localisation in HeLa cells. Therefore, a different pool of lipids may interact with βDG in HEK cells compared to HeLa cells. This emphasizes that future studies should focus on the identification of protein-SL interactions in the respective cell type to identify functionally relevant protein-SL interactions.

Conclusively, knockout of UGCG in HEK cells led to altered pacSL profiles, but did not allow an unambiguous identifications of the interacting lipid class in protein-lipid pulldown assays. Furthermore, it would be necessary to include e.g., a GM3-interacting protein such as EGFR[71] or FGFR[195] as a control. To circumvent the generation of multiple pacSL classes, a combination of different clickable head groups in combination with a photocrosslinkable sphingosine could be considered for future experiments. This would further allow the identification of proteins specifically interacting with SM that could not be targeted so far.

4.1.4. Role of the TMD in Dystroglycan-Sphingolipid Interactions

In this thesis, a specific interaction of proteins with SLs with a particular acyl chain length was investigated. To investigate if specific amino acids in the TMD of dystroglycan were involved in the interaction with SLs, the TMD was replaced by TMD sequences of proteins known to not interact with SLs. These included ASGR1[113,217] and CD63 TMD3[166] as well as the TMD of CD8 as a control for plasma membrane localisation[218]. Initial experiments were performed using overexpression of TMD-swapped constructs in HeLa *SGPL1*$^{-/-}$ and HeLa *SGPL1*$^{-/-}$

CERS2$^{-/-}$ cells, however the results of three independent experiments were inconsistent and showed a high deviation (Section 3.4.1). A pulldown assay performed with the overexpressed proteins showed false positive protein-lipid interactions before (Section 4.1.2). Interestingly, a trend towards a lower efficiency of βDG recovery in pulldowns of HeLa *SGPL1*$^{-/-}$ *CERS2*$^{-/-}$ cells compared to the parental cells was observed. However, it also appeared that swapped protein variants showed a higher amount of protein in pulldowns in general. The TMD-swaps might have affected the intracellular trafficking of βDG which might have led to a stronger localisation in intracellular organelles. This would in turn lead to different amounts of protein in protein-lipid pulldown assays. With this experimental setup it was not possible to conclude about the influence of the TMD of βDG on interactions to SLs. Confocal microscopy analysis would be able to reveal differences in cellular localisations of the swap mutants compared to wild type dystroglycan.

A CRISPR-Cas9-engineered knockout of endogenous dystroglycan in HeLa cells was performed, since in this experimental system overexpressed dystroglycan might be targeted to the same intracellular sites as the endogenous protein, and thus would better reflect the physiological situation. The knockout of DAG1 in HeLa cells was confirmed by Western blot analysis, but still needs to be confirmed by sequencing of the respective genomic locus. In these DAG1 knockout cells, the previously seen elevated interaction of the CD8a swap mutant with pacSL species was comparable to wild-type dystroglycan. This indicates an improved intracellular localisation of the overexpressed swap mutant in DAG1 knockout cells.

The interaction of CD8a swapped βDG was not diminished compared to wild-type DAG1 which could imply that the TMD is not involved in SL interactions to βDG. Nevertheless, the immunofluorescence staining and confocal microscopy analysis of DAG1 knockout cells still suggested a strong localisation in the biosynthetic compartments even though the localisation in vesicles was diminished compared to SGPL1 knockout cells. Thus, the deletion of endogenous DAG1 already led to an improved cellular localisation of the overexpressed DAG1 constructs even though a strong Golgi localisation is assumable which was not detectable for endogenous dystroglycan. The application of a low expression vector might help to overcome the strong localisation of DAG1 in the biosynthetic pathway. CRISPR-Cas9-mediated tagging of endogenous dystroglycan is likely to result in more

reliable data. Under these conditions the endogenously-modified swapped dystroglycan would more likely occupy the physiological localisation. Conclusively, due to technical problems, the role of the TMD in βDG SL interaction could not be interpreted so far.

4.2. Exploring the Role of Dystroglycan-VLCFA-SL Interactions in Oligodendrocytes

Next, the functional role of dystroglycan-VLCFA SL interactions in OLGs was investigated. VLCFA SLs are described to be important for myelin stability[54] and their synthesis is strongly upregulated during active myelination[34]. Likewise the expression of dystroglycan increases during myelination and a role of dystroglycan in myelin stability is described[128,139]. The loss of dystroglycan leads to delayed myelination[130,137] and inefficient OLG differentiation[134–136]. However, the underlining molecular functions of VLCFA SLs and dystroglycan in myelin stability as well as the functional mechanisms that regulate myelination and long-term stability is not understood in detail. Based on these data, the interaction of dystroglycan with SLs was investigated in OLGs. In the following sections, the lipidomic and phenotypic changes of an immortalised OPC cell line are discussed as well as the generation of knockout cell lines to investigate the functional association between dystroglycan and VLCFA SLs is depicted.

4.2.1. Lipidomic and Morphologic Changes During Initiation of Oligodendrocyte Progenitor Cell Maturation

Primary OPC cultures are limited in their availability, their isolation results in relatively low cell numbers per preparation and genetic modification is difficult which limits their application for detailed biochemical analysis. Therefore Oli-*neu* cells, which are an immortalized OPC cell line from E16 mouse brains and can be induced to recapitulate several features of differentiating OPCs *in vitro*[170,219]*,* were selected as model cell line to study myelination. Prior functional investigations, the morphologic changes as well as lipidomic changes of Oli-*neu* cells during initiation of myelination were analysed (Section 3.5.1). The quantitative lipidomic changes during the first days of differentiation have not been investigated before.

Oli-*neu* cells showed a mostly bipolar or multipolar shape when cultured without dbcAMP. The treatment with dbcAMP initiated the formation of highly arborized protrusions which formed membranous sheets after 5 days of treatment, indicating a successful induction of OLG maturation (Section 3.5.1), as described before[170]. cAMP triggers a protein kinase A (PKA)-dependent activation and phosphorylation of the transcription factors Cyclic AMP response element-binding protein (CREB) and Activator protein 1 (AP-1) thereby leading to differentiation and myelination[220]. Untreated Oli-*neu* cells are arrested in a progenitor state and therefore reflect the lipid composition of the OPC state[175]. The most abundant lipid species in mature myelin are cholesterol, GalCer and ethanolamine plasmalogen[21]. Undifferentiated Oli-*neu* cells contain lower amounts of HexCer, cholesterol and plasmalogens compared to mature myelin[175]. In response to dbcAMP, Oli-*neu* cells showed an increase of ePC, pI-PE 18:0, HexCer and sulfatide species whereas the synthesis of aPE, and cholesterol was reduced. This lipidomic analysis indicated that the observed initial increase in ePC and pI-PE plays an important role during the early phases of myelination and was induced by cAMP-mediated metabolic changes within the cell. The biological role of the initial increase of ether lipid synthesis during myelination is not described so far, however in mature myelin ether lipids form a compact and stable structure[41] and might protect cells from oxidation[65]. Especially plasmalogens and phospholipids with C18:1 fatty acids were elevated during the initial phases of OLG development. This is in line with previous observations describing a strong enrichment of C18:1 fatty acids in mature myelin[21,175]. Oleic acid (C18:1 fatty acid) is the major monounsaturated fatty acid in myelin[221]. PC 36:1, containing oleic acid, is decreased in the demyelinating disease multiple sclerosis[221]. Especially in myelin and other brain cells, there is a strong increase of oleic acid synthesis when dietary oleic acid is lacking[222]. The ability of OLGs to self-regulate their oleic acid composition points to important functional roles of oleic acid-containing lipids in myelin. Furthermore a strong decrease in polyunsaturated has been described[175] and was discovered to occur already in early stages of OLG differentiation. The saturated lipid profile of myelin makes it extraordinary stable[24]. The myelin stability is further promoted by an enrichment of GSL and cholesterol[24]. However, the strong accumulation of GalCer and cholesterol could not be detected after 3-5 days differentiation and might increase in later stages, e.g. during myelin wrapping. Alternatively, under the given

experimental conditions cAMP might have not been a sufficient stimulus to activate the synthesis of cholesterol, which was described to increase with the start of myelination[30]. The growth of myelin in CNS is regulated by the PI3 kinase/Akt/TOR signalling pathway[51]. Downstream of its activation are the transcriptional programs for cholesterol synthesis[51] which was presumably not activated in Oli-*neu* cells by adding dbcAMP. The addition of neuron-conditioned medium might help to better mimic the differentiation of Oli-*neu* cells. Nevertheless, initial changes towards an elevation of HexCer species, sulfatide, a strongly decreasing overall unsaturation and a strong elevation of plasmalogen lipids were observed, indicating that myelination was initiated under these conditions.

GalCer and sulfatides with 24:0 and 24:1 FAs are among the most common myelin lipids[27,33]. Especially VLCFA GalCer is enriched in myelin[21]. Oli-*neu* cells differentiated by cAMP showed increased values of VLCFA HexCer as well as VLCFA ceramide and VLCFA SM species which further indicates that cAMP induced the myelination of Oli-*neu* cells. Clearly, as sheets in culture are obviously not able to wrap around axons, the total lipid composition would differ compared to mature myelin sheaths *in vivo*. The extension of the dbcAMP incubation time in Oli-*neu* cells might be able to increase the elevation of especially VLCFA SLs which will be important for assays analysing the protein-VLCFA SL interactions in this context (discussed in section 4.2.2). Conclusively, Oli-*neu* cells showed typical differentiation changes and were therefore capable to study the myelination *in vitro* even though not all common changes occurred upon treatment with cAMP.

4.2.2. Oli-*neu SGPL1*$^{-/-}$ Cells as a Model System to Study Protein-Sphingolipid Interactions

To investigate cellular functions of the protein-VLCFA SL interactions in HeLa cells[124], Oli-*neu* cells were subjected to CRISPR-Cas9 genetic engineering (Section 3.5.2). To analyse the interaction of proteins with sphingolipids using pacSph, SGPL1 knockouts were introduced in Oli-*neu* cells. Two different clones were analysed and both showed a knockout of SGPL1, resulting in an incorporation of pacSph into SL but not into GPL species. Mass spectrometric analysis of pacSph metabolism revealed a pac-labelling of all measured SL classes including HexCer and sulfatide species (Section 3.5.1). The dbcAMP treatment resulted in elevated levels of pac-VLCFA sulfatides[165]. Initial protein-lipid pulldown assays using these

Oli-*neu SGPL*$^{-/-}$ cells showed an interaction of βDG with SLs in these cells. However, confocal microscopic analyses revealed a localisation of βDG to the plasma membrane and intracellular vesicles in undifferentiated cells Oli-*neu SGPL*$^{-/-}$ cells. In wild-type cells, a plasma membrane localisation only occured in differentiated cells. The knockout of SGPL1 might have altered the lipidome in a way that promoted the localisation of βDG to the plasma membrane. Therefore, a lipidomic comparison of SGPL1 S6 knockout cells to Oli-*neu* wild-type cells should be performed. The generation of OLG SGPL1 knockout cells could allow the analysis of proteome-wide protein-sphingolipid interactions before and after induction of myelination. The interaction of dystroglycan and ITGB1 was detected in Oli-*neu* cells, but additional experiments are required to further characterise this interaction and its functional implications during myelination.

4.2.3. Role of VLCFA SL-Dystroglycan Interactions in Oligodendrocytes

To elucidate the functional role of an interaction of VLCFA SLs with dystroglycan in OLGs, CerS2 and dystroglycan knockout cells were generated in Oli-*neu* cells (Section 3.5.2). The Oli-*neu* cells lacking CerS2 showed strongly diminished VLCFA SL species (Section 3.5.1). The strong reduction of VLCFA SLs in Oli-*neu* CerS2 knockout cells makes them a suitable tool to elucidate the functional role of these lipids in OLGs.

VLCFA SLs might be important for protein trafficking during myelination and maintaining their localisation in sheaths. Similar processes are described for other lipids[21,55,60]. For example, cholesterol is involved in trafficking of myelin components to the membrane and is required for PLP to be retained within myelin membranes[21,223]. Further positioning of MBP in membranes[55] is described to depend on the lipid environment and sulfatides are involved in trafficking and stabilisation of NF-155 at paranodes[60]. In general, the knowledge of the functions of lipids in organising proteins during myelination is limited. The mislocalisation of βDG in CerS2 knockout cells upon stimulation of differentiation by dbcAMP indicated that the trafficking of βDG to the plasma membrane relies on VLCFA SLs (Section 3.5.3). However, further experiments are required to support this observation:

Firstly, the ability to differentiate upon stimulation with dbcAMP in Oli-*neu* CerS2 knockout cells needs to be investigated. The differentiation might be unaffected in CerS2 knockout cells if VLCFA SLs are important for differentiation steps upstream of cAMP-mediated signalling. Moreover, OLGs from CerS2 knockout mice are still able to differentiate and myelin is formed[54]. The investigation of the localisation of dystroglycan in myelinating OLGs of CerS2 knockout mice would further show if dystroglycan is mislocalised in mature myelin sheaths of these mice.
Secondly, the endogenous localisation of βDG in undifferentiated OLGs and Oli-*neu* knockout cells needs to be investigated by co-localising with endosomal and other subcellular markers. The identification of the precise localisation of the vesicular βDG pool would support the investigation of the molecular trafficking pathways. Especially the function of the cell-adhesion receptor dystroglycan is thought to be regulated by its targeting to different subcellular sites where it is interacting with its diverse interactions partners[126]. This highlights that lipids could be involved in dystroglycan receptor localisation and therefore regulate its function.

βDG was found to be present in sheets upon differentiation with dbcAMP (Section 3.5.3). Further localisations of βDG to filopodia tips and in focal adhesions of OGLs are described[135] which suggests an interaction with GalCer lipids localised in compact myelin[22] rather than sulfatides. However, GalCer is not essential for myelin and could partially compensated by GlcCer species[62]. Therefore βDG might “unspecifically” interact with a HexCer species. Moreover, the interaction of βDG and VLCFA SLs was discovered in HeLa cells (Section 4.1) showing only minor amounts of GalCer[224] whereas the interacting lipid class of plasma membrane-localised dystroglycan remains to be elucidated (Section 4.1.3).
As mentioned above, besides the possible functional role in trafficking, the stabilisation of βDG in myelin sheaths via VLCFA SLs might be an additional functional role of the discovered interaction as CerS2 and dystroglycan knockouts show negative effects on myelin stability[54,139,141]. The ability of βDG to connect to the actin-cytoskeleton via the DGC complex provides stability in multiple mammalian tissues including myelinating Schwann cells[128]. Interestingly, SGCE belongs to the DGC complex and was also identified by the proteomic approach to specifically interact with VLCFA SLs (Section 4.1)[124]. This suggests that both proteins might be trafficked by VLCFA SLs to the same site and are maintained in

the membrane to provide long-term stability. Oli-*neu* cells cannot be used to study the potential role of the VLCFA SL-βDG interaction in myelin stability as Oli-*neu* cells are not able to myelinate axons when re-transplanted into experimentally demyelinated rat spinal cord[170].

Summarising, an interaction of dystroglycan with SLs was observed in Oli-*neu* cells and a possible role of VLCFA SL in dystroglycan trafficking to the plasma membrane was identified. Furthermore, the established cellular system would help to elucidate specific interactions of sphingolipids with dystroglycan as well as other proteins to understand their functional implications during myelination in OLGs.

5. Materials and Methods

5.1. Cell culture

5.1.1. Materials for Cell Culture

All materials were suitable for cell culture if available, otherwise of analytical grade or of higher purity.

Table 5.1 Cell Lines
WT, wild-type.

Cell line	Origin	Source	Features
HeLa *SGPL1*$^{-/-}$	Human cervical carcinoma	Gerl et al., 2016[115]	SGPL1 knockout
HeLa *SGPL1*$^{-/-}$ *CERS2*$^{-/-}$	Human cervical carcinoma	Ostkotte MSc thesis[124]	SGPL1 and CerS2 knockouts
Oli-*neu*	Immortalised Oligodendroglial progenitor	Jung et al., 1995[170]	WT
Oli-*neu SGPL1*$^{-/-}$ (S2 clone)	Immortalised Oligodendroglial progenitor	This study	SGPL1 knockout
Oli-*neu SGPL1*$^{-/-}$ (S6 clone)	Immortalised Oligodendroglial progenitor	This study	SGPL1 knockout
Oli-*neu CERS2*$^{-/-}$	Immortalised Oligodendroglial progenitor	This study	CerS2 knockout
Oli-*neu DAG1*$^{-/-}$	Immortalised Oligodendroglial progenitor	This study	DAG1 knockout
HEK *SGPL1*$^{-/-}$ (S2 clone)	Immortalised human embryonic kidney	Hannah Olschowski (AG Brügger)	SGPL1 knockout
HEK *SGPL1*$^{-/-}$ *UGCG*$^{-/-}$	Immortalised human embryonic kidney	Provided by P. Haberkant	SGPL1 and UGCG knockout

Table 5.2 Chemicals, Solvents and Reagents used for Cell Culture

Reagent	Company
Apo-Transferrin, human	Sigma-Aldrich
Collagen	Merck
Dibutyryl-Cyclic Adenosine Monophosphate cAMP (dbcAMP)	Sigma-Aldrich
DMEM-Powder	Gibco
DNase I	Roche

Dulbecco's Modified Eagle's Medium (DMEM; 4.5 mg/mL glucose)	Sigma-Aldrich
Ethylenediaminetetraacetic Acid (EDTA)	Roth
Fetal Bovine Serum (FBS) Superior	Merck
FuGENE® HD	Promega
Gentamicin	Invitrogen
Glycerol	Sigma-Aldrich
Hank's Balanced Salt Solution (HBSS)	Gibco
Horse Serum (HS)	Thermo Fisher Scientific
Hybri-Max TM Dimethyl sulfoxide (DMSO)	Sigma-Aldrich
Insulin (10 mg/mL)	Sigma-Aldrich
JetPrime®	PolyPlus
L-Thyroxine	Sigma-Aldrich
Opti-Minimal Essential Medium (Opti-MEM®)	Gibco
Penicillin-Streptomycin (P/S)	Sigma-Aldrich
Phosphate Buffered Saline (PBS)	Sigma-Aldrich
Poly-L-Lysine (PLL)	Sigma-Aldrich
Progesteron	Sigma-Aldrich
Putrescine	Sigma-Aldrich
Roswell Park Memorial Institute (RPMI) 1640	Invitrogen
Sodium Bicarbonate ($NaHCO_3$)	Roth
Sodium hydroxide (NaOH)	Sigma-Aldrich
Sodium Selenite	Sigma-Aldrich
Tri-Iodo-Thyrodine (TIT)	Fluka
Trypan Blue	Sigma-Aldrich
Trypsin-EDTA Solution	Sigma-Aldrich

5.1.2. Cultivation of HeLa and HEK Cells

The cells were cultured at 37°C and 5% CO_2 in DMEM supplemented with 10% FBS and 1% penicillin/streptomycin (P/S). The cultures were kept in monolayers and split 1:10 after 3 to 4 days. The plates were washed 1x with PBS and trypsinised with Trypsin-EDTA solution for 5 min at 37°C, 5% CO_2. The reaction was quenched by addition of 10x pre-warmed (37°C) DMEM (10% FCS, 1%P/S). Then the cells were transferred to a new cell culture dish. HEK cells were plated on collagen-coated dishes. Prior seeding, collagen (200 µL collagen + 1.8 mL PBS) was added to the plates, incubated for 30 min at 37°C and washed 3x with PBS.

5.1.3. Cultivation of Oli-*neu* Cells

The cells were cultured at 37°C and 5% CO_2 in SATO media (Table 5.3) supplemented with 1.5% HS on PLL-coated dishes. To coat with PLL, 7-9 mL of

1x PLL (0.01% w/v in ddH_2O) was incubated for 30 min in a 15 cm dish. After 2x washing with ddH_2O, 18 mL SATO media was added and pre-incubated at 37°C, 5% CO_2 for at least 10 min.

Cells were kept in monolayers and split 1:3 or 1:10 after 3-6 days. Media was removed and 7 mL pre-warmed TE-low (Table 5.4) was added for 2 min. The last minute the cells were rinsed by pipetting. After transfer to a falcon containing 8 mL cold PBS with 10% HS to stop the trypsin digestion, cells were pelleted for 10 min with 800 rpm at 4°C. The supernatant was discarded and the cell pellet was resuspended in SATO media with 1.5% HS and added to the prepared PLL-coated culture dish.

Table 5.3 SATO Media Composition

	1 L	**Final Concentration**
DMEM-Powder	13.4 g	1x
$NaHCO_3$	2 g	2 g/L
Apo-Transferrin	0.01 g	10 µg/mL
Dissolve in 950 mL ddH_2O		
Insulin	1 mL	10 µg/mL
Putrescine	10 mL	100 µM
Progesteron	100 µL	200 nM
Tri-Iodo-Thyrodine	1 mL	500 nM
Sodium-Selenite	740 µL	220 nM
L-Thyroxin	130 µL	520 nM
Adjust with ddH_2O to 1 L		
Gentamicin	500 µl	1x
Filtration through 0.2 µm filter		

Table 5.4 TE (Trypsin-EDTA) low

	Volume
1 % Trypsin	4 mL
0.2% EDTA in HBSS	40 mL
Adjust with HBSS to	400 mL
Filtration through 0.2 µm filter	

Table 5.5 1% Trypsin

	Volume
2.5 % Trypsin	100 mL
10x HBSS	15 mL
ddH_2O	135 mL
DNase I	125 mg
Adjust pH 7.8 with 2 N NaOH	
Filtration through 0.2 µm filter	

5.1.4. Freezing and Thawing of HeLa and HEK Cells

The cells were grown to 70-80% confluency on a 15 cm dish, washed once with PBS and detached with 3 mL Trypsin-EDTA solution. Then the reaction was quenched 1:10 with DMEM (10% FBS, 1% P/S), transferred into a 50 mL falcon and pelleted (5 min, 300 xg at 4°C). Cell pellets were resuspended in 1.5 mL ice-cold FBS, distributed to three cryovials and incubated on ice for 20 min. Per vial, 500 µL of ice-cold 20% DMSO in DMEM was added to cells and the cryovial was inverted a few times. Cells were stored at -80°C for 3 days then transferred to liquid N_2. To thaw cells, cryovials were incubated in a 37°C water bath and transferred into a 15 mL falcon with 10 mL cold DMEM, centrifuged (5 min, 300 xg at 4°C). Obtained cell pellets were resuspended in 1 mL pre-warmed DMEM (10% FBS, 1% P/S) prior transfer to a 10 cm dish filled with 9 mL warm DMEM (10% FBS, 1% P/S). HEK cells were plated on collagen-coated dishes.

5.1.5. Freezing and Thawing of Oli-neu Cells

In each cryovial, one half of subconfluent cells from a 15 cm dish cells were frozen in 1.8 mL freezing medium. Cells were incubated with 7 mL warm TE-low (Table 5.4) for 2 min. The last minute the cells were rinsed by pipetting. After transfer to a falcon containing 8 mL cold PBS with 10% HS to stop the trypsin digestion, cells were pelleted for 10 min with 800 rpm at 4°C. The cell pellet was resuspended in 1.8 mL freezing media per one half of a subconfluent 15 cm dish and the suspension was transferred into cryotubes. Cells were stored at -80°C for 3 days and then transferred to liquid nitrogen.

Table 5.6 Freezing Medium

	Final Concentration
RPMI 1640	70%
FBS	20%
DMSO	10%
Filtration through 0.2 µm filter	

5.1.6. Transfection

To overexpress specific genes, HeLa, HEK and Oli-*neu* cells were transfected with FuGene® HD at a ratio 1:3 of plasmid DNA to transfection reagent. The

transfection reaction set up was prepared as suggested by the supplier. For siRNA-mediated knockdown, HeLa cells were transfected with jetPRIME® transfection reagent according to the manufacturer's instructions.

Table 5.7 List of Plasmids
CMV, Cytomegalo Virus; SRα: Simian Virus 40 (SV40) fused early promoter and the R segment and part of the U5 sequence (R-U5') of the long terminal repeat of human T-cell Leukemia Virus Type 1

Plasmid	Characteristic	Resistance	Promoter	Source
pBJ5-DAG1_WT_FLAG		Ampicillin	SRα	This study
pBJ5-DAG1_ASGR1_FLAG	TMD swap with ASGR1	Ampicillin	SRα	This study
pBJ5-DAG1_CD8a_FLAG	TMD swap with CD8a	Ampcillin	SRα	This study
pBJ5-DAG1_CD63_FLAG	TMD swap with CD63	Ampcillin	SRα	This study
pCMV6-CerS2		Kanamycin	CMV	AG Brügger
pcDNA3.1-CerS1		Ampicillin	CMV	Genescript
pSpCas9(BB)-2A-GFP (PX458)	Empty CRISPR plasmid	Ampicillin	CMV	Feng Zhang Fa. Addgene #48138
pCMV3-DAG1_FLAG		Kanamycin	CMV	Sino Biological Inc.

Table 5.8 siRNAs for Transient Knockdown Experiments

Gene-target	Company	Order number
UGCG	Ambion	AM51334
SGMS1	MISSION® esiRNA; Sigma Aldrich	EHU126521

5.1.7. CRISPR-Cas9 Mediated Knockouts

For CRISPR-Cas9 mediated knockouts, sgRNA targets with very few off-targets were designed according to Ran *et al*., 2013[169] and by employing CCTop[168]. The pair of 5'phosphorylated forward and reverse oligos (Table 5.9) was annealed and ligated into the BbsI digested vector pSpCas9(BB)-2A-GFP (Addgene # PX458[169]). Correct insertion was confirmed by sequencing (Eurofins). The cells were transfected with the generated CRISPR-plasmids and after 48 h and subjected to single cell sorting (FACS facility, ZMBH). GFP-positive cells were sorted into a 96-

well plate containing conditioned medium. Conditioned medium was obtained from respective cell culture supernatants which was filter-sterilised (0.2 µm) and supplemented with 20% FCS. The cells were grown until confluency was reached and expanded. Western Blot analysis (Section 5.3.5), gDNA sequencing (Section 5.2.5) and pacSph metabolism analysis by HPTLC for some knockouts (Section 5.5.2) were employed to identify a successful knockout of individual clones.

Table 5.9 sgRNA Sequences used for CRISPR/Cas9-Mediated Knockouts

sgRNA primer	Species	Sequence (5`-3`)	Cell clones
SGPL1_S2_fwd	Mouse	CACCgCTGCAAAGCTTACCGGGACT	Oli-*neu SGPL1*$^{-/-}$ S2
SGPL1_S2_rev	Mouse	CACCgTGCAAAGCTTACCGGGACT	
SGPL1_S6_fwd	Mouse	CACCGTGCATCAAGGCGGCCCAAC	Oli- *neu SGPL1*$^{-/-}$ S6
SGPL1_S6_rev	Mouse	AAACGTTGGGCCGCCTTGATGCAC	
CerS2_C7_fwd	Mouse	CACCGGTCCCTGCCCGGACGTAAT	Oli- *neu CERS2*$^{-/-}$
CerS2_C7_rev	Mouse	AAACATTACGTCCGGGCAGGGACC	
DAG1_fwd	Mouse	CACCgTACGGAGGGGGTGATCGGTA	Oli- *neu DAG1*$^{-/-}$
DAG1_rev	Mouse	CACCgACGGAGGGGGTGATCGGTA	
DAG1_fwd_h	Human	CACCGCTCCTGGATAGCCGTGGTT	HeLa *SGPL1*$^{-/-}$*DAG1*$^{-/-}$
DAG1_rev_h	Human	AAACAACCACGGCTATCCAGGAGC	

5.2. Molecular Cloning

5.2.1. Materials for Molecular Cloning

All chemicals were of analytical grade or of higher purity. Buffers were prepared in ddH_2O.

Table 5.10 Chemicals, Solvents and Reagents used for Nucleic Acid Biochemistry

Reagent	Company
2-Log DNA ladder (N3200S)	New England BioLabs®
6x DNA loading dye (B7024S)	New England BioLabs®
Acetic acid (AcOH)	Merck
Agarose	Carl Roth
Ampicillin Sodium Salt	Sigma-Aldrich
Bacto™ Agar	BD Biosciences
Bacto™ Tryptone	BD Biosciences
Bacto™ Yeast Extract	BD Biosciences
Bromphenol Blue	Waldeck
Deoxynucleotide (dNTP) Mix, long range, peqGOLD	Peqlab (VWR brand)
Dimethyl Sulfoxide (DMSO)	Sigma-Aldrich
Ethylenediaminetetraacetic acid (EDTA)	Carl Roth
Glacial Acetic Acid	Sigma-Aldrich

SERVA DNA Stain Clear G	SERVA
Glycerol	Sigma-Aldrich
Kanamycin-sulfate	Sigma-Aldrich
Sodium Chloride (NaCl)	Carl Roth
Taq-polymerase	Axon
Tris(hydroxymethyl)aminomethane (Tris)	Carl Roth

5.2.2. Cultivation of Bacteria

E. coli DH5α was cultivated in liquid or on solid LB media (10 g Tryptone, 5 g NaCl, 5 g Yeast Extract, -/+ 15 g Agar per 1 L) and placed at 37°C, liquid cultures were additionally shaken at 180 rpm. All media were autoclaved prior use. LB was supplemented with either Kanamycin (30 µg/mL) or Ampicillin (100 µg/mL).

5.2.3. Heat Transformation of Chemically Competent Bacteria

Chemically competent *E.coli* (Thermo Fisher) were thawed on ice for 10 min and gently mixed with the ligation reaction or plasmid. The mixture was incubated on ice for 30 min before the heat shock was applied (1 min, 42°C) followed by shortly placing on ice again. Afterwards, 950 µL of pre-warmed LB medium was added and the cells were shaken and incubated at 37°C for 1 h. The bacteria were spread on LB agar plates, supplemented with respective antibiotic and incubated at 37°C overnight.

5.2.4. Freezing of Bacterial Cells

For long-term storage of the desired plasmid DNA glycerol stocks were prepared. 850 µL of an overnight culture was mixed with 150 µl of sterile 100 % (v/v) glycerol. The glycerol stock was stored at -80°C until usage. For recovery, a sterile pipette tip was used to scrape some of the frozen material from the glycerol stock. The tip was directly used to inoculate 4 ml of LB medium supplemented with the respective antibiotic. The culture was grown at 37°C overnight.

5.2.5. Agarose Gels

Agarose gels were prepared prior electrophoresis with the desired percentage (w/v) of agarose (1-2%) dissolved in 1x TAE buffer (40 mM Tris, 20 mM Glacial

Acetic Acid, 1 mM EDTA, pH 8) by heating. To visualise DNA, SERVA DNA Stain Clear G was added to the gel.

5.2.6. DNA Isolation and Sequencing

Genomic DNA (gDNA) was isolated using the DNeasy® Blood & Tissue Kit and the target sequence was amplified by the Titanium® Taq PCR Kit. The forward and reverse primer sequences for gDNA amplification (Section 5.2.6) are listed in table 5.11. DNA fragments were sub-cloned into a pCR™2.1 Vector using the TA Cloning™ Kit (Thermo Fisher Scientific) and transformed into *E.coli* cells (Section 5.2.3). Plasmids were isolated using the QIAspin® Spin Miniprep Kit (QIAGEN®), Plasmid Midi or Maxi Kit (QIAGEN®) according to the manufacturer's instructions. Plasmids were sent to sequencing by Eurofins and stored in ddH_2O at -20°C.

5.2.7. Amplification of Gene Fragments

DNA was amplified by polymerase chain reaction (PCR). The following concentrations of ingredients were applied: dNTPs (10 mM each), $MgCl_2$ (25 mM), primer molecules (100 pmol/µl), Polymerase (5 U/µl). The PCR products were purified by QIAquick® PCR Purification Kit (QIAGEN®) and eluted in 30 µL ddH_2O. The DNA yields were measured by Nanodrop™ 2000c.

Table 5.11 Primers Used for gDNA Amplification
Primers were synthesised by Thermo Fisher Scientific.

	5'-3' Sequence	Application
CerS2 gDNA_fwd	CAAGCGAAAGGTGGGTAAAGAGAC	gDNA amplification
CerS2 gDNA_rev	CATAGACAGTAGTATTTGCATGTGGCTAG	gDNA amplification
DAG1 gDNA_fwd (mouse)	CCAAAGTCTCTCCAGCAGCTTTG	gDNA amplification
DAG1 gDNA_rev (mouse)	CAAGCTGACCCTTGAGGACCAG	gDNA amplification
SGPL1 S2_fwd	CACATGCCTTTAATCCCAGCACTTC	gDNA amplification
SGPL1 S2_rev	GAGCAGGCTGTACCTCCTGATACC	gDNA amplification
SGPL1 S6_fwd	GCTCAAAGGGTGTGCCAC	gDNA amplification
SGPL1 S6_rev	CTTCTCCCCTCAGTATGGCTATG	gDNA amplification
DAG1_KpnI_fwd	tttGGTACCATGCGAATGTCCGTG	subcloning
DAG1_XbaI_rev	tttTCTAGATCACTTATCGTCATCGTCCTTATAATC	subcloning

5.2.8. Restriction Digest

All restriction enzymes were purchased from NEB. The digestion of template DNA (vector, PCR product) was performed with type II restriction endonucleases in CutSmart® buffers as suggested by the supplier (NEBcloner). The standard protocol has a reaction volume of 20 µl containing 1-2 µg DNA, 2 U of the restriction endonuclease and was incubated at the corresponding temperature for 1 h. The digest was confirmed by Agarose gel electrophoresis (Section 5.2.5). The DNA was extracted from the gel using the QIAquick® Gel Extraction Kit (QIAGEN®) were eluted in 30 µL ddH_2O.

5.2.9. Ligation

DNA ligation was performed with Quick T4 DNA ligase using the Quick Ligation™ Kit (NEB) according to the manufacturer's instructions. Ligations were either stored at -20°C or 5 µL were directly used for heat transformation of *E. coli* DH5α (Section 5.2.3).

5.2.10. Cloning

Digested vectors (Section 5.2.7) and amplified and digested PCR products (Section 5.2.7) from synthetic gene fragments (obtained from Genscript) were ligated and heat transformed into *E. coli* DH5α (Section 5.2.3). PCR product size was confirmed by Agarose gel electrophoresis (Section 5.2.5) using a DNA ladder. The correct insertion was confirmed by sequencing (Eurofins).

5.3. Protein Assays

5.3.1. Materials for Protein Assays

All chemicals were of analytical grade or of higher purity. Buffers were prepared in ddH_2O.

Table 5.12 Chemicals, Solvents and Reagents Used for Biochemical Protein Assays

Reagent	Company
2-Mercaptoethanol	Carl Roth
Acrylamide-bisacrylamide stock (37.5:1) 30% (v/v)	Carl Roth
Ammoniumperoxodisulfate (APS)	Carl Roth
Bromphenol Blue	Waldeck
Chloroform ($CHCl_3$)	VWR
Copper(II) Sulfate Pentahydrate ($CuSO_4$)	Sigma-Aldrich
Dimethyl Sulfoxide (DMSO)	Sigma-Aldrich
Fumonisin B1 (FB1)	Cayman Chemical
Glycine	LaboChem international
Hydrochloric acid (HCl)	Honeywell
Isopropanol	Sigma-Aldrich
Methanol (MeOH)	VWR
Methyl-β-Cylcodextrin	Sigma-Aldrich
Milk Powder, low fat	Carl Roth
N, N, N', N'-Tetramethylethylendiamine (TEMED)	Carl Roth
Nonidet P40 (NP40) Substitute	Roche
PEG4-Carboxamid-6-Azidohexanyl-Biotin (Biotin-azide)	Invitrogen
Phosphate Buffered Saline (PBS)	Sigma-Aldrich
Precision Plus Protein™ All Blue Prestained Protein Standards (#1610373)	Bio-Rad
Protease Inhibitor Cocktail (PIC), EDTA-free	Roche
Sodium Chloride (NaCl)	Carl Roth
Sodium Dodecyl Sulfate (SDS)	Serva
Triethylamine (TEA)	Sigma-Aldrich
Tris(2carboxyethyl)phosphine Hydrochloride (TCEP)	Sigma-Aldrich
Tris(hydroxymethyl)aminomethane (Tris)	Carl Roth
Tris[(1-benzyl-1H-1,2,3- triazol-4-yl)methyl]amine (TBTA)	Sigma-Aldrich
Triton X-100	Merck
Tween® 20	Carl Roth

5.3.2. Metabolic Labelling of Cultured Cells

The cells were labelled with 6 or 0.5 µM pacSph, or 50 µM pacFA (Table 5.13) for 4 h or 24 h in the respective cell culture media. The cells treated with Fumonisin B1 (50 µM, freshly dissolved in PBS) were pre-incubated for 20 h prior labelling experiments. Methyl-β-Cylcodextrin (5 mM final) was added for the last hour of the labelling time. Afterwards, the cells were subjected to UV-crosslinking and subsequent protein-lipid complex analysis (Section 5.3.3 and 5.3.4) or lipid analysis (Section 5.5.2 and 5.5.3).

Table 5.13 List of Bifunctional Lipids

Bifunctional Lipid	Stock Concentration	Company	Order Number
pacSph	20 mM in EtOH	AG Brügger (T. Sachsenheimer)	
pacFA	50 mM in EtOH	Avanti	900401P

5.3.3. Protein-Lipid Pulldown Assay with Overexpression of Proteins

A confluent 10 cm dish of cells was transfected (Section 5.1.6) for 24 h. After metabolic labelling (Section 5.3.2), the cells were placed on ice and washed twice with ice-cold PBS, overlayed with PBS and subjected to UV-irradiation (365 nm, UVP Blak-Ray®, 100 W) for 5 min on ice. The PBS was removed and the cells were scraped off and transferred into a 1.5 mL tube. Cells were centrifuged (3 min, 3000 rpm at 4°C) and the obtained cell pellet was resuspended in 200 µL lysis buffer (PBS, 1% SDS, 2x PIC) followed by an incubation for 1 h at 4°C on a rotating wheel. A post-nuclear supernatant (PNS) was created by centrifugation for 8 min, 16000 g at 4°C. The protein concentration was determined by the Pierce™ BCA™ Protein-Assay Kit according to the manufacturer's instructions. Per click reaction 200 µg protein was diluted in 187 µL 1% SDS in PBS. For click reaction 5 µL $CuSO_4$, 2 µL Biotin-azide, 4 µL TCEP and 2 µL TBTA (stock and final concentrations in table 5.14) were mixed and added to the protein lysates.

Table 5.14 Click Master Mix
$CuSO_4$, TCEP and TBTA were freshly prepared.

Substance	Solvent	Stock (mM)	Concentration (µM)
$CuSO_4$	H_2O	40	500
Biotin-azide	DMSO	10	50
TCEP	H_2O	50	500
TBTA	DMSO	10	50

After incubation for 4 h at 800 rpm at RT, cell lysates were precipitated according to the method described by Wessel & Flügge 1983[225]. The obtained precipitated protein pellets were washed 2x with ice-cold MeOH and resuspended in 4% SDS in PBS. After dilution to 0.2%, Input samples were taken and the remaining lysate was added to 40 µL washed High Capacity Neutravidin Agarose Resin (Thermo Fisher) to enrich Biotin-clicked protein-lipid complexes. After 3 h incubation at RT on a rotating wheel, the affinity purification was washed 10x with 1 mL 1% SDS in PBS. For Elution, 15 µL 4x Laemmli sample buffer[226] (with freshly added 20% 2-mercaptoethanol) was added and incubated for 15 min at 70°C. After a short centrifugation, the supernatant was yielded and 15 µL new sample buffer was applied and incubated for 95°C for 15 min. Both elutions were combined and loaded along with the Input on an SDS-PAGE gel (Section 5.3.5). Overexpressed proteins were detected with an α-FLAG antibody (Table 5.16).

5.3.4. Protein-Lipid Pulldown Assay with Endogenous Proteins

Two confluent 10 cm dishes were metabolically labelled (Section 5.3.2). After the extact labelling time, cells were placed on ice and washed twice with ice-cold PBS, overlayed with PBS and subjected to UV-irradiation (365 nm, UVP Blak-Ray®, 100W) for 5 min on ice. PBS was removed and cells were scraped off and transferred into a 1.5 mL tube. Cells were pelleted (3 min, 3000 rpm at 4°C) and resuspended in 200 µL NP-40 lysis buffer (50 mM TEA pH 7.4, 150 mM NaCl, 1% (v/v) NP-40, 2x PIC) per 10 cm dish and incubated for 1 h at 4°C on a rotor wheel. A post-nuclear supernatant (PNS) was created at 8 min, 16000 g at 4°C centrifugation. The protein concentration was determined by the Pierce™ BCA™ Protein-Assay Kit according to the manufacturer's instructions. Per click reaction 200 µg protein was diluted in 187 µL NP-40 lysis buffer. For click reaction 5 µL

$CuSO_4$, 2 µL Biotin-azide, 4 µL TCEP and 2 µL TBTA (stock and final concentrations in table 5.14) were mixed and added to the protein lysates.
After incubation for 1 h at 800 rpm (RT), the cell lysates were precipitated according to Wessel & Flügge 1983[225]. Obtained precipitated protein pellets were washed 2x with ice-cold MeOH and resuspended in 4% SDS in PBS by sonication. After dilution to 0.2%, Input samples were taken and the remaining lysate was added to 40 µL washed High Capacity Neutravidin Agarose Resin (Thermo Fisher) to enriched Biotin-clicked protein-lipid complexes. After 3 h incubation at RT on a rotating wheel, the affinity purification was washed 10x with 1 mL 1% SDS in PBS. For Elution, 15 µL 4x Laemmli sample buffer[226] (with freshly added 20% 2-mercaptoethanol) was added and incubated for 15 min at 70°C. After a short centrifugation, the supernatant was yielded and 15 µL new sample buffer was applied and incubated for 15 min at 95°C. Both elutions were combined and loaded along with the Input on an SDS-PAGE gel (section 5.3.5). Endogenous proteins were detected with specific antibodies antibody (Table 5.16).

5.3.5. SDS-PAGE and Western Blot

Protein separation was performed by one-dimensional discontinuous SDS-PAGE as described by Laemmli[226]. The composition of the separation (12%) and stacking gel (4%) is shown in table 5.15. If not stated otherwise, protein samples were mixed with 4x Laemmli sample buffer to 1x concentration and placed for 5 min at 95°C. The gels were run in 1x SDS gel electrophoresis buffer (25 mM (w/v) Tris, 192 mM (w/v) Glycine, 0.1% (w/v) SDS) at 30 mA/gel using the Mini-PROTEAN® Tetra System.

Table 5.15 SDS-Gel Composition
Volume for 2x 0.75 mm gels or 1x 1.5. mm gel.

Reagent	Volume
Separating gel	
ddH_2O	4.05 mL
Tris (1.5 M) pH 8.8	2.5 mL
Acrylamide	3.3 mL
SDS 10% (w/v)	100 µL
TEMED	10 µL
APS 10% (w/v)	100 µL
Stacking gel	
ddH_2O	3.05 mL
Tris (1.5 M) pH 6.8	1.25 mL
Acrylamide	0.64 mL
SDS 10% (w/v)	50 µL
TEMED	10 µL
APS 10% (w/v)	50 µL

Separated proteins on the SDS-PAGE gels were transferred to PVDF membranes by a wet tank electrotransfer. The PVDF membranes were pre-wetted in 100% methanol for 10 s and the blot was assembled as a “sandwich” (2x blotting paper-SDS gel/ activated PVDF membrane/ 2x blotting paper). The protein transfer was performed for 1.5 h, 100 V at 4°C or overnight at 30 V, 4°C (Mini-PROTEAN® Tetra System) in transfer buffer (25 mM (w/v) Tris, 192 mM (w/v) glycine, 10% (v/v) methanol). The membrane was blocked for 60 min at RT or overnight at 4°C in 5% (w/v) low fat milk diluted in PBS with 0.1% (v/v) Tween 20 (PBS-T). The incubation of the membrane with the primary antibody was performed for 1 h at RT or overnight at 4°C, incubation with the second antibody for 60 min at RT or overnight at 4°C (list of antibodies see table 5.16). Before, after as well as in between incubation with antibodies, the membrane was washed 3x with PBS-T for 10 min. The scanning to detect the fluorescent secondary antibodies was performed by a LiCor Odyssey CLx.

Table 5.16 Antibodies Used for Western Blot Analysis
Poly=polyclonal; Mono=monoclonal

Anti-	Species, Clonality	Company (Order Number)	Dilution
FLAG® M2	Mouse, mono	Sigma-Aldrich (F1804)	1:5000
GAPDH	Mouse, mono	Abcam (ab8245)	1:5000
ITGB1	Rabbit, poly	Abcam (ab179471)	1:5000
TFR	Mouse, mono	Thermo Fischer Scientific (13-6800)	1:500
β-Dystroglycan	Mouse, mono	Santa Cruz (sc-165998)	1:1000
STX6	Rabbit, poly	Proteintech (10841-1-AP)	1:2000
TGOLN2	Rabbit, poly	Atlas Antibodies (HPA012609)	1:5000
Anti-mouse IgG (H+L) antibody, IRDye® 800CW Conjugate	Donkey, poly	Rockland (600-145-098)	1:10000
Anti-rabbit IgG (H+L) antibody IRDye® 800 CW	Goat, poly	Rockland (611-131-002)	1:10000

5.4. Microscopy

5.4.1. Materials for Microscopy

All chemicals were of analytical grade or of higher purity. Buffers were prepared in ddH_2O.

Table 5.17 Chemicals, Solvents and Reagents Used for Microscopy

Reagent	Company
4',6-diamidino-2-phenylindole (DAPI)	ThermoFisher Scientific
Albumin Fraction V (BSA)	Carl Roth
Alexa Fluor™ 647 Phalloidin	Thermo Fischer Scientific
Methanol (MeOH)	VWR
Paraformaldehyd (PFA)	Sigma-Aldrich
Phosphate Buffered Saline (PBS)	Sigma-Aldrich
Prolong™ Gold Diamond Antifade Mountant	ThermoFisher Scientific
Sodium Chloride (NaCl)	Carl Roth
Sodium Dodecyl Sulfate (SDS)	Serva
Triton X-100	Merck

5.4.2. Sample Preparation for Microscopy

Oli-*neu* cells were grown on PLL-coated ibi-Treat cell-culture dishes. HeLa cells were grown on coverslips that were added into the cell culture dish. After removal of the cell culture media, the cells were washed 3x with PBS and Oli-*neu* cells were fixed with 4% (w/v) paraformaldehyde (PFA) for 10 min at RT. The HeLa cells were fixed with ice-cold MeOH for 10 min at -20°C. Cells were rinsed 3x with PBS. PFA-treated samples were permeabilised for 10 min with 0.1% (v/v) Triton X-100 at RT. Blocking was performed with 2.5% (w/v) BSA in PBS overnight at 4°C. Incubation with primary (1:50 or 1:100 in 2.5% (w/v) BSA in PBS) and secondary (1:1000 in 2.5% (w/v) BSA in PBS) antibodies (antibodies in table 5.18) was performed for 1 h at RT. Cell nuclei were stained with DAPI (300 nM in PBS) for 10 min at RT. F-actin was stained with Alexa Fluor™ 647 Phalloidin (1x, 5 µL of 40x MeOH stock solution in 200 µL PBS) for 1 h. Coverslips containing HeLa cells were mounted on glass slides with ProLong™ Gold Diamond Antifade Mountant. Oli-*neu* samples on ibiTreat dishes were overlayed with PBS.

Table 5.18 List of Antibodies Used for Microscopy
Poly=polyclonal; Mono=monoclonal

Anti-	Species, Clonality	Company (Order Number)	Dilution
FLAG® M2	Mouse, mono	Sigma-Aldrich (F1804)	1:100
ITGB1	Rabbit, poly	Abcam (ab179471)	1:50
TFR	Mouse, mono	Thermo Fischer Scientific (13-6800)	1:100
β-Dystroglycan	Mouse, mono	Santa Cruz (sc-165998)	1:50
STX6	Rabbit, poly	Proteintech (10841-1-AP)	1:50
TGOLN2	Rabbit, poly	Atlas Antibodies (HPA012609)	1:100
Calnexin (CNX)	Rabbit, poly	Enzo (ADI-SPA-860)	1:100
Anti-rabbit IgG (H+L), Alexa Fluor® 488 Conjugate	Goat, poly	Thermo Fischer Scientific (A11008)	1:1000
Anti-mouse IgG (H+L), Alexa Fluor® 647 Conjugate	Goat, poly	(A21236)	1:1000
Anti-mouse IgG (H+L), Alexa Fluor® 488 Conjugate	Goat, poly	Thermo Fischer Scientific (A11029)	1:1000

5.4.3. Confocal Microscopy

Multicolour fluorescent images were captured using a Zeiss LSM 800 microscope with an 63x/1.4NA Oil Ph3 Plan-Apochromat (a=0.28 mm) objective. The microscope was operated with a ZEN Black software using 405 nm, 488 nm and 640 nm laser diodes.

The following emission bandpass (BP) filters were used. DAPI: BP 425/30; Alexa Fluor®488: BP 514/30; Alexa Fluor®647: BP629/62. The data were exported as *.czi* format files and were analysed with Fiji[227].

5.5. Lipid Assays

5.5.1. Chemicals for Lipid Assays

All chemicals were of analytical grade or of higher purity. Buffers were prepared in ddH_2O.

Table 5.19 Chemicals, Solvents and Reagents Used for Lipid Assays

Reagent	Company
3-Azido-7-Hydroxycoumarin (Coumarin-azide)	Jena Bioscience
Acetonitrile	Sigma-Aldrich
Ammonium Acetate	Sigma-Aldrich
Ammonium Bicarbonate	Honeywell
Chloroform ($CHCl_3$)	VWR
Copper(II) sulfate pentahydrate ($CuSO_4$)	Sigma-Aldrich
Dimethyl Sulfoxide (DMSO)	Sigma-Aldrich
Ethanol (EtOH), 100% (v/v)	VWR
Ethyl Acetate	Zentralbereich Universität Heidelberg
Formic Acid	Merck
Glacial Acetic Acid	Sigma-Aldrich
Hexane	Sigma-Aldrich
Hydrochloric Acid (HCl)	Honeywell
Methanol (MeOH)	VWR
N',N'-diisopropylethylamine	Sigma-Aldrich
Sodium Hydroxide (NaOH)	Sigma-Aldrich
Sulfuric Acid	Sigma-Aldrich
Tetrakis(acetonitrile)copper(I) tetrafluoroborate ($CuBF_4$)	Sigma-Aldrich
Tris(2carboxyethyl)phosphine hydrochloride (TCEP)	Sigma-Aldrich
Tris(hydroxymethyl)aminomethane (Tris)	Sigma-Aldrich

Tris[(1-benzyl-1H-1,2,3- triazol-4-yl)methyl]amine (TBTA)	Sigma-Aldrich
Water HPLC Grade	Merck

5.5.2. HPTLC Analysis

The cells were labelled with bifunctional lipids (Section 5.3.2). After the indicated labelling times, the cells were washed 2x with PBS, detached with 250 µL trypsin and mixed with 1 mL cold DMEM (10% FBS, 1% P/S). The cells were pelleted at 3000 rpm, 3 min at 4°C and washed 2x with 1 mL ice-cold PBS. After resuspension in 300 µL PBS, the cells were subjected to lipid extraction (according to the method described by Thiele *et al*., 2012)[228]. 600 µL MeOH and 150 µL $CHCl_3$ were added and samples were mixed by vortexing for 30 s. After centrifugation at 14000 rpm, 5 min at RT, the supernatant was transferred into a 2 mL tube and was mixed with 300 µL $CHCl_3$ and 600 µL 0.1% (v/v) acetic acid in ddH_2O and were again centrifuged (14000 rpm, 5 min at RT). The lower organic phase was transferred into a fresh 1.5 mL tube and dried in a rotational vacuum concentrator (Christ, RVC 2-18) for 20 min at 30°C. The lipid extracts were resuspended in 7 µL $CHCl_3$ and 30 µL of a freshly prepared Coumarin-click mix was added (Table 5.20):

Table 5.20 Coumarin-azide Click Master Mix
$CuBF_4$ was freshly prepared.

Substance	Solvent	Stock (mM)	Volume (µL)
$CuBF_4$	Acetonitile	10	250
Coumarin-azide	DMSO	44.5	2.5
Ethanol			1000

The click reaction was incubated for 20 min at 45°C in the rotational vacuum concentrator. The lipids were resuspended in 20 µL of mobile phase I ($CHCl_3$:MeOH:H_2O:AcOH at 65:25:4:1), applied to a HPTLC silica gel 60 plate (1.05641.0001, Merck) with the CAMAG Linomat 5 applicator. The plates were developed to 80% in mobile phase I in a CAMAG ADC2 system followed by a development to 100% in mobile phase II (hexane:ethyl actetate at 1:1). The plates were sprayed with 4% (v/v) N,N-diisopropylethylamine in hexane. The Coumarin-clicked lipids were visualized with the Amersham Imager 600 with an excitation at 460 nm and a Cy2 emission filter (525BP20). Charring of lipids was performed by

spraying the TLC plate with 20% (v/v) sulfuric acid in ddH_2O, incubation for 10 min at 125°C and subsequent scanning of the charred lipid bands.

5.5.3. Lipidomics

Lipid extractions were performed by I. Leibrecht, C. Lüchtenborg and T. Sachsenheimer. The lipidomic measurements and data evaluation was provided by C. Lüchtenborg and T. Sachsenheimer (AG Brügger).

5.5.3.1. Sample Preparation for Lipidomics

The cells were washed once with PBS, trypsinised, quenched with 1 mL cold DMEM and transferred to a 1.5 mL tube. The cells were centrifuged for 5 min with 3,000 rpm at 4°C. The obtained cell pellet was washed 3x with DMEM without FBS to remove lipids possibly originating from FBS. The cell pellets were resolved in 100 µL 150 mM NH_4HCO_3 and snap frozen in liquid nitrogen.

5.5.3.2. Lipid Extraction for Lipidomics

For lipid extraction (according to the method described by Bligh & Dyer, 1959[229]), the cells comprising approximately 1-4 nmol of total lipid, were transferred in a Wheaton tube spiked with lipid standards (Table 5.21) and filled up with water to a final volume of 500 µL. 1.9 mL SBD solution (10 mL MeOH, 5 mL $CHCl_3$, 0.75 mL HCl) or 1.9 mL neutral extraction solution (10 mL MeOH, 5 mL $CHCl_3$) was added to the samples and vortexed for 10 s. 500 µL of $CHCl_3$ and HPLC-grade water were added and mixed by vortexing for 30 s. After centrifugation for 2 min with 2,000 rpm at 4°C, the organic phase was transferred into a new Wheaton tube (II). To the new tube II, 500 µL water and $CHCl_3$ were added and to tube I another 500 µL $CHCl_3$ for re-extraction was added. Both tubes were mixed by vortexing and phase separation was performed by centrifugation. The organic phase from tube II was transferred into a new tube (III). The organic phase from tube I was transferred to tube II, vortexed and centrifuged (2 min, 2,000 rpm, 4°C). The resulting organic phase was combined with tube III and the solvent was removed under a nitrogen stream at 37°C. The dried lipids were stored at -20°C. For mass spectrometric analysis, lipids were resolved in 50 µL 10 mM ammonium acetate in methanol.

Table 5.21 List of Lipid Standards
Listed are the name of the lipid standard mixtures and their components. SM, PE, PS, Cer, GlcCer and PG were semi-synthesised as described in Özbalci, Sachsenheimer, & Brügger, 2013[230] and pI-PE was semi-synthesised as described by Paltauf & Hermetter, 1994[231]. PC, phosphatidylcholine; SM, sphingomyelin; PI, phosphatidylinositol; PE, phosphatidylethanolamine; PS, phosphatidylserine; PG, phosphatidylglycerol; PA, phosphatidic acid (PA); pI-PE, ethanolamine plasmalogen; Cer, ceramide; GlcCer, glucosylceramide

Lipid Class	Lipid Composition
Cer, GlcCer	d18:1 with N-acylated 15:0, 17:0, 25:0
Cholesterol-ester (CE)	9:0, 19:0, 24:1 (Sigma Aldrich GmbH)
D6-Cholsterol	D6-Chol (Cambridge Isotope Laboratory, Inc.)
DAG	17:0/17:0 (Larodan Fine Chemicals AB)
PA	PA 17:0/20:4 (Avanti Polar Lipids)
PC	13:0/13:0, 14:0/14:0, 20:0/20:0; 21:0/21:0 (Avanti Polar Lipids)
PE, PS	14:1/14:1, 20:1/20:1, 22:1/22:1
PG	14:1/14:1, 20:1/20:1, 22:1/22:1
PI	16:0/16:0, 17:0/20:4 (Avanti Polar Lipids)
pI-PE	33 pmol pI PE-Mix 1 (16:0p/15:0, 16:0p/19:0, 16:0p/25:0) 46.5 pmol pI PE - Mix 2 (18:0p/15:0, 18:0p/19:0, 18:0p/25:0) 64.5 pmol pI PE - Mix 3 (18:1p/15:0, 18:1p/19:0, 18:1p/25:0)
SM	d18:1 with N-acylated 15:0, 17:0, 25:0
TAG	D5-TAG-Mix, LM- 6000 / D5-TAG 17:0,17:1,17:1 (Avanti Polar Lipids)

5.5.3.3. Derivatization of Cholesterol

For quantification of cholesterol, a single step chemical derivatization to cholesterol acetate was performed[232]. The former solvent was evaporated and 50 µL acetylchloride/chloroform (1:5, v/v) was added and left open for 2 h at RT under a fume hood. If necessary, the remaining solvent was evaporated and the derivatised lipids were re-suspended in 50 µL 10 mM ammonium acetate in MeOH and subjected to mass spectrometric analysis (Section 5.5.3.4).

5.5.3.4. Mass Spectrometric Analysis by ESI-MS/MS

The mass spectrometric analysis was performed using a QTRAP 6500+ mass spectrometer (Sciex), equipped with chip-based (HD-D ESI Chip, Advion Biosciences) electrospray infusion, and ionisation via Triversa Nanomate (Advion Biosciences) for lipid infusion and ionization. 5 µL of the diluted samples were added into a 96-well plate filled with 15 µL 10 mM ammonium acetate, sealed to avoid evaporation and placed into the Nanomate plate holder. The scan settings

of QTRAP 6500+ for the different lipid species according to Özbalci et al., 2013[230]. The obtained data were analysed using the LipidView software (Sciex) and the in-house developed software ShinyLipids.

5.6. Statistical Analysis

Data obtained from protein-lipid pulldown experiments (Section 5.3.3 and 5.3.4) were analysed by two-tailed t-tests for depended (matched) groups due to experimental differences between the replicates (e.g. click-reaction efficiency). The remaining data were analysed by two-tailed unpaired t-tests corrected for multiple comparisons by the Holm-Sidak method, if applicable. *p*-values lower than 0.05 were considered as statistically significant. Values are represented as the mean ± SEM.

6. References

1. Lamari, F., Mochel, F., Sedel, F. & Saudubray, J. M. Disorders of phospholipids, sphingolipids and fatty acids biosynthesis: toward a new category of inherited metabolic diseases. *J. Inherit. Metab. Dis.* **36**, 411–425 (2013).
2. Harayama, T. & Riezman, H. Understanding the diversity of membrane lipid composition. *Nat. Rev. Mol. Cell Biol.* **19**, 281–296 (2018).
3. van Meer, G., Voelker, D. R. & Feigenson, G. W. Membrane lipids: where they are and how they behave. *Nat. Rev. Mol. Cell Biol.* **9**, 112–124 (2008).
4. Russo, D., Parashuraman, S. & D'Angelo, G. Glycosphingolipid–Protein Interaction in Signal Transduction. *Int. J. Mol. Sci.* **17**, 1732 (2016).
5. Lingwood, D. & Simons, K. Lipid rafts as a membrane-organizing principle. *Science* **327**, 46–50 (2010).
6. Bieberich, E. Sphingolipids and lipid rafts: Novel concepts and methods of analysis. *Chem. Phys. Lipids* **216**, 114–131 (2018).
7. Lingwood, D., Kaiser, H.-J., Levental, I. & Simons, K. Lipid rafts as functional heterogeneity in cell membranes. *Biochem. Soc. Trans.* **37**, 955–960 (2009).
8. Zidovetzki, R. & Levitan, I. Use of cyclodextrins to manipulate plasma membrane cholesterol content: Evidence, misconceptions and control strategies. *Biochim. Biophys. Acta - Biomembr.* **1768**, 1311–1324 (2007).
9. Hannun, Y. A. & Obeid, L. M. Sphingolipids and their metabolism in physiology and disease. *Nat. Rev. Mol. Cell Biol.* **19**, 175–191 (2018).
10. Gault, C. R., Obeid, L. M. & Hannun, Y. A. An overview of sphingolipid metabolism: From synthesis to breakdown. *Adv. Exp. Med. Biol.* **688**, 1–23 (2010).
11. Grösch, S., Schiffmann, S. & Geisslinger, G. Chain length-specific properties of ceramides. *Prog. Lipid Res.* **51**, 50–62 (2012).
12. Mullen, T. D., Hannun, Y. A. & Obeid, L. M. Ceramide synthases at the centre of sphingolipid metabolism and biology. **802**, 789–802 (2012).
13. Levy, M. & Futerman, A. H. Mammalian ceramide synthases. *IUBMB Life* **62**, 347–356 (2010).
14. Ben-David, O. *et al.* Encephalopathy caused by ablation of very long acyl chain ceramide synthesis may be largely due to reduced galactosylceramide levels. *J. Biol. Chem.* **286**, 30022–30033 (2011).
15. Sassa, T. & Kihara, A. Metabolism of Very Long-Chain Fatty Acids : Genes and Pathophysiology. *Biomol. Ther. (Seoul).* **22**, 83–92 (2014).
16. Ogretmen, B. Sphingolipid metabolism in cancer signalling and therapy. *Nat. Rev. Cancer* **18**, 33–50 (2017).
17. Fyrst, H. & Saba, J. D. An update on sphingosine-1-phosphate and other sphingolipid mediators. *Nat. Chem. Biol.* **6**, 489–497 (2010).
18. Tafesse, F. G. *et al.* Both sphingomyelin synthases SMS1 and SMS2 are required for sphingomyelin homeostasis and growth in human HeLa cells. *J. Biol. Chem.* **282**, 17537–17547 (2007).
19. Ohno, Y. *et al.* ELOVL1 production of C24 acyl-CoAs is linked to C24 sphingolipid synthesis. *Proc. Natl. Acad. Sci. U. S. A.* **107**, 18439–18444 (2010).
20. Poitelon, Y., Kopec, A. M. & Belin, S. Myelin Fat Facts : An Overview of Lipids and Fatty Acid Metabolism. *Cells* **9**, 812 (2020).
21. Schmitt, S., Cantuti Castelvetri, L. & Simons, M. Metabolism and functions of lipids in myelin. *Biochim. Biophys. Acta - Mol. Cell Biol. Lipids* **1851**, 999–1005 (2015).
22. Baron, W. & Hoekstra, D. On the biogenesis of myelin membranes: Sorting, trafficking and cell polarity. *FEBS Lett.* **584**, 1760–1770 (2010).
23. Buttermore, E. D., Thaxton, C. L. & Bhat, M. A. Organization and maintenance of molecular domains in myelinated axons. *J. Neurosci. Res.* **91**, 603–622 (2013).
24. Simons, M. & Nave, K. A. Oligodendrocytes: Myelination and axonal support. *Cold Spring Harb. Perspect. Biol.* **8**, 1–16 (2016).
25. Gard, A. L. & Pfeiffer, S. E. Two proliferative stages of the oligodendrocyte lineage (A2B5+O4- and O4+GalC-) under different mitogenic control. *Neuron* **5**, 615–625 (1990).
26. Jackman, N., Ishii, A. & Bansal, R. Oligodendrocyte development and myelin biogenesis: parsing out the roles of glycosphingolipids. *Physiology (Bethesda).* **24**, 290–7 (2009).
27. Hirahara, Y. *et al.* Sulfatide species with various fatty acid chains in oligodendrocytes at

different developmental stages determined by imaging mass spectrometry. *J. Neurochem.* **140**, 1–16 (2016).
28. Ranscht, B., Clapshaw, P. A., Price, J., Noble, M. & Seifert, W. Development of oligodendrocytes and Schwann cells studied with a monoclonal antibody against galactocerebroside. *Proc. Natl. Acad. Sci. U. S. A.* **79**, 2709–2713 (1982).
29. Ellen Gielen, Wia Baron, Martin Vandeven, Paul Streels, Dick Hoekstra, M. A. Rafts in Oligodendrocytes: Evidence and Structure–Function Relationship. *Glia* **54**, 523–532 (2006).
30. Saher, G. *et al.* High cholesterol level is essential for myelin membrane growth. *Nat. Neurosci.* **8**, 468–475 (2005).
31. Koper, J. W., Lopes-Cardozo, M. & Van Golde, L. M. G. Preferential utilization of ketone bodies for the synthesis of myelin cholesterol in vivo. *Biochim. Biophys. Acta - Lipids Lipid Metab.* **666**, 411–417 (1981).
32. Arenas, F., Garcia-Ruiz, C. & Fernandez-Checa, J. C. Intracellular Cholesterol Trafficking and Impact in Neurodegeneration. *Front. Mol. Neurosci.* **10**, 382 (2017).
33. Chrast, R., Saher, G., Nave, K.-A. & Verheijen, M. H. G. Lipid metabolism in myelinating glial cells: lessons from human inherited disorders and mouse models. *J. Lipid Res.* **52**, 419–434 (2011).
34. Becker, I., Wang-Eckhardt, L., Yaghootfam, A., Gieselmann, V. & Eckhardt, M. Differential expression of (dihydro)ceramide synthases in mouse brain: Oligodendrocyte-specific expression of CerS2/Lass2. *Histochem. Cell Biol.* **129**, 233–241 (2008).
35. Boggs, J. M. Early glycolipid (POA) in pro-oligodendroblasts revealed to be sulfatide. *J. Neurochem.* **140**, 4–6 (2016).
36. Eckhardt, M., Yaghootfam, A., Fewou, S. N., Zoller, I. & Gieselmann, V. A mammalian fatty acid hydroxylase responsible for the formation of alpha-hydroxylated galactosylceramide in myelin. *Biochem. J.* **388**, 245–254 (2005).
37. Ishibashi, Y., Kohyama-Koganeya, A. & Hirabayashi, Y. New insights on glucosylated lipids: Metabolism and functions. *Biochim. Biophys. Acta - Mol. Cell Biol. Lipids* **1831**, 1475–1485 (2013).
38. Gould, R. M. & Dawson, R. M. C. Incorporation of newly formed lecithin into peripheral nerve myelin. *J. Cell Biol.* **68**, 480–496 (1976).
39. Gould, R. M. Incorporation of Glycoproteins into Peripheral Nerve Myelin. *J. Cell Biol.* **75**, 326–338 (1977).
40. Maier, O., Hoekstra, D. & Baron, W. Polarity development in oligodendrocytes: Sorting and trafficking of myelin components. *J. Mol. Neurosci.* **35**, 35–53 (2008).
41. Braverman, N. E. & Moser, A. B. Functions of plasmalogen lipids in health and disease. *Biochim. Biophys. Acta - Mol. Basis Dis.* **1822**, 1442–1452 (2012).
42. Rog, T. & Koivuniemi, A. The biophysical properties of ethanolamine plasmalogens revealed by atomistic molecular dynamics simulations. *Biochim. Biophys. Acta* **1858**, 97–103 (2016).
43. Da Silva, T. F., Sousa, V. F., Malheiro, A. R. & Brites, P. The importance of ether-phospholipids: A view from the perspective of mouse models. *Biochim. Biophys. Acta - Mol. Basis Dis.* **1822**, 1501–1508 (2012).
44. Aureli, M., Grassi, S., Prioni, S., Sonnino, S. & Prinetti, A. Lipid membrane domains in the brain. *Biochim. Biophys. Acta* **1851**, 1006–16 (2015).
45. Ozgen, H., Baron, W., Hoekstra, D. & Kahya, N. Oligodendroglial membrane dynamics in relation to myelin biogenesis. *Cell. Mol. Life Sci.* **73**, 3291–3310 (2016).
46. Marbois, B. N., Faull, K. F., Fluharty, A. L., Raval-Fernandes, S. & Rome, L. H. Analysis of sulfatide from rat cerebellum and multiple sclerosis white matter by negative ion electrospray mass spectrometry. *Biochim. Biophys. Acta* **1484**, 59–70 (2000).
47. Zhou, Y. *et al.* A neutral lipid-enriched diet improves myelination and alleviates peripheral nerve pathology in neuropathic mice. *Exp. Neurol.* **321**, 113031 (2019).
48. Czubowicz, K., Jesko, H., Wencel, P., Lukiw, W. J. & Strosznajder, R. P. The Role of Ceramide and Sphingosine-1-Phosphate in Alzheimer's Disease and Other Neurodegenerative Disorders. *Mol. Neurobiol.* **56**, 5436–5455 (2019).
49. Sherman, D. L. & Brophy, P. J. Mechanisms of axon ensheathment and myelin growth. *Nat. Rev. Neurosci.* **6**, 683–90 (2005).
50. Maier, O. *et al.* The function of neurofascin155 in oligodendrocytes is regulated by metalloprotease-mediated cleavage and ectodomain shedding. *Exp. Cell Res.* **312**, 500–511 (2006).
51. Saher, G. & Stumpf, S. K. Cholesterol in myelin biogenesis and hypomyelinating disorders. *Biochim. Biophys. Acta - Mol. Cell Biol. Lipids* **1851**, 1083–1094 (2015).

52. German, D. . *et al.* Neurodegeneration in the Niemann–Pick C mouse: glial involvement. *Neuroscience* **109**, 437–450 (2002).
53. Yu, T. & Lieberman, A. P. Npc1 Acting in Neurons and Glia Is Essential for the Formation and Maintenance of CNS Myelin. *PLoS Genet.* **9**, e1003462 (2013).
54. Imgrund, S. *et al.* Adult ceramide synthase 2 (CERS2)-deficient mice exhibit myelin sheath defects, cerebellar degeneration, and hepatocarcinomas. *J. Biol. Chem.* **284**, 33549–60 (2009).
55. Min, Y. *et al.* Interaction forces and adhesion of supported myelin lipid bilayers modulated by myelin basic protein. *Proc. Natl. Acad. Sci. U. S. A.* **106**, 3154–3159 (2009).
56. Mueller, N. *et al.* De novo mutation in ELOVL1 causes ichthyosis, acanthosis nigricans, hypomyelination, spastic paraplegia, high frequency deafness and optic atrophy. *J. Med. Genet.* **56**, 1–12 (2018).
57. Sassa, T. *et al.* Impaired Epidermal Permeability Barrier in Mice Lacking Elovl1, the Gene Responsible for Very-Long-Chain Fatty Acid Production. *Mol. Cell. Biol.* **33**, 2787–2796 (2013).
58. Zöller, I., Büssow, H., Gieselmann, V. & Eckhardt, M. Oligodendrocyte-specific ceramide galactosyltransferase (CGT) expression phenotypically rescues CGT-deficient mice and demonstrates that CGT activity does not limit brain galactosylceramide level. *Glia* **52**, 190–198 (2005).
59. Grassi, S. *et al.* The role of 3-O-sulfogalactosylceramide, sulfatide, in the lateral organization of myelin membrane. *Neurochem. Res.* **41**, 130–143 (2016).
60. Poliak, S. & Peles, E. The local differentiation of myelinated axons at nodes of Ranvier. *Nat. Rev. Neurosci.* **4**, 968–980 (2003).
61. Boggs, J. M. *et al.* Participation of galactosylceramide and sulfatide in glycosynapses between oligodendrocyte or myelin membranes. *FEBS Lett.* **584**, 1771–1778 (2010).
62. Saadat, L. *et al.* Absence of oligodendroglial glucosylceramide synthesis does not result in CNS myelin abnormalities or alter the dysmyelinating phenotype of CGT-deficient mice. *Glia* **58**, 391–398 (2010).
63. Yang, L. J. *et al.* Gangliosides are neuronal ligands for myelin-associated glycoprotein. *Proc. Natl. Acad. Sci. U. S. A.* **93**, 814–818 (1996).
64. Rodemer, C. *et al.* Inactivation of ether lipid biosynthesis causes male infertility, defects in eye development and optic nerve hypoplasia in mice. *Hum. Mol. Genet.* **12**, 1881–1895 (2003).
65. Broniec, A. *et al.* Interactions of plasmalogens and their diacyl analogs with singlet oxygen in selected model systems. *Free Radic. Biol. Med.* **50**, 892–898 (2011).
66. Lessig, J. & Fuchs, B. Plasmalogens in biological systems: their role in oxidative processes in biological membranes, their contribution to pathological processes and aging and plasmalogen analysis. *Curr. Med. Chem.* **16**, 2021–2041 (2009).
67. Haberkant, P. *et al.* Protein-sphingolipid interactions within cellular membranes. *J. Lipid Res.* **49**, 251–262 (2008).
68. Contreras, F., Ernst, A. M., Wieland, F. & Brugger, B. Specificity of Intramembrane Protein − Lipid Interactions. *Cold Spring Harb. Perspect. Biol.* **3**, 6 (2011).
69. Gubbens, J. & de Kroon, A. I. P. M. Proteome-wide detection of phospholipid-protein interactions in mitochondria by photocrosslinking and click chemistry. *Mol. Biosyst.* **6**, 1751–1759 (2010).
70. Ernst, A. M., Contreras, F. X., Brügger, B. & Wieland, F. Determinants of specificity at the protein-lipid interface in membranes. *FEBS Lett.* **584**, 1713–1720 (2010).
71. Coskun, Ü., Grzybek, M., Drechsel, D. & Simons, K. Regulation of human EGF receptor by lipids. *Proc. Natl. Acad. Sci. U. S. A.* **108**, 9044–9048 (2011).
72. Contreras, F.-X. *et al.* Molecular recognition of a single sphingolipid species by a protein's transmembrane domain. *Nature* **481**, 525–529 (2012).
73. Saliba, A.-E., Vonkova, I. & Gavin, A.-C. The systematic analysis of protein–lipid interactions comes of age. *Nat. Rev. Mol. Cell Biol.* **16**, 753–761 (2015).
74. Lee, A. G. Lipid-protein interactions in biological membranes: a structural perspective. *Biochim. Biophys. Acta* **1612**, 1–40 (2003).
75. Schreiber, G. Kinetic studies of protein-protein interactions. *Curr. Opin. Struct. Biol.* **12**, 41–47 (2002).
76. Anderson, R. G. W. & Jacobson, K. A role for lipid shells in targeting proteins to caveolae, rafts, and other lipid domains. *Science (80-.).* **296**, 1821–1825 (2002).
77. Pliotas, C. *et al.* The role of lipids in mechanosensation. **22**, (2015).

78. Perozo, E., Kloda, A., Cortes, D. M. & Martinac, B. Physical principles underlying the transduction of bilayer deformation forces during mechanosensitive channel gating. *Nat. Struct. Biol.* **9**, 696–703 (2002).
79. Luecke, H., Schobert, B., Richter, H. T., Cartailler, J. P. & Lanyi, J. K. Structure of bacteriorhodopsin at 1.55 A resolution. *J. Mol. Biol.* **291**, 899–911 (1999).
80. Murata, T., Yamato, I., Kakinuma, Y., Leslie, A. G. W. & Walker, J. E. Structure of the rotor of the V-Type Na+-ATPase from Enterococcus hirae. *Science* **308**, 654–659 (2005).
81. Li, H., Yao, Z., Degenhardt, B., Teper, G. & Papadopoulos, V. Cholesterol binding at the cholesterol recognition/ interaction amino acid consensus (CRAC) of the peripheral-type benzodiazepine receptor and inhibition of steroidogenesis by an HIV TAT-CRAC peptide. *Proc. Natl. Acad. Sci. U. S. A.* **98**, 1267–1272 (2001).
82. Hanson, M. A. *et al.* A specific cholesterol binding site is established by the 2.8 A structure of the human beta2-adrenergic receptor. *Structure* **16**, 897–905 (2008).
83. Gimpl, G., Burger, K. & Fahrenholz, F. A closer look at the cholesterol sensor. *Trends in biochemical sciences* **27**, 596–599 (2002).
84. Gimpl, G., Wiegand, V., Burger, K. & Fahrenholz, F. Cholesterol and steroid hormones: modulators of oxytocin receptor function. *Prog. Brain Res.* **139**, 43–55 (2002).
85. Bremers, E. G., Schlessinger, J. & Hakomoris, S. Ganglioside-mediated Modulation of Cell Growth. **261**, 2434–2440 (1986).
86. Deák, F. *et al.* Novel Cellular Functions of Very Long Chain-Fatty Acids: Insight From ELOVL4 Mutations. *Front. Cell. Neurosci.* **13**, 428 (2019).
87. Sandhoff, R. Very long chain sphingolipids: Tissue expression, function and synthesis. *FEBS Lett.* **584**, 1907–1913 (2010).
88. Hannun, Y. A. & Obeid, L. M. Many Ceramides. *J. Biol. Chem.* **286**, 27855–27862 (2011).
89. Pewzner-Jung, Y. *et al.* A critical role for ceramide synthase 2 in liver homeostasis: I. alterations in lipid metabolic pathways. *J. Biol. Chem.* **285**, 10902–10910 (2010).
90. Kurz, J., Parnham, M. J., Geisslinger, G. & Schiffmann, S. Ceramides as Novel Disease Biomarkers. *Trends Mol. Med.* **25**, 20–32 (2019).
91. Garić, D., De Sanctis, J. B., Shah, J., Dumut, D. C. & Radzioch, D. Biochemistry of very-long-chain and long-chain ceramides in cystic fibrosis and other diseases: The importance of side chain. *Prog. Lipid Res.* **74**, 130–144 (2019).
92. Silva, L. C. *et al.* Ablation of ceramide synthase 2 strongly affects biophysical properties of membranes. *J. Lipid Res.* **53**, 430–436 (2012).
93. Simons, K. & Ikonen, E. Functional rafts in cell membranes. *Nature* **387**, 569–572 (1997).
94. Kasahara, K. & Sanai, Y. Functional roles of glycosphingolipids in signal transduction via lipid rafts. *Glycoconj. J.* **17**, 153–162 (2000).
95. Sonnino, S. *et al.* Role of very long fatty acid-containing glycosphingolipids in membrane organization and cell signaling: the model of lactosylceramide in neutrophils. *Glycoconj. J.* **26**, 615–621 (2009).
96. Iwabuchi, K. *et al.* Involvement of very long fatty acid-containing lactosylceramide in lactosylceramide-mediated superoxide generation and migration in neutrophils. *Glycoconj. J.* **25**, 357–374 (2008).
97. Obara, K., Kojima, R., Kihara, A. & Gtpase, R. Effects on vesicular transport pathways at the late endosome in cells with limited very long-chain fatty acids. **54**, 831–842 (2013).
98. Hurst, L. R. *et al.* Sphingolipids with Very Long-chain Fatty Acids Regulate Vacuole Fusion During Tethering and Docking. *bioRxiv* 1–40 (2020).
99. Turpin, S. M. *et al.* Obesity-Induced CerS6-Dependent C16:0 Ceramide Production Promotes Weight Gain and Glucose Intolerance. *Cell Metab.* **20**, 678–686 (2014).
100. Hammerschmidt, P. *et al.* CerS6-Derived Sphingolipids Interact with Mff and Promote Mitochondrial Fragmentation in Obesity. *Cell* **177**, 1536-1552.e23 (2019).
101. Yamaji, T. *et al.* Role of intracellular lipid logistics in the preferential usage of very long chain-ceramides in glucosylceramide. *Int. J. Mol. Sci.* **17**, 1–16 (2016).
102. Tafesse, F. G. *et al.* Intact sphingomyelin biosynthetic pathway is essential for intracellular transport of influenza virus glycoproteins. *Proc. Natl. Acad. Sci. U. S. A.* **110**, 6406–11 (2013).
103. Wegner, M.-S., Schiffmann, S., Parnham, M. J., Geisslinger, G. & Grösch, S. The Enigma Of Ceramide Synthase Regulation In Mammalian Cells. *Prog. Lipid Res.* **63**, 93–119 (2016).
104. Brügger, B. *et al.* Evidence for segregation of sphingomyelin and cholesterol during formation of COPI-coated vesicles. *J. Cell Biol.* **151**, 507–518 (2000).
105. Haberkant, P. & Holthuis, J. C. M. Fat & fabulous: Bifunctional lipids in the spotlight. *Biochim.*

Biophys. Acta - Mol. Cell Biol. Lipids **1841**, 1022–1030 (2014).
106. Amrich, M. J. & Bell, J. A. Photoisomerization of diazirine. *J. Am. Chem. Soc.* **86**, 292–293 (1964).
107. Haberkant, P. & van Meer, G. Protein-lipid interactions: paparazzi hunting for snap-shots. *Biol. Chem.* **390**, 795–803 (2009).
108. Offord, R. E. Protection of peptides of biological origin for use as intermediates in the chemical synthesis of proteins. *Nature* **221**, 37–40 (1969).
109. Ross, A. H., Radhakrishnan, R., Robson, R. J. & Khorana, H. G. The transmembrane domain of glycophorin A as studied by cross-linking using photoactivatable phospholipids. *J. Biol. Chem.* **257**, 4152–4161 (1982).
110. Kolb, H. C., Finn, M. G. & Sharpless, K. B. Click Chemistry: Diverse Chemical Function from a Few Good Reactions. *Angew. Chem. Int. Ed. Engl.* **40**, 2004–2021 (2001).
111. Gaebler, A., Penno, A., Kuerschner, L. & Thiele, C. A highly sensitive protocol for microscopy of alkyne lipids and fluorescently tagged or immunostained proteins. **57**, (2016).
112. Liang, L. & Astruc, D. The copper(I)-catalyzed alkyne-azide cycloaddition (CuAAC) 'click' reaction and its applications. An overview. *Coord. Chem. Rev.* **255**, 2933–2945 (2011).
113. Haberkant, P. *et al.* Bifunctional Sphingosine for Cell-Based Analysis of Protein-Sphingolipid Interactions. *ACS Chem. Biol.* **11**, 222–230 (2016).
114. Gaebler, A., Penno, A., Kuerschner, L. & Thiele, C. A highly sensitive protocol for microscopy of alkyne lipids and fluorescently tagged or immunostained proteins. *J. Lipid Res.* **57**, 1934–1947 (2016).
115. Gerl, M. J. *et al.* Sphingosine-1-Phosphate Lyase Deficient Cells as a Tool to Study Protein Lipid Interactions. *PLoS One* **11**, e0153009 (2016).
116. Suzuki, E., Handa, K., Toledo, M. S. & Hakomori, S. Sphingosine-dependent apoptosis: a unified concept based on multiple mechanisms operating in concert. *Proc. Natl. Acad. Sci. U. S. A.* **101**, 14788–14793 (2004).
117. Saha, S. *et al.* Diffusion of GPI-anchored proteins is influenced by the activity of dynamic cortical actin. *Mol. Biol. Cell* **26**, 4033–4045 (2015).
118. Goswami, D. *et al.* Nanoclusters of GPI-anchored proteins are formed by cortical actin-driven activity. *Cell* **135**, 1085–1097 (2008).
119. Levental, I. & Veatch, S. The continuing mystery of lipid rafts. **428**, 4749–4764 (2017).
120. Reverter, M. *et al.* Cholesterol Regulates Syntaxin 6 Trafficking at trans-Golgi Network Endosomal Boundaries. *Cell Rep.* **7**, 883–897 (2014).
121. Taylor, C. M., Coetzee, T. & Pfeiffer, S. E. Detergent-insoluble glycosphingolipid/cholesterol microdomains of the myelin membrane. *J. Neurochem.* **81**, 993–1004 (2002).
122. Leitinger, B. & Hogg, N. The involvement of lipid rafts in the regulation of integrin function. *J. Cell Sci.* **115**, 963–972 (2002).
123. Percherancier, Y. *et al.* HIV-1 entry into T-cells is not dependent on CD4 and CCR5 localization to sphingolipid-enriched, detergent-resistant, raft membrane domains. *J. Biol. Chem.* **278**, 3153–3161 (2003).
124. Ostkotte, D. Lipidomic Characterization of Ceramide Synthase Knockout Cells and Identification of Very-Long Chain Sphingolipid Interacting Proteins. (Ruprecht-Karls-Universität Heidelberg, 2016).
125. Adams, J. C. & Brancaccio, A. The evolution of the dystroglycan complex, a major mediator of muscle integrity. *Co. Biol.* **4**, 1163–1179 (2015).
126. Moore, C. J. & Winder, S. J. Dystroglycan versatility in cell adhesion: a tale of multiple motifs. *Cell Commun. Signal.* **8**, 3 (2010).
127. Holmberg, J. & Durbeej, M. Laminin-211 in skeletal muscle function. *Cell Adhes. Migr.* **7**, 111–121 (2013).
128. Walko, G. *et al.* Stabilization of the dystroglycan complex in Cajal bands of myelinating Schwann cells through plectin-mediated anchorage to vimentin filaments. *Glia* **61**, 1274–1287 (2013).
129. Cotton, S. M., Voudouris, N. J. & Greenwood, K. M. Association between intellectual functioning and age in children and young adults with Duchenne muscular dystrophy: further results from a meta-analysis. *Dev. Med. Child Neurol.* **47**, 257–265 (2005).
130. Aranmolate, A., Tse, N. & Colognato, H. Myelination is delayed during postnatal brain development in the mdx mouse model of Duchenne muscular dystrophy. *BMC Neurosci.* **18**, 63 (2017).
131. Chun, S. J., Rasband, M. N., Sidman, R. L., Habib, A. A. & Vartanian, T. Integrin-linked kinase is required for laminin-2-induced oligodendrocyte cell spreading and CNS

myelination. *J. Cell Biol.* **163**, 397–408 (2003).
132. Relucio, J., Menezes, M. J., Miyagoe-Suzuki, Y., Takeda, S. & Colognato, H. Laminin regulates postnatal oligodendrocyte production by promoting oligodendrocyte progenitor survival in the subventricular zone. *Glia* **60**, 1451–1467 (2012).
133. Relucio, J., Tzvetanova, I. D., Ao, W., Lindquist, S. & Colognato, H. Laminin alters fyn regulatory mechanisms and promotes oligodendrocyte development. *J. Neurosci.* **29**, 11794–11806 (2009).
134. Colognato, H. *et al.* Identification of dystroglycan as a second laminin receptor in oligodendrocytes, with a role in myelination. *Development* **134**, 1723–1736 (2007).
135. Eyermann, C., Czaplinski, K. & Colognato, H. Dystroglycan promotes filopodial formation and process branching in differentiating oligodendroglia. *J. Neurochem.* **120**, 928–947 (2012).
136. Galvin, J., Eyermann, C. & Colognato, H. Dystroglycan modulates the ability of insulin-like growth factor-1 to promote oligodendrocyte differentiation. *J. Neurosci. Res.* **88**, 3295–3307 (2010).
137. Sharma, H. *et al.* Dystroglycan Suppresses Notch to Regulate Stem Cell Niche Structure and Function in the Developing Postnatal Subventricular Zone Article Dystroglycan Suppresses Notch to Regulate Stem Cell Niche Structure and Function in the Developing Postnatal Subventri. *Dev. Cell* **38**, 1–19 (2016).
138. Vajda, Z. *et al.* Delayed onset of brain edema and mislocalization of aquaporin-4 in dystrophin-null transgenic mice. *Proc. Natl. Acad. Sci. U. S. A.* **99**, 13131–13136 (2002).
139. Cai, H. *et al.* The sarcoglycan complex in Schwann cells and its role in myelin stability. *Exp. Neurol.* **205**, 257–269 (2007).
140. Leiton, C. V. *et al.* Laminin promotes metalloproteinase-mediated dystroglycan processing to regulate oligodendrocyte progenitor cell proliferation. *J. Neurochem.* **135**, 522–538 (2015).
141. Nickolls, A. R., Bonnemann, C. G. & Bo, C. G. The roles of dystroglycan in the nervous system: insights from animal models of muscular dystrophy. *Dis. Model. Mech.* **11**, 1–17 (2018).
142. Satz, J. S. *et al.* Distinct Functions of Glial and Neuronal Dystroglycan in the Developing and Adult Mouse Brain. *J. Neurosci.* **30**, 14560–14572 (2010).
143. Li, S. *et al.* Laminin-sulfatide binding initiates basement membrane assembly and enables receptor signaling in Schwann cells and fibroblasts. *J. Cell Biol.* **169**, 179–189 (2005).
144. Waite, A., Tinsley, C. L., Locke, M. & Blake, D. J. The neurobiology of the dystrophin-associated glycoprotein complex. *Ann. Med.* **41**, 344–359 (2009).
145. Haenggi, T. & Fritschy, J.-M. Role of dystrophin and utrophin for assembly and function of the dystrophin glycoprotein complex in non-muscle tissue. *Cell. Mol. Life Sci.* **63**, 1614–1631 (2006).
146. Sotgia, F. *et al.* Localization of phospho-β-dystroglycan (pY892) to an intracellular vesicular compartment in cultured cells and skeletal muscle fibers in vivo. *Biochemistry* **42**, 7110–7123 (2003).
147. Ilsley, J. L., Sudol, M. & Winder, S. J. The interaction of dystrophin with beta-dystroglycan is regulated by tyrosine phosphorylation. *Cell. Signal.* **13**, 625–632 (2001).
148. Ilsley, J. L., Sudol, M. & Winder, S. J. The WW domain: linking cell signalling to the membrane cytoskeleton. *Cell. Signal.* **14**, 183–189 (2002).
149. Eich, C. *et al.* Changes in membrane sphingolipid composition modulate dynamics and adhesion of integrin nanoclusters. *Sci. Rep.* **6**, 1–15 (2016).
150. Legate, K. R., Wickstrom, S. A. & Fassler, R. Genetic and cell biological analysis of integrin outside-in signaling. *Genes Dev.* **23**, 397–418 (2009).
151. Rezniczek, G. A. *et al.* Plectin 1f scaffolding at the sarcolemma of dystrophic (mdx) muscle fibers through multiple interactions with beta-dystroglycan. *J. Cell Biol.* **176**, 965–977 (2007).
152. Thompson, O. *et al.* Modulation of cell spreading and cell-substrate adhesion dynamics by dystroglycan. *J. Cell Sci.* **123**, 118–127 (2010).
153. Chen, Y.-J. *et al.* Direct interaction of beta-dystroglycan with F-actin. *Biochem. J.* **375**, 329–337 (2003).
154. Batchelor, C. L. *et al.* Recruitment of Dbl by ezrin and dystroglycan drives membrane proximal Cdc42 activation and filopodia formation. *Cell Cycle* **6**, 353–363 (2007).
155. Sotgia, F. *et al.* Caveolin-3 directly interacts with the C-terminal tail of beta -dystroglycan. Identification of a central WW-like domain within caveolin family members. *J. Biol. Chem.* **275**, 38048–38058 (2000).

156. Mann, M. Functional and quantitative proteomics using SILAC. *Nat. Rev. Mol. cell Biol.* **7**, 952–958 (2006).
157. Singh, S. & Mittal, A. Transmembrane Domain Lengths Serve as Signatures of Organismal Complexity and Viral Transport Mechanisms. *Sci. Rep.* **6**, 22352 (2016).
158. Bailey, T. L. *et al.* MEME Suite: Tools for motif discovery and searching. *Nucleic Acids Res.* **37**, 202–208 (2009).
159. von Mering, C. *et al.* STRING: A database of predicted functional associations between proteins. *Nucleic Acids Res.* **31**, 258–261 (2003).
160. Teng, H., Wang, Y. & Tang, B. L. Protein family review The syntaxins. *Genome* 1–7 (2001).
161. Haberkant, P. *et al.* In vivo profiling and visualization of cellular protein-lipid interactions using bifunctional fatty acids. *Angew. Chemie - Int. Ed.* **52**, 4033–4038 (2013).
162. Park, J.-W. W., Park, W.-J. J. & Futerman, A. H. Ceramide synthases as potential targets for therapeutic intervention in human diseases. *Biochim. Biophys. Acta - Mol. Cell Biol. Lipids* **1841**, 671–681 (2014).
163. Wang, E., Norred, W. P., Bacon, C. W., Riley, R. T. & Merrill, A. H. J. Inhibition of sphingolipid biosynthesis by fumonisins. Implications for diseases associated with Fusarium moniliforme. *J. Biol. Chem.* **266**, 14486–14490 (1991).
164. Wegner, M. S., Gruber, L., Mattjus, P., Geisslinger, G. & Grösch, S. The UDP-glucose ceramide glycosyltransferase (UGCG) and the link to multidrug resistance protein 1 (MDR1). *BMC Cancer* **18**, 1–10 (2018).
165. Sachsenheimer, T. Monitoring the intracellular metabolic fate of photoactivatable and clickable sphingosine. (Ruprecht-Karls-Universität Heidelberg, 2019).
166. Zhou, K. *et al.* A Ceramide-Regulated Element in the Late Endosomal Protein LAPTM4B Controls Amino Acid Transporter Interaction. *ACS Cent. Sci.* **4**, 548–558 (2018).
167. Bernsel, A., Viklund, H., Hennerdal, A. & Elofsson, A. TOPCONS: consensus prediction of membrane protein topology. *Nucleic Acids Res.* **37**, W465-8 (2009).
168. Stemmer, M., Thumberger, T., Del Sol Keyer, M., Wittbrodt, J. & Mateo, J. L. CCTop: An intuitive, flexible and reliable CRISPR/Cas9 target prediction tool. *PLoS One* **10**, 1–11 (2015).
169. Ran, F. A. *et al.* Genome engineering using the CRISPR-Cas9 system. *Nat. Protoc.* **8**, 2281–2308 (2013).
170. Jung, M. *et al.* Lines of Murine Oligodendroglial Precursor Cells Immortalized by an Activated neu Tyrosine Kinase Show Distinct Degrees of Interaction with Axons In Vitro and In Vivo. *Eur. J. Neurosci.* **7**, 1245–1265 (1995).
171. Buttery, P. C. & ffrench-Constant, C. Process extension and myelin sheet formation in maturing oligodendrocytes. *Prog. Brain Res.* **132**, 115–130 (2001).
172. Azevedo, M. M. *et al.* Jmy regulates oligodendrocyte differentiation via modulation of actin cytoskeleton dynamics. *Glia* **66**, 1826–1844 (2018).
173. Nawaz, S. *et al.* Actin filament turnover drives leading edge growth during myelin sheath formation in the central nervous system. *Dev. Cell* **34**, 139–151 (2015).
174. Davis, D. L. *et al.* Dynamics of sphingolipids and the serine palmitoyltransferase complex in rat oligodendrocytes during myelination. *J. Lipid Res.* **61**, 505–522 (2020).
175. Yurlova, L. *et al.* Self-Segregation of Myelin Membrane Lipids in Model Membranes. *Biophys. J.* **101**, 2713–2720 (2011).
176. Stangl, M. & Schneider, D. Functional competition within a membrane: Lipid recognition vs. transmembrane helix oligomerization. *Biochim. Biophys. Acta - Biomembr.* **1848**, 1886–1896 (2015).
177. Pinto, S. N., Silva, L. C., De Almeida, R. F. M. & Prieto, M. Membrane domain formation, interdigitation, and morphological alterations induced by the very long chain asymmetric C24:1 ceramide. *Biophys. J.* **95**, 2867–2879 (2008).
178. Kiessling, V. *et al.* A molecular mechanism for calcium-mediated synaptotagmin-triggered exocytosis. *Nat. Struct. Mol. Biol.* **25**, 911–917 (2018).
179. Head, B. P., Patel, H. H. & Insel, P. A. Interaction of membrane/lipid rafts with the cytoskeleton: Impact on signaling and function: Membrane/lipid rafts, mediators of cytoskeletal arrangement and cell signaling. *Biochim. Biophys. Acta - Biomembr.* **1838**, 532–545 (2014).
180. Kleene, R., Yang, H., Kutsche, M. & Schachner, M. The Neural Recognition Molecule L1 is a Sialic Acid-binding Lectin for CD24, Which Induces Promotion and Inhibition of Neurite Outgrowth. *J. Biol. Chem.* **276**, 21656–21663 (2001).
181. Ashburner, M. *et al.* Gene ontology: tool for the unification of biology. The Gene Ontology

Consortium. *Nat. Genet.* **25**, 25–29 (2000).
182. Fujishima, K., Galbraith, K. & Kengaku, M. Dendritic Self-Avoidance and Morphological Development of Cerebellar Purkinje Cells Parallel fibers (granule cell axons) Purkinje cell Granule cell Coronal axis. *The Cerebellum* **17**, 701–708 (2018).
183. Beesley, P. W., Herrera-Molina, R., Smalla, K. H. & Seidenbecher, C. The Neuroplastin adhesion molecules: Key regulators of neuronal plasticity and synaptic function. *J. Neurochem.* **131**, 268–283 (2014).
184. Desai, T. M. *et al.* IFITM3 restricts influenza A virus entry by blocking the formation of fusion pores following virus-endosome hemifusion. *PLoS Pathog.* **10**, e1004048 (2014).
185. Wei, Y. *et al.* Roles of the putative integrin-binding motif of the human metapneumovirus fusion (f) protein in cell-cell fusion, viral infectivity, and pathogenesis. *J. Virol.* **88**, 4338–4352 (2014).
186. Weigel-Kelley, K. A., Yoder, M. C. & Srivastava, A. Alpha5beta1 integrin as a cellular coreceptor for human parvovirus B19: requirement of functional activation of beta1 integrin for viral entry. *Blood* **102**, 3927–3933 (2003).
187. Rojek, J. M., Spiropoulou, C. F., Campbell, K. P. & Kunz, S. Old World and clade C New World arenaviruses mimic the molecular mechanism of receptor recognition used by alpha-dystroglycan's host-derived ligands. *J. Virol.* **81**, 5685–5695 (2007).
188. Imperiali, M. *et al.* O Mannosylation of -Dystroglycan Is Essential for Lymphocytic Choriomeningitis Virus Receptor Function. *J. Virol.* **79**, 14297–14308 (2005).
189. Kunz, S. Receptor binding and cell entry of Old World arenaviruses reveal novel aspects of virus-host interaction. *Virology* **387**, 245–249 (2009).
190. Suo, Y. *et al.* ICAM-1 depletion in the center of immunological synapses is important for calcium releasing in T-cells. *J. Innov. Opt. Health Sci.* **11**, 1–14 (2018).
191. Dupré, L. *et al.* Wiskott-Aldrich syndrome protein regulates lipid raft dynamics during immunological synapse formation. *Immunity* **17**, 157–166 (2002).
192. Gilsanz, A. *et al.* ALCAM/CD166 adhesive function is regulated by the tetraspanin CD9. *Cell. Mol. Life Sci.* **70**, 475–493 (2013).
193. Kurita-Taniguchi, M. *et al.* Molecular assembly of CD46 with CD9, alpha3-beta1 integrin and protein tyrosine phosphatase SHP-1 in human macrophages through differentiation by GM-CSF. *Mol. Immunol.* **38**, 689–700 (2002).
194. Hemler, M. E. Tetraspanin functions and associated microdomains. *Nat. Rev. Mol. Cell Biol.* **6**, 801–811 (2005).
195. Toledo, M. S., Suzuki, E., Handa, K. & Hakomori, S. Effect of ganglioside and tetraspanins in microdomains on interaction of integrins with fibroblast growth factor receptor. *J. Biol. Chem.* **280**, 16227–16234 (2005).
196. Kagawa, T., Mekada, E., Shishido, Y. & Ikenaka, K. Immune system-related CD9 is expressed in mouse central nervous system myelin at a very late stage of myelination. *J. Neurosci. Res.* **50**, 312–320 (1997).
197. Terada, N. *et al.* The tetraspanin protein, CD9, is expressed by progenitor cells committed to oligodendrogenesis and is linked to beta1 integrin, CD81, and Tspan-2. *Glia* **40**, 350–359 (2002).
198. Ishibashi, T. *et al.* Tetraspanin Protein CD9 Is a Novel Paranodal Component Regulating Paranodal Junctional Formation. *J. Neurosci.* **24**, 96–102 (2004).
199. Schafer, D. P., Bansal, R., Hedstrom, K. L., Pfeiffer, S. E. & Rasband, M. N. Does paranode formation and maintenance require partitioning of neurofascin 155 into lipid rafts? *J. Neurosci.* **24**, 3176–3185 (2004).
200. Bröer, A., Rahimi, F. & Bröer, S. Deletion of amino acid transporter ASCT2 (SLC1A5) Reveals an essential role for transporters SNAT1 (SLC38A1) and SNAT2 (SLC38A2) to sustain glutaminolysis in cancer cells. *J. Biol. Chem.* **291**, 13194–13205 (2016).
201. Scalise, M., Pochini, L., Galluccio, M., Console, L. & Indiveri, C. Glutamine transporters as pharmacological targets: From function to drug design. *Asian J. Pharm. Sci.* **15**, 207–219 (2020).
202. Eskelinen, E.-L. Roles of LAMP-1 and LAMP-2 in lysosome biogenesis and autophagy. *Mol. Aspects Med.* **27**, 495–502 (2006).
203. Stepanenko, A. A. & Heng, H. H. Transient and stable vector transfection: Pitfalls, off-target effects, artifacts. *Mutat. Res. - Rev. Mutat. Res.* **773**, 91–103 (2017).
204. Park, J. W. *et al.* Ablation of very long acyl chain sphingolipids causes hepatic insulin resistance in mice due to altered detergent-resistant membranes. *Hepatology* **57**, 525–532 (2013).

205. Lingwood, D. & Simons, K. Detergent resistance as a tool in membrane research. *Nat. Protoc.* **2**, 2159–2165 (2007).
206. Noël, G., Tham, D. K. L. & Moukhles, H. Interdependence of laminin-mediated clustering of lipid rafts and the dystrophin complex in astrocytes. *J. Biol. Chem.* **284**, 19694–19704 (2009).
207. Sharma, P. *et al.* beta-Dystroglycan binds caveolin-1 in smooth muscle: a functional role in caveolae distribution and Ca2+ release. *J. Cell Sci.* **123**, 3061–3070 (2010).
208. Keshet, G. I., Bar-Peled, O., Yaffe, D., Nudel, U. & Gabizon, R. The cellular prion protein colocalizes with the dystroglycan complex in the brain. *J. Neurochem.* **75**, 1889–1897 (2000).
209. Saslowsky, D. E., Lawrence, J. C., Henderson, R. M. & Edwardson, J. M. Syntaxin is efficiently excluded from sphingomyelin-enriched domains in supported lipid bilayers containing cholesterol. *J. Membr. Biol.* **194**, 153–164 (2003).
210. Laviad, E. L. *et al.* Characterization of Ceramide Synthase 2: TISSUE DISTRIBUTION, SUBSTRATE SPECIFICITY, AND INHIBITION BY SPHINGOSINE 1-PHOSPHATE. *J. Biol. Chem.* **283**, 5677–5684 (2008).
211. Abbas, H. K. *et al.* Fumonisin- and AAL-Toxin-Induced Disruption of Sphingolipid Metabolism with Accumulation of Free Sphingoid Bases. *Plant Physiol.* **106**, 1085–1093 (1994).
212. Harrer, H., Humpf, H. U. & Voss, K. A. In vivo formation of N-acyl-fumonisin B1. *Mycotoxin Res.* **31**, 33–40 (2014).
213. Luttgeharm, K. D., Cahoon, E. B. & Markham, J. E. Substrate specificity, kinetic properties and inhibition by fumonisin B1of ceramide synthase isoforms from Arabidopsis. *Biochem. J.* **473**, 593–603 (2016).
214. Bolla, J. R. *et al.* A Mass-Spectrometry-Based Approach to Distinguish Annular and Specific Lipid Binding to Membrane Proteins. *Angew. Chem. Int. Ed. Engl.* **59**, 3523–3528 (2020).
215. Hussain, M. M., Jin, W. & Jiang, X. C. Mechanisms involved in cellular ceramide homeostasis. *Nutr. Metab.* **9**, 1 (2012).
216. Hayashi, Y. *et al.* Complex formation of sphingomyelin synthase 1 with glucosylceramide synthase increases sphingomyelin and decreases glucosylceramide levels. *J. Biol. Chem.* **293**, 17505–17522 (2018).
217. Björkholm, P. *et al.* Identification of novel sphingolipid-binding motifs in mammalian membrane proteins. *Biochim. Biophys. Acta - Biomembr.* **1838**, 2066–2070 (2014).
218. Nickel, W., Sohn, K., Bünning, C. & Wieland, F. T. p23, A major COPI-vesicle membrane protein, constitutively cycles through the early secretory pathway. *Proc. Natl. Acad. Sci. U. S. A.* **94**, 11393–11398 (1997).
219. Winterstein, C., Trotter, J. & Krämer-Albers, E. M. Distinct endocytic recycling of myelin proteins promotes oligodendroglial membrane remodeling. *J. Cell Sci.* **121**, 834–842 (2008).
220. Erb, M., Steck, A. J., Nave, K. A. & Schaeren-Wiemers, N. Differential expression of L- and S-MAG upon cAMP stimulated differentiation in oligodendroglial cells. *J. Neurosci. Res.* **71**, 326–337 (2003).
221. Trépanier, M. O. *et al.* Phosphatidylcholine 36:1 concentration decreases along with demyelination in the cuprizone animal model and in post-mortem multiple sclerosis brain tissue. *J. Neurochem.* **145**, 504–515 (2018).
222. Bourre, J. M., Dumont, O. L., Clément, M. E. & Durand, G. A. Endogenous synthesis cannot compensate for absence of dietary oleic acid in rats. *J. Nutr.* **127**, 488–493 (1997).
223. Simons, M., Krämer, E. M., Thiele, C., Stoffel, W. & Trotter, J. Assembly of myelin by association of proteolipid protein with cholesterol- and galactosylceramide-rich membrane domains. *J. Cell Biol.* **151**, 143–153 (2000).
224. Yamaji, T. & Hanada, K. Establishment of HeLa Cell Mutants Deficient in Sphingolipid-Related Genes Using TALENs. *PLoS One* **9**, (2014).
225. Wessel, D. & Flügge, U. I. A method for the quantitative recovery of protein in dilute solution in the presence of detergents and lipids. *Anal. Biochem.* **138**, 141–143 (1984).
226. Laemmli, U. K. Cleavage of Structural Proteins during the Assembly of the Head of Bacteriophage T4. *Nature* **227**, 680–685 (1970).
227. Schindelin, J. *et al.* Fiji: an open-source platform for biological-image analysis. *Nat. Methods* **9**, 676–682 (2012).
228. Thiele, C. *et al.* Tracing fatty acid metabolism by click chemistry. *ACS Chem. Biol.* **7**, 2004–2011 (2012).
229. Bligh, E. G. & Dyer, W. J. A rapid method of total lipid extraction and purification. *Can. J.*

Biochem. Physiol. **37**, 911–917 (1959).
230. Özbalci, C., Sachsenheimer, T. & Brügger, B. Quantitative analysis of cellular lipids by nano-electrospray ionization mass spectrometry. in *Membrane Biogenesis* 3–20 (Springer, 2013).
231. Paltauf, F. & Hermetter, A. Strategies for the synthesis of glycerophospholipids. *Prog. Lipid Res.* **33**, 239–328 (1994).
232. Liebisch, G. *et al.* High throughput quantification of cholesterol and cholesteryl ester by electrospray ionization tandem mass spectrometry (ESI-MS/MS). *Biochim. Biophys. Acta (BBA)-Molecular Cell Biol. Lipids* **1761**, 121–128 (2006).

7. Supplement

Table 7.1 Proteins Interacting with Very Long Chain Fatty Acid-Containing Sphingolipid Species

List shows identified proteins with log_2 H/L <0.66 and p-value <0.05, expect for grey shaded proteins. Grey: proteins used as controls during validation. Blue: validated proteins. Sorted by the lowest log_2(H/L) value on top. Dataset from previous work[124].

Protein name	Gene name	log_2 H/L	-log_{10} t-test
Epsilon-sarcoglycan	SGCE	-1.97	2.66
CD83 antigen	CD83	-1.93	1.85
Membrane cofactor protein	CD46	-1.91	3.31
Dystroglycan;Alpha-dystroglycan;Beta-dystroglycan	DAG1	-1.82	2.08
Syntaxin-6	STX6	-1.50	2.96
Syntaxin-4	STX4	-1.49	2.70
Feline leukemia virus subgroup C receptor-related protein 1	FLVCR1	-1.49	1.97
Trans-Golgi network integral membrane protein 2	TGOLN2	-1.46	2.57
Vang-like protein 1	VANGL1	-1.44	1.33
CD276 antigen	CD276	-1.29	1.57
Basigin	BSG	-1.28	2.21
Intercellular adhesion molecule 1	ICAM1	-1.28	1.54
CD166 antigen	ALCAM	-1.27	1.31
EF-hand calcium-binding domain-containing protein 14	EFCAB14	-1.27	1.48
Embigin	EMB	-1.26	3.35
Keratinocyte-associated transmembrane protein 2	KCT2	-1.26	1.85
Choline transporter-like protein 1	SLC44A1	-1.24	3.17
Presenilin-1;Presenilin-1 NTF subunit;Presenilin-1 CTF subunit;Presenilin-1 CTF12;Presenilin;Presenilin-2;Presenilin-2 NTF subunit;Presenilin-2 CTF subunit	PSEN1, PSEN2	-1.22	3.56
Endonuclease domain-containing 1 protein	ENDOD1	-1.20	2.90
Aldo-keto reductase family 1 member C2	AKR1C2	-1.19	1.79
Neuroplastin	NPTN	-1.13	3.12
Neural cell adhesion molecule L1	L1CAM	-1.12	1.82
Syntaxin-7	STX7	-1.11	2.70
Transmembrane protein 87A	TMEM87A	-1.08	1.68
Tetraspanin;CD81 antigen	CD81	-1.06	2.03
Podocalyxin	PODXL	-1.03	1.70
Transmembrane protein 165	TMEM165	-1.02	2.81
Tetraspanin; CD9 antigen	CD9	-1.01	2.97
Serum paraoxonase/arylesterase 2	PON2	-1.00	3.65
Vesicle transport protein GOT1B	GOLT1B	-1.00	1.91
Golgi integral membrane protein 4	GOLIM4	-0.92	2.34
Neutral amino acid transporter B(0);Amino acid transporter	SLC1A5	-0.92	1.41
Heparan sulfate 2-O-sulfotransferase 1	HS2ST1	-0.92	4.33

CMP-N-acetylneuraminate-beta-galactosamide-alpha-2,3-sialyltransferase 1	ST3GAL1	-0.92	1.77
Tetraspanin-6	TSPAN6	-0.91	2.28
Cell surface glycoprotein MUC18	MCAM	-0.90	2.00
Syntaxin-10	STX10	-0.90	1.42
Zinc transporter 1	SLC30A1	-0.85	1.51
Very-long-chain 3-oxoacyl-CoA reductase	HSD17B12	-0.81	2.72
Lysosome-associated membrane glycoprotein 2	LAMP2	-0.81	2.54
Sodium-coupled neutral amino acid transporter 2	SLC38A2	-0.81	1.38
Atrial natriuretic peptide receptor 3	NPR3	-0.80	3.60
Reticulon-4; Reticulon	RTN4	-0.80	2.84
Integrin alpha-5;Integrin alpha-5 heavy chain;Integrin alpha-5 light chain	ITGA5	-0.80	1.64
Interferon-induced transmembrane protein 3	IFITM3	-0.80	1.49
Protein FAM114A2	FAM114A2	-0.75	1.32
Lysosome-associated membrane glycoprotein 1	LAMP1	-0.74	1.67
C-type mannose receptor 2	MRC2	-0.74	1.65
Solute carrier family 12 member 2	SLC12A2	-0.72	2.27
Signal recognition particle receptor subunit beta	SRPRB	-0.70	2.23
Tubulin alpha-4A chain	TUBA4A	-0.68	1.59
Vasorin	VASN	-0.67	1.93
Transmembrane protein 245	TMEM245	-0.61	3.14
Transferrin receptor protein 1;Transferrin receptor protein 1, serum form	TFRC	-0.12	0.54
Tetraspanin;CD63 antigen	CD63	-0.11	0.37
Integrin beta-1	ITGB1	0.37	3.06

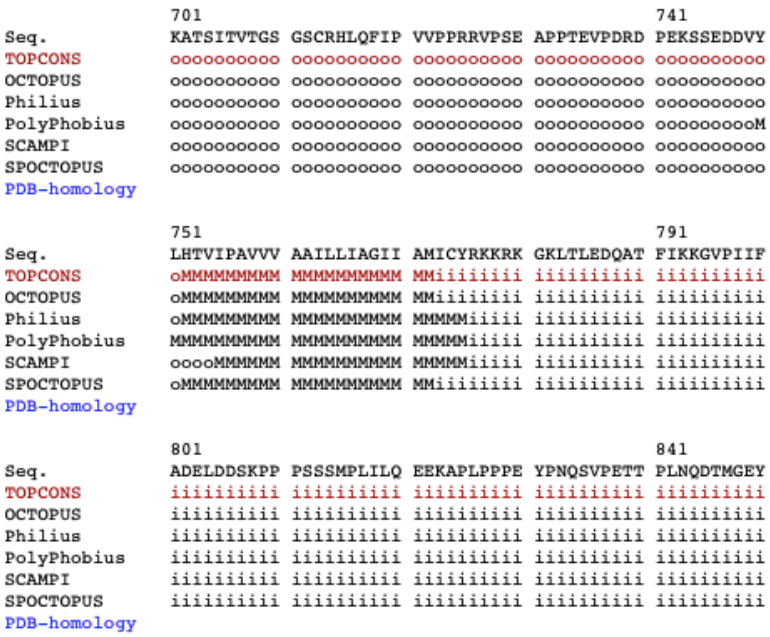

Figure 7.1 TOPCONS analysis of human DAG1
Consensus prediction of membrane topology. Seq: amino acid sequence human of dystroglycan (Uniprot ID: Q14118) from amino acids 700-750; M: transmembrane; o: extracellular; i: intracellular

Danksagung

An erster Stelle möchte ich mich bei Frau Prof. Dr. Britta Brügger bedanken, die mir die Möglichkeit gab, meine Dissertation im Rahmen dieses Projektes zu verfassen und mir stets mit Rat zur Seite stand. Zudem danke ich allen Mitgliedern des TAC Komitees für die wissenschaftliche Begleitung dieser Doktorarbeit.

Des Weiteren bedanke ich mich bei Frau Prof. Dr. Eva-Maria Krämer-Albers für die Bereitstellung der Oli-*neu* Zellen und bei Herrn Dr. Per Haberkant für die Bereitstellung der HEK Zellen.
Innerhalb der Gruppe danke ich Iris Leibrecht für die Aufbereitung der Lipidproben, sowie Timo Sachsenheimer und Christian Lüchtenborg für die Lipidmessungen und Auswertung der Lipidomdaten. Zudem danke ich insbesondere Ellen Kraus für die tolle Unterstützung im Labor - vor allem während meiner Schwangerschaft. Weitergehend möchte ich allen Kolleginnen und Kollegen für ihre Unterstützung und Hilfsbereitschaft, lebhaften Diskussionen, sowie die schöne gemeinsame Zeit danken.

Weiterhin geht ein großer Dank an meine Familie. Insbesondere an meine Eltern, die mich von Anfang an in meinem Studienvorhaben unterstützt haben. Zudem bedanke ich mich bei meinen Schwiegereltern für ihre Unterstützung.

Ein besonderer Dank gilt meiner Tochter Ida, die so gut schlief, dass ich genügend Zeit hatte, um diese Dissertation zu verfassen.

Zu guter Letzt bedanke ich mich bei meinem Ehemann Kornelius, der mich in der Zeit des Zusammenschreibens sehr unterstützt hat.